NTNU
Norwegian University of Science and Technology
Department of Marine Technology

M.Sc.THESIS

Title:	**Delivered:**
Simulation of Trawl Loads on Subsea Pipelines	14.06.10
	Availability: Open
Student: Vegard Longva	**Number of pages:** 110

Abstract:

The main objectives in this thesis was to investigate the effect of oblique trawl board crossings, increased trawl board added mass due to seabed proximity and the effect of a more rectangular trawl board geometry. In addition a new hydrodynamic load model which handles the seabed proximity and forward speed in a more consistent way was examined.

All simulations in this thesis are performed by means of the computer software SIMLA. A brief description of methods applied in SIMLA and nonlinear finite element analysis is therefore included. The thesis contains also a chapter which describes trawling concepts and trawl boards used in Norwegian waters.

Design loads from trawl gears on subsea pipelines are nowadays based on recommendations from the DNV-RP-F111 code. Simulation models with a 4500 kg polyvalent trawl board were established to verify the DNV recommendations for free spans of height 0 m and 1 m.

The simulations demonstrated that increasing trawl board added mass due to seabed proximity did not have any influence on neither pull-over loading nor pipeline response.

The effect of a rectangular trawl board geometry was most pronounced for a span height of 0 m because the duration increased by 0.5 s and the horizontal pull-over force was kept constant throughout the pull-over. A slighty larger pull-over loading compared to the polyvalent board was observed for a span height of 1 m.

Oblique trawl board crossings were examined for 6 different hit angles. The major finding was that a perpendicular crossing did not predict the largest pull-over load. On a general basis the simulations for a span height of 1 m underpredicted maximum pull-over force, duration and pipeline displacement compared to the DNV-RP-F111 recommendations. The 0 m span height simulations indicate that DNV predicts a different shape of the load time history and is slightly nonconservative in terms of maximum pull-over load.

The new hydrodynamic load model which includes the effect of forward speed and seabed proximity was used to simulate a perpendicular trawl board crossing. Here the span height of 0 m indicated that the DNV-RP-F111 code is nonconservative in terms of the pull-over load. The simulation for a span height of 1 m was however in very good agreement with the DNV-RP-F111 code in terms of duration and horizontal pull-over load. Therefore it is recommended that future simulations are based on the new hydrodynamic load model.

Keyword:

Trawl gear
Pipeline

Advisor:

Prof. Svein Sævik

Address:
NTNU
Department of Marine Technology
N-7491 Trondheim

Location:
Marinteknisk Senter
O. Nielsens vei 10

Tel. +47 73 595501
Fax +47 73 595697

NTNU Trondheim
Norges teknisk-naturvitenskapelige universitet
Institutt for marin teknikk

THESIS WORK SPRING 2010

for

Stud. tech. Vegard Longva

Simulation of trawl loads on subsea pipelines

Simulering av trållaster på offshore rørledninger

A large network of subsea pipelines have been installed at the Norwegian continental shelf and for large diameter cases (> 16") these are in most cases left exposed on the seabed. The fishing activity in the area is often based on bottom trawl gear, consisting of a trawl net kept open by a trawl door, one at each side of the net. The trawl doors are further pulled by a cable connected to the vessel, the purpose of the doors being to keep the cables separated and the trawl net open.

The trawl board design has traditionally been based on the "Otter"-trawl concept which is based on applying a flat steel plate, connected to a chain arrangement that introduces a rotational moment forcing the doors to open outwards when pulled forward. This gives a transverse hydrodynamic lift force that keeps the trawl board separated and the trawl net open. Lately, more advanced designs have been developed, focusing on increasing the lift force to drag force ratio, thus improving the fuel economy.

The trawl board mass, including hydrodynamic mass may be in the order of 10000 kg and when the trawl board hits a pipeline, two load effects govern:

1. An initial impact that may damage the coating and cause steel wall denting.
2. A "Pull-over" force which is a more long periodic force needed to pull the trawlboard over the pipeline. This force depending on the several parameters such as the mass, cable stiffness, free span height etc.

Item 2 above are in many cases governing the design with respect to external loads on subsea pipelines, specially for high temperature pipelines.

This master work therefore focus on the "Pull-over" load and continuing the work done during the project work in order to explain the differences between the results obtained by the software SIMLA and the results obtained from DnV Recommended Practice DnV-RP-F11 for low free-spans. The work is to include:

1. Investigate the effect of hit angle for increasing added mass.
2. Investigate the effect from an alternative trawlboard geometry, e.g. a more rectangular geometry.

3. Use a new model that include model test results and which handles the increased added mass effect from seabed in a more consistent way.
4. Conclusions and recommendations for further work

The work scope may prove to be larger than initially anticipated. Subject to approval from the supervisors, topics may be deleted from the list above or reduced in extent.

In the thesis the candidate shall present his personal contribution to the resolution of problems within the scope of the thesis work

Theories and conclusions should be based on mathematical derivations and/or logic reasoning identifying the various steps in the deduction.

The candidate should utilise the existing possibilities for obtaining relevant literature.

Thesis format
The thesis should be organised in a rational manner to give a clear exposition of results, assessments, and conclusions. The text should be brief and to the point, with a clear language. Telegraphic language should be avoided.

The thesis shall contain the following elements: A text defining the scope, preface, list of contents, summary, main body of thesis, conclusions with recommendations for further work, list of symbols and acronyms, references and (optional) appendices. All figures, tables and equations shall be numerated.

The supervisors may require that the candidate, in an early stage of the work, presents a written plan for the completion of the work.

The original contribution of the candidate and material taken from other sources shall be clearly defined. Work from other sources shall be properly referenced using an acknowledged referencing system.

The report shall be submitted in two copies:
- Signed by the candidate
- The text defining the scope included
- In bound volume(s)
- Drawings and/or computer prints which cannot be bound should be organised in a separate folder.

Ownership
NTNU has according to the present rules the ownership of the thesis. Any use of the thesis has to be approved by NTNU (or external partner when this applies). The department has the right to use the thesis as if the work was carried out by a NTNU employee, if nothing else has been agreed in advance.

Thesis supervisors
Prof. Svein Sævik

Deadline: 14th June, 2010

Trondheim, Januar 17, 2010

Svein Sævik

Preface

The content in thesis is based upon research carried out during the spring semester 2010 at the Department of Marine Technology, NTNU. The research is performed as a part of my Master degree in Marine Technology, with specialization in Marine Structures. The thesis is a continuation of the work I did in my Project thesis during the fall semester 2009.

The main objective of this thesis was to compare simulated trawl loads on a subsea pipeline with the recommended design loads in the DNV-RP-F111 code. The effect of oblique crossings for increasing trawl board added mass and the effect of a rectangular-shaped trawl board were also investigated. All simulations in this report are based on the computer software SIMLA.

Enclosed with this report is a CD, which aside from a digital copy of the report includes SIMLA input files for all simulations executed in this thesis.

My supervisor was Prof. Svein Sævik at the Department of Marine Technology, NTNU. I would like to thank him for excellent counselling during my thesis work. Especially his great knowledge of the SIMLA software has been of very good use regarding modelling tips and code debugging. I would also thank Statoil for providing hydrodynamic trawl board coefficients. In addition MARINTEK should be acknowledged regarding license of SIMLA.

Vegard Longva
Trondheim, June 2010

Contents

List of Figures

List of Tables

List of Symbols

A_e	Cross-sectional area exposed to external pressure
A_i	Cross-sectional area exposed to internal pressure
C_a	Added mass coefficient
C_{ii}	Drag coefficient for DOF $i = 1, 2, ..., 6$
$\tilde{C}_{ii}$	Forward speed drag coefficient for DOF $i = 1, 2, ..., 6$
c_c	Concentrated damping of contact element
C_D	Drag coefficient
C_F	Empirical coefficient of pull-over force
d	Water depth
D_x	Drag force in x-direction, verification test
D_y	Drag force in y-direction, verification test
D_z	Drag force in z-direction, verification test
D_m	Mean steel diameter
D_o	Coating diameter
EA	Axial stiffness
E	Young's modulus
E_T	Tangent modulus
F_x	Maximum horizontal pull-over force, DNV-RP-F111
$\hat{F}_x$	Sampled horizontal pull-over load
F_z	Maximum vertical downward pull-over force, DNV-RP-F111
$\hat{F}_z$	Sampled vertical pull-over load
$\overline{H}$	Dimensionless height
h	Height of trawl board
h_{sp}	Span height, measured as seabed to pipeline gap
I	Impulse of sampled pull-over load
k_c	Normal stiffness of contact element

k_w	Warpline stiffness
l	Length of trawl board
l_{fs}	Length of free span
L	Length of pipeline model
l_s	Length of sweepline
l_{uw}	Length of upper warpline
l_{lw}	Length of lower warpline
m	Structural mass
m_{aii}	Added mass coefficient for DOF $i = 1, 2, 3$
m_{ajj}	Added moment of inertia coefficient for DOF $j = 4, 5, 6$
m_{ii}	Mass moment of inertia for DOF $i = 4, 5, 6$
$\hat{m}_{aii}$	Seabed proximity added mass coefficient for DOF $i = 1, 2, 3$
$\hat{m}_{ajj}$	Seabed proximity added moment of inertia coefficient for DOF $j = 4, 5, 6$
m_p	Mass of trawl board plate
m_s	Mass of trawl board ski
m_t	Steel mass of trawl board
p_e	External pressure
p_i	Internal pipeline pressure
R_D	Hydrofoil drag force
R_e	Reynolds number
R_x	Reaction force in x-direction, verification test
R_y	Reaction force in y-direction, verification test
R_z	Reaction force in z-direction, verification test
t	Thickness of trawl board
t_w	Wall thickness of steel pipe
T_w	True axial force in pipe wall, positive in tension
T_e	Effective axial force, positive in tension
T_p	Duration of pull-over
u_x, u_y, u_z	Surge, sway and heave displacements of trawl board
u	Axial displacement in co-rotated reference frame
V	Trawling velocity
V_c	Current velocity
V_R	Relative forward velocity

v	Horizontal displacement in co-rotated reference frame
w_s	Submerged weight
w_x, w_y, w_z	Water particle displacement in x-, y- and z-direction
w	Vertical displacement in co-rotated reference frame
x_D, y_D, z_D	Coordinates of drag center
x_M, y_M, z_M	Coordinates of hydrodynamic center
$\mathbf{C}^m$	Elasticity tensor
$\mathbf{C}$	System damping matrix
$\mathbf{C}_0$	System diagonal damping matrix
$\mathbf{c}$	Element total damping matrix
$\mathbf{c}_0$	Element concentrated damping matrix
D_{ijkl}	Component of 4$^{\text{th}}$ order constitutive tensor for plastic range
$\Delta\epsilon_{kl}$	Total strain increment, component of 2$^{\text{nd}}$ order tensor
$\Delta\boldsymbol{\epsilon}^P$	Plastic Strain increment, Eulerian strain tensor
$\mathbf{E}$	Green strain tensor
E_{ijkl}	Component of 4$^{\text{th}}$ order constitutive tensor for elastic range
E_{xx}	Longitudinal Green strain for a pipe element
$\hat{\mathbf{K}}$	Effective stiffness matrix
$\mathbf{k}_\sigma$	Initial stress stiffness matrix
$\mathbf{k}_m$	Material stiffness matrix
$\mathbf{k}_T$	Element tangent stiffness matrix
$\mathbf{K}_T$	System tangent stiffness matrix
$\mathbf{M}$	System mass matrix
$\mathbf{m}$	Element mass matrix
$\mathbf{N}$	Matrix containing interpolation polynomials
$\mathbf{r}$	Displacement vector
$\Delta\mathbf{r}$	Displacement increment
$\Delta\hat{\mathbf{R}}$	Effective load vector increment
$\Delta\mathbf{R}$	Load vector increment
$\mathbf{R}^E$	System external force vector
$\mathbf{R}^I$	System internal force vector
$\mathbf{S}$	2$^{\text{nd}}$ Piola-Kirchoff stress tensor
$\boldsymbol{\sigma}$	Cauchy stress tensor

$\Delta\sigma_{ij}$	Stress increment, component of 2nd order tensor
$\mathbf{T}$	Transformation matrix
$\mathbf{t}$	Referential surface traction vector
$\mathbf{u}$	Displacement field
α	Parameter in HHT-α method
β	Parameter in HHT-α method
δ_p	Maximum global pipeline deflection at point of trawl board pull-over
Δ	Seabed to trawl board gap
Δt	Time increment
ϵ_D	Convergence norm parameter for displacements
γ	Parameter in HHT-α method
J_2	2nd Deviatoric stress invariant
κ	Hardening parameter
λ	Damping ratio
ν	Kinematic viscosity coefficient
∇	Displaced water volume of body
ϕ	Sweepline angle
Φ	Roll angle of trawl board
Ψ	Heading angle of trawl board
ψ	Pipeline hit angle
ρ	Density of water
ρ_s	Density of structural element
σ_1	1st Principal Cauchy stress
σ_2	2st Principal Cauchy stress
σ_Y	Yield stress
$\sigma_{0.2}$	Offset yield strength
θ	Torsional rotation in co-rotated reference frame
θ_x, θ_y, θ_z	Roll, pitch and yaw rotations of trawl board
$\overline{\theta}_x$, $\overline{\theta}_z$	Mean roll and yaw angle
ζ_1, ζ_2	Mass and stiffness proportional Rayleigh damping coefficients

Chapter 1

Introduction

1.1 Background and Motivation

Before offshore pipelines are installed a trench is sometimes made along parts of the planned pipeline path. Long free spans are prone to fatigue damage and in extreme cases the spans can be reduced by for instance rock dumping. Even though these actions are applied, current and severe sea states will result in erosion which can produce free spans and excavate initially buried parts. Moreover, there will certainly exist short free spans with evident heights and parts where the pipeline is laid freely on the seabed. In connection with bottom trawling this clearly represents a potential risk of interference.

The Norwegian authorities requires that subsea installations shall not unnecessarily or to an unreasonable extent impede or obstruct fishing activities [3]. With this invariable requirement the oil companys must install their pipelines distant to fishing zones or ensure that proper safety measures are fulfilled if crossings are unavoidable. To fishermen it is well known that subsea installations attract fishes and therefore the hazard of overtrawling cannot be completely eliminated even if the pipeline is laid outside of the fishing banks.

The largest trawl gears operated today are used in the seas surrounding Svalbard. Ship owners which operates in these waters will probably use the same trawl gears in the Norwegian Sea and in the North Sea. It must therefore be anticipated that trawl gears used nearby subsea pipelines will be of the same size as the equipment used in the Greenland Sea and in the Barents Sea. According to DNV [3] the largest trawl boards used in the Barents Sea can have a mass of 6000 kg, while clump weights can have a mass of up to 10000 kg. In addition it must be expected that the hydrodynamic mass will be of the same order as the mass. The trawling velocity is governed by the swimming speed of the fish which pursuant to DNV [3] will be maximum 3 m/s. The loading in case of interference can therefore cause severe damages of the pipeline.

1.2 Scope of Thesis

The trawl gear design loads on subsea pipelines are nowadays determined by the DNV-RP-F111 code [3]. From the pipeline designers point of view this code is believed to overestimate the pipeline response. This was confirmed in the Master thesis of Møller [15] by interference simulations of a trawl board and a pipeline. His major finding was that the DNV-RP-F111 code overestimated the lateral pipeline

displacement for free spans with height less than 2 m. Based on his observations it was decided to focus on span heights of 0 m and 1 m in this thesis.

In the DNV-RP-F111 code the effect of a oblique trawl board crossing is not explicitly taken into account in the recommended pull-over loading. The validity of the DNV code is examined by simulations of 6 different hit angles with a polyvalent trawl board which has a circular-shaped front. From the field of hydrodynamics it is known that seabed proximity will result in an increase of the added mass coefficients. The trawl board added mass increase will be examined together with the effect of hit angle in this report.

It is plausible that the pull-over characteristics depend on the trawl board geometry. This hypothesis is investigated by simulations with a rectangular-shaped trawl board. Conclusions regarding the effect of a more rectangular geometry must be based on several analysis runs such that the uncertainty level is reduced. The simulations are hence executed for the same hit angles which was used to examine the effect of oblique crossings. Conclusions regarding the effect of hit angle is therefore provided for the rectangular-shaped board as well.

When the trawl board is towed along the seabed there will be induced a transverse lift force which must be included in the simulations. In addition the hydrodynamic coefficients will depend on the distance to the seabed. These effects will be investigated with a new hydrodynamic load model for the case of a perpendicular crossing.

All simulations in this report are based on the computer software SIMLA. The simulation models have been made such that they provoke large pipeline responses and pull-over loads. To provoke large pipeline displacements the coating stiffness contribution is neglected and the selected pipeline diameter is located at the lower range of the DNV-RP-F111 validity interval. Furthermore, the trawl board is modelled by pipe elements with a very high bending stiffness such that deformations related to the board will be neglectable during interference. The maximum trawling velocity, which pursuant to DNV [3] is equal to 3 m/s, has been used in all simulations. In addition is the towing line conservatively modelled as a straight cable.

Several assumptions and simplifications have been introduced in the simulation models. The pipeline is for instance assumed to be located at the Skarv field in the North Sea. The modelled seafloor is completely flat and is assigned a rather high vertical stiffness in order to avoid large seabed penetrations. Moreover, the pipeline steel shell is assumed to remain intact without any denting deformations during interference. The thickness of the board is not represented since the contact geometry is defined by small diameter pipe elements which are located in the same plane. In addition there are other minor modelling simplifications which will be mentioned as they come along in Chapter 5.

1.3 Thesis Structure

Chapter 2 Describes trawling concepts and trawl boards used in Norwegian waters.

Chapter 3 Gives a brief introduction of dynamic analysis with nonlinear finite element methods. The basic methods applied in SIMLA are in focus throughout the chapter.

Chapter 4 Contains a short presentation of the DNV-RP-F111 code and the recommended pull-over loading for the polyvalent trawl board used in the simulations.

Chapter 5 Provides a detailed presentation of the trawl gear configuration, the pipeline, the two trawl boards and the hydrodynamic load models. Estimates of the trawl board dynamic properties are made for all six degrees of freedom. Further the material curves which describe interaction between pipeline,

trawl board and seabed are presented. In addition a pull-over convergence test and a description of the simulation execution are included.

Chapter 6 Results from the simulations are presented in this chapter. This includes pull-over load impulses and history plots of pull-over forces and horizontal pipeline displacements. Minor amendments which have been made to the model presented in Chapter 5 are mentioned here. Comments of the results are provided for all simulations and in specific cases the observed trawl board behaviour is also described.

Chapter 7 Here trends from the simulations are briefly summarized before concluding statements are made. Recommendations for further work are also included based on observations during the thesis work and the simulation results.

Chapter 2

Trawl Gears

A vessel performs a trawling process when it tows a fishing net with an opening in the direction of travel. In this context the fishing net is referred to as a trawl bag. The trawling process can be executed at any altitude in the water column and is governed by the biological behaviour of the species which are harvested. This chapter will focus only on bottom trawling concepts in Norwegian waters which are based on the use of trawl boards. The chapter was written in connection with the Project thesis in the fall semester 2009 and is based on textbooks by Ludvig Karlsen [8, 9].

2.1 Otter Trawl

The configuration of an otter trawl is seen in Figure 2.1. At both sides the trawl bag is connected to the trawl boards through sweeplines. The trawl boards are further connected to the surface vessel by means of warplines. An angle of attack relative to the direction of travel is achieved by connecting the sweepline and the warpline at suitable positions on the trawl boards. According to foil theory the boards will produce lift forces which act outwards. Around the circumference of the trawl bag mouth there are mounted weights on the lower part and floats on the upper part. The combined action of the boards, the floats and the weights will retain the opening of the mouth during the trawling process. As the boards are dragged along the seabed they make noise and set up a cloud of mud. This will affect the fish to swim forward in front of the trawl. Eventually the fish will lose speed and get trapped in the trawl net. The otter trawl is today common to use in Norwegian waters.

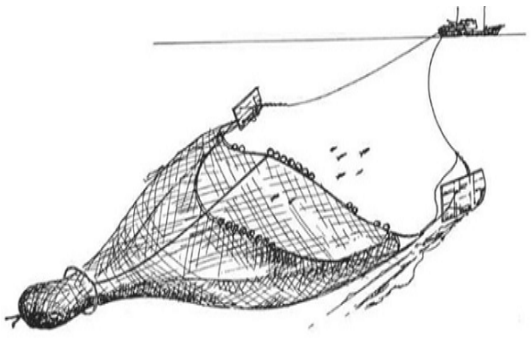

Figure 2.1: Otter trawl [2]

2.2 Twin Trawl

The twin trawl in Figure 2.2 is an extension of the otter trawl concept. In Ludvig Karlsens textbook [9] the twin trawl is categorized as an otter trawl instead of an own trawl gear type. The twin trawl is a relatively new concept which has been developed during the last decades. The design is based on a heavy clump weight located at the end of the centre warpline. The clump weight will together with the trawl boards keep the bags apart and their mouths open. The harvesting capacity is obviously raised compared to the single otter trawl. Most of the towing force is transferred in the centre warpline. This will reduce the tension in the warplines connected to the trawl doors, and the hydrodynamic lift force will give a larger mouth opening compared to the single otter trawl. Another advantage is that the whole catch is not lost if one of the warplines are cut off during operation. Today the twin trawl concept is in common use by Norwegian ship owners.

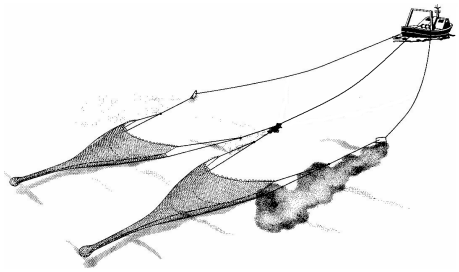

Figure 2.2: Twin trawl [5]

2.3 Trawl Boards

The development of different boards is a result of various operation conditions and the demand for improved fuel economy. In the recent years designers have developed boards with spoilers to increase the lift force and reduce the viscous pressure resistance. The design and degree of robustness depends on the seabed appearance. If the seafloor is hard it is desirable to have a small contact area, while for soft bottoms a large contact area is advantageous. The edge which slides along the seabed is fitted with a heavy steel ski to avoid wear and tear. In a bottom trawling process it is crucial that the boards have enough weight to prevent the warpline tension from lifting it upwards during harvesting. The lateral stability must be adequate such that the lift force is not suppressed. Therefore the bottom trawl boards are long compared to the height and equipped with a heavy ski.

2.3.1 V-Board

The V-board has a knuckleline in the longitudinal direction which gives different attack lines of the hydrodynamic lift forces on the upper and lower part. This makes the board self-righting to some extent and improves the lateral stability. The slope of the lower part improves the ability to pass small obstacles. When the trawl gear is launched from the vessel this board has a very good ability to obtain rapid spreading such that the gear will not get tangled. The main drawback is that the knuckleline design produces a smaller hydrodynamic lift resultant compared to other boards. It is also claimed by fishermen that the board is fragile when used at very hard seafloors.

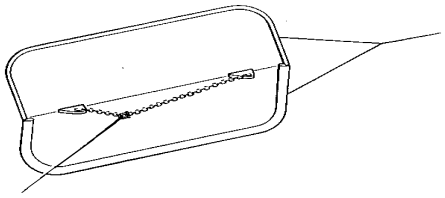

Figure 2.3: V-Board [6]

2.3.2 Polyvalent Board

These boards have a curved surface with an oval shape which improves the ability to slide over obstacles. In case of a hard seabed the oval shape is significant since it is desirable to have a small contact area. When used at muddy seafloors the contact area should be large and hence the oval shape is more faded out. By selecting a medium oval shape the boards will get reasonable abilities to operate on both soft and hard seabeds. The drawback of this trawl board is the high producing costs related to the complex geometry.

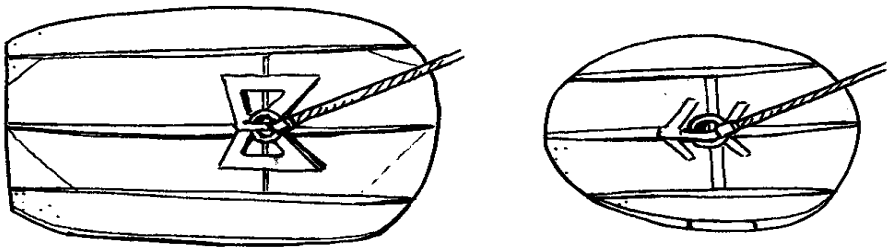

Figure 2.4: Polyvalent boards [9]

2.3.3 Polyfoil Board

This is the most modern board and consists of 3 or 4 foils mounted in series. The aspect ratio of each foil is hence increased and a larger hydrodynamic lift force can be produced. This arrangement will retain the length and height dimensions such that the lateral stability is maintained. The separated foils will behave like single beams when lateral impacts occur and the robustness is therefore reduced. In Norway this trawl board has been used on small trawlers.

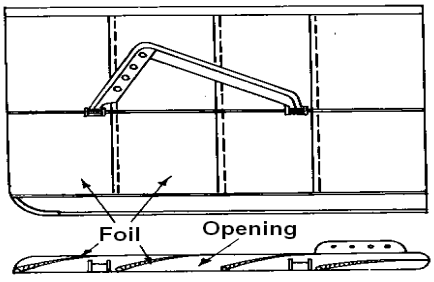

Figure 2.5: Polyfoil board [8]

Chapter 3

Nonlinear Finite Element Analysis

The content of this chapter is taken from a literature study of nonlinear finite element methods carried out in the Project thesis during the fall semester 2009. It is included here to enhance the knowledge of methods applied in the SIMLA software which has been used throughout the thesis work.

3.1 Nonlinear Effects

The finite element method is a widely used numerical method which can solve for instance elasticity, diffusion and heat transfer problems. In this report the focus will be on structural analysis where the following nonlinearities are present,

- Material,
- Geometry,
- Boundary conditions.

In brief the material behaviour becomes nonlinear when the stress exceeds the yield limit. Geometric nonlinearity will arise when the structure deforms such that the equilibrium equations must be expressed with respect to the deformed configuration. Nonlinear boundary conditions can for instance be related to contact problems.

3.2 Basics of the Finite Element Method

Three basic principles must be dealt with in both linear and nonlinear finite element methods,

- Compatibility,
- Equilibrium,
- Constitutive equations.

3.2.1 Compatibility

The compatibility requirement for a beam assures that adjacent cross-sections get the same deformation and that the material is continuous when it deforms. This is fulfilled by describing the displacements with continuous interpolation functions and ensuring that the strain is finite at the element boundaries [16]. In SIMLA the pipe elements obey the Bernoulli-Euler deformation hypothesis which assumes that plane cross-sections perpendicular to the neutral axis will remain plane and perpendicular to the neutral axis in the deformed configuration, i.e. shear deformations are neglected. In SIMLA the Green strain definition is applied and the 2nd order longitudinal engineering strain term is neglected [18],

$$E_{xx} = u_{,x} - yv_{,xx} - zw_{,xx} + \frac{1}{2}(v_{,x}^2 + w_{,x}^2) + \theta_{,x}(yw_{,x} - zv_{,x}) + \frac{1}{2}\theta_{,x}^2(y^2 + z^2). \tag{3.1}$$

(3.1) is based on the Bernoulli-Euler compatibility requirement which is valid also in the elastoplastic range. In (3.1) the neutral axis coincides with the x-axis and u, v and w are respectively the axial, horizontal and vertical displacements. The torsional rotation of the neutral axis is denoted θ. The compatibility requirement is taken into account by including (3.1) in the equilibrium formulation.

3.2.2 Equilibrium

Equilibrium is expressed by means of the Principle of Virtual Displacements. This principle states that the work performed by the constant true internal stresses and the constant external forces is zero when the structure is exposed to a virtual displacement field which satisfies the boundary conditions. The principle is valid if the stresses and external forces represent an equilibrium state. In the formulation in SIMLA the volume forces are neglected while initial stresses are accounted for [19]. The Principle of Virtual Displacements expressed by tensors for the static case can then be written as [21]

$$\int_{V_0} (\mathbf{S} - \mathbf{S}_0) : \delta\mathbf{E}\, \mathrm{d}V - \int_{\partial V_0} \mathbf{t} \cdot \delta\mathbf{u}\, \mathrm{d}S = 0. \tag{3.2}$$

Here subscript 0 refers to the initial state, $\mathbf{S}$ is the 2nd Piola-Kirchoff stress tensor, $\mathbf{t}$ is the surface traction vector, $\delta\mathbf{u}$ is a virtual compatible displacement field and $\delta\mathbf{E}$ is the corresponding virtual Green strain tensor.

(3.2) can also be derived by the Method of Weighted Residuals [21]. Before this method is applied, the static equilibrium equation which contains the divergence of the stress tensor must in principle be satisfied at every point in the continuum. The method will have two consequences for the equilibrium condition. Firstly, the differentiability requirement of the stress tensor is removed. Secondly, equilibrium is not satisfied at every point, but rather in an averaged sense expressed by the integral in (3.2). Hence (3.2) represents a weaker formulation of the original equilibrium condition, and an approximation of the true solution is obtained instead.

3.2.3 Constitutive Equations

The stresses in (3.2) must be related to the strains. This is done with a constitutive equation which for the elastic case is given by Hooke's law. The effect of internal and external pressure will result in a circumferential stress in a subsea pipeline. In the elastoplastic case this stress must be included in the

finite element formulation [19]. Nonlinear problems are solved by incremental methods and therefore a flow rule which gives the plastic strain increments at every point in the load history must be found.

Three features must be defined in order to calculate the plastic strain:

- An initial yield condition,
- A hardening rule,
- A flow rule.

Initial Yield Criterion

The initial yield condition defines the stress state where plastic deformation first occurs. This state can for instance be expressed in terms of the von Mises yield criterion. Furthermore, in metal structures the strains are usually small such that the 2nd Piola-Kirchoff stress tensor coincides with the Cauchy stress tensor [16]. The 2-dimensional von Mises yield criterion expressed by the principal stresses is given as

$$f_{initial} = \sqrt{\sigma_1^2 + \sigma_2^2 - \sigma_1\sigma_2} - \sigma_Y = 0. \tag{3.3}$$

Hardening Rule

The hardening rule describes how the yield criterion changes as the plastic flow proceeds [19]. Both isotropic and kinematic hardening is included in the material models in SIMLA. In Figure 3.1 the features of these two concepts are illustrated for a uniaxial state of stress.

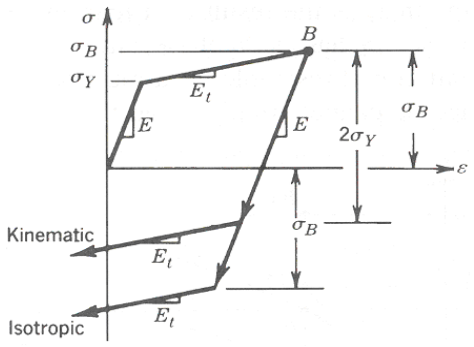

Figure 3.1: Isotropic and kinematic hardening [16]

As depicted in Figure 3.1 the difference between isotropic and kinematic hardening rules appear when the loading is reversed. In case of isotropic hardening the yield criterion is unaltered if the loading is reversed. Many metals are in conflict with the isotropic hardening feature and can better be described by kinematic hardening [16]. Kinematic hardening for the uniaxial stress state implies that an elastic range equal to twice the yield strength is preserved. In the literature this behaviour is called the Bauschinger effect.

Flow Rule

The flow rule determines the plastic strain increment at every point in the load history. The starting point in the derivation of the flow rule is to define the yield surface, f. In SIMLA the yield surface is assumed

to depend on the 2nd deviatoric stress invariant J_2, and a hardening parameter κ [19],

$$f(J_2, \kappa) = 0. \tag{3.4}$$

The domain of the yield function,

- $f < 0$: Elastic range,
- $f = 0$: Plastic range,
- $f > 0$: Inadmissible.

Further Drucker's postulate of a stable material is utilized [16],

- The yield surface is convex,
- The plastic strain increment $\Delta\boldsymbol{\epsilon}^P$ is normal to the yield surface,
- The plastic strain increment is a linear function of the stress increment.

A complete and formal derivation of the flow rule based on the assumptions above can be found in the SIMLA theory manual [19]. The result is a constitutive equation which gives the relation between the total strain increment and the increment in stress. In component form with Einstein summation convention this relation can be written as

$$\Delta\sigma_{ij} = D_{ijkl}(E_{ijkl}, \boldsymbol{\sigma}, \kappa)\, \Delta\epsilon_{kl}. \tag{3.5}$$

In the elastic range where $f < 0$, the incremental constitutive equation is given by Hooke's law. In component form it is formally given as

$$\Delta\sigma_{ij} = E_{ijkl}\, \Delta\epsilon_{kl}. \tag{3.6}$$

3.3 Total and Updated Lagrange Formulation

When the finite element method is formulated for a nonlinear geometrical problem in structural engineering it is common to distinguish between two methods,

- Updated Lagrangian formulation,
- Total Lagrangian formulation.

The difference between the methods is related to the frame of reference. In the total Lagrange method the incremental equations are formulated such that stresses and strains refer to a coordinate system which is fixed with respect to the initial element configuration. Contrary, the updated Lagrange method uses a curvilinear coordinate system which is fixed to the deformed body and continuously updated as the body deforms. In Figure 3.2 the updated Lagrange formulation uses C_n as reference, while the total Lagrange formulation uses C_0 as reference [11].

In SIMLA the formulation is however based on a co-rotational reference. This method resembles on the updated Lagrange formulation since a Cartesian coordinate system is attached to the element and is continuously updated as the element deforms. The difference between a co-rotational formulation and an updated Lagrange formulation will be neglectable for small strains. For a beam element the co-rotated coordinate system is defined such that the longitudinal coordinate axis intersects the end nodes in the last known equilibrium configuration. When the coordinate system is defined in this manner, the rigid body motions will be separated from the relative element deformation [19]. In Figure 3.2 the co-rotated formulation will have the ghost configuration C_{0n} as the reference [11].

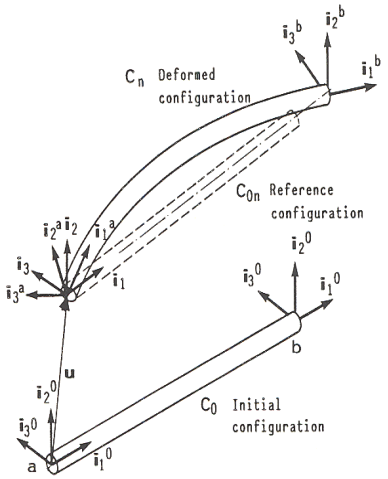

Figure 3.2: Reference frames [11]

3.4 Incremental Stiffness Matrix

The solution of a problem which is nonlinear in terms of material behaviour or geometry is obtained by means of incremental methods. Therefore it is necessary to formulate an incremental stiffness matrix. The first step is to apply the Principle of Virtual Displacements in (3.2) on two configurations which are close to each other in terms of stresses and strains. Thereafter the integrated equilibrium equations are subtracted from each other. When 2nd order contributions are neglected the result can be expressed as [19],

$$\int_{V_{0n}} (\mathbf{C}^m \colon \Delta\mathbf{E}) : \delta\mathbf{E}\,\mathrm{d}V + \int_{V_{0n}} \mathbf{S} \colon \delta\Delta\mathbf{E}\,\mathrm{d}V - \int_{\partial V_{0n}} \Delta\mathbf{t} \cdot \delta\mathbf{u}\,\mathrm{d}S - \int \mathbf{t} \cdot \delta\mathbf{u}\,(\Delta\mathrm{d}S) = 0. \tag{3.7}$$

Here $\mathbf{C}^m$ is the elasticity tensor, $\mathbf{S}$ is the 2nd Piola-Kirchoff stress tensor, $\mathbf{E}$ is the Green strain tensor, δ is a virtual quantity and Δ denotes the increment between the two configurations. The first term in (3.7) corresponds to the material stiffness matrix, the second term gives the initial stress stiffness matrix and the two last terms will result in an incremental load vector. A load correction stiffness matrix will appear if the loading depend on the motion of the element [11]. This will not be discussed in the following.

The incremental stiffness relation is found on matrix form when the strain measure from (3.1) is inserted into (3.7) together with the constitutive relation and the selected displacement interpolation functions. When the numerical integration has been executed the tangent stiffness matrix can be expressed as

$$\mathbf{k}_T = \mathbf{k}_m + \mathbf{k}_\sigma. \tag{3.8}$$

Here $\mathbf{k}_m$ is the material stiffness matrix and $\mathbf{k}_\sigma$ is the initial stress stiffness matrix on element level. The orientation of the co-rotated coordinate system will in general not coincide with the global coordinate system used for assembly of global matrices. Therefore it is necessary to transform both local displacements and local forces into the global coordinates. This can be expressed by means of transformation matrices as

$$\mathbf{k}_T^{global} = \mathbf{T}^\mathsf{T} \mathbf{k}_T^{local} \mathbf{T}. \tag{3.9}$$

In the co-rotated formulation the continuous updating of transformation matrices accounts for the nonlinear geometry which arises for large rotations [16].

The system equations is obtained by adding the transformed incremental load vectors and element tangent stiffness matrices into a global matrix system. For a static problem the system incremental relation can be expressed as

$$\mathbf{K}_T \Delta \mathbf{r} = \Delta \mathbf{R}. \tag{3.10}$$

Here $\Delta \mathbf{r}$ is the displacement increment and $\Delta \mathbf{R}$ the load increment. A static problem is solved stepwise by incrementing the load until a given load level is achieved. In addition equilibrium iterations are typically performed at each load step. Solution methods for static problems are not given any focus in the following since all simulations in this thesis are based on dynamic analysis.

3.5 Dynamic Analysis

The structural mass matrix can be found from the Principle of Virtual Displacement or simple considerations regarding the kinetic energy. On element level the mass matrix is given as

$$\mathbf{m} = \int_{V_0} \rho_s \mathbf{N}^{\mathsf{T}} \mathbf{N} \, \mathrm{d}V \qquad \mathbf{u} = \mathbf{N}\mathbf{v}. \tag{3.11}$$

Here ρ_s is the structural density and $\mathbf{N}$ is a matrix which contains interpolation functions. The $\mathbf{N}$-matrix gives the relation between the nodal degrees of freedom $\mathbf{v}$ and the displacement vector $\mathbf{u}$ at arbitrary locations within the element. It should also be mentioned that submerged elements will have a hydrodynamic mass matrix as well.

Structural damping in SIMLA can be included as Rayleigh proportional damping and concentrated damping as shown in (3.12). In a linear analysis it is beneficial to use Rayleigh damping since an uncoupled system of equations can be found if the eigenmodes are known. The response from the uncoupled equations can then be superposed to give the total solution. In a nonlinear analysis this approach cannot be used since the principle of superposition is not valid. It can be shown that modes with very low frequency are damped out by mass proportional damping and higher frequency modes by stiffness proportional damping. Therefore Rayleigh damping is typically introduced in a nonlinear analysis to damp out high frequency modes by means of a stiffness proportional damping matrix.

$$\mathbf{c} = \mathbf{c}_0 + \zeta_1 \mathbf{m} + \zeta_2 \mathbf{k}_T \tag{3.12}$$

The global equilibrium equation system is found by adding all the transformed element contributions into the global matrix system. The global equilibrium equation can then be expressed as

$$\mathbf{M}\ddot{\mathbf{r}} + \mathbf{C}\dot{\mathbf{r}} + \mathbf{R}^I = \mathbf{R}^E. \tag{3.13}$$

Here $\mathbf{M}$ is the global mass matrix, $\mathbf{C}$ the global damping matrix, $\mathbf{R}^I$ a vector with internal forces and $\mathbf{R}^E$ a vector with external forces. (3.13) is solved stepwise and therefore $\mathbf{R}^I$ can be found by summation over the incremental steps which was used to calculate the given equilibrium state. (3.13) is a result of a discretization in space, and when it is solved a discretization in time must be applied.

3.6 Solution Methods

In SIMLA both static and dynamic analysis can be performed. In this thesis SIMLA is used in a dynamic analysis of a trawl gear and pipeline interference. Therefore the focus in this section will be on the solution method for dynamic problems. Nonlinear dynamic problems cannot be solved by modal superposition or the impulse-response method and therefore direct time integration of the equation of motion is necessary. This can be performed either by an explicit method or an implicit method.

Explicit Methods

Explicit methods can typically be expressed as (3.14), where the subscript refers to the time step. Here displacements at the next time step will be determined exclusively on information from the current time step and previous steps. Explicit methods are conditionally stable and therefore very small time steps must be used. If these methods are formulated in terms of lumped mass and lumped damping matrices it is not necessary to solve a coupled equation system in the time march [16]. This results in very small computational efforts per time step. In analysis of impulse type response it is necessary to use small time steps in order to achieve sufficient accuracy. Therefore explicit methods are typically used in explosion and impact analysis.

$$\mathbf{r}_{k+1} = f(\ddot{\mathbf{r}}_k, \dot{\mathbf{r}}_k, \mathbf{r}_k, \mathbf{r}_{k-1}, ...) \tag{3.14}$$

Implicit Methods

As expressed in (3.15) the displacements in an implicit method depend on quantities at the next time step, together with information from the current step. Since implicit methods use information at the next time step they have better numerical stability than explicit methods. The various implicit methods differ in terms of how the acceleration is assumed to vary between the time steps and at which time the equilibrium equation is fulfilled. By for instance assuming constant average acceleration between the time steps the result will be an unconditionally stable method [10]. This means that numerical stability is provided regardless of the time step size. In case of long analysis durations it is beneficial to use such methods. When implicit methods are used a coupled equation system must be solved at every time step, and hence they will become uneconomical if short time steps are unavoidable due to accuracy. In case of nonlinear systems the guarantee of unconditional stability does not hold, but in practical cases this is not considered to be an issue [10].

$$\mathbf{r}_{k+1} = f(\ddot{\mathbf{r}}_{k+1}, \ddot{\mathbf{r}}_k, \dot{\mathbf{r}}_{k+1}, \dot{\mathbf{r}}_k, \mathbf{r}_k, ...) \tag{3.15}$$

In a dynamic analysis the response of high frequency modes are usually not of interest and are described with less accuracy than the lower modes. Therefore it is desirable to remove these modes and at the same time describe the lower modes with good accuracy. It can be shown that increasing the damping ratio or introducing Rayleigh damping in the well known Newmark-β method will damp out mainly the medium modes, leaving lower and higher modes almost unaffected [12]. Higher modes can however be damped out by numerical damping. In the Newmark-β method numerical damping can be introduced at the cost of reducing the accuracy from 2$^{\text{nd}}$ order to 1$^{\text{st}}$ order. The drawback of reduced accuracy can however be eliminated by applying the implicit HHT-α method proposed by Hilbert, Hughes and Taylor. The HHT-α method will damp out high frequency modes and at the same time retain 2$^{\text{nd}}$ order accuracy [12].

3.6.1 Incremental Time Integration Scheme

In SIMLA the HHT-α method is used in the time integration scheme. Since the system equilibrium equation is nonlinear the solution is obtained by an incremental method. In the following the formulation of the incremental time integration scheme is presented. The material in this section is based on the PhD thesis of Kjell Magne Mathisen [11].

In the HHT-α method the modified global equilibrium equation for the system is given as

$$\mathbf{M}\ddot{\mathbf{r}}_{k+1} + (1+\alpha)\mathbf{C}\dot{\mathbf{r}}_{k+1} - \alpha\mathbf{C}\dot{\mathbf{r}}_k + (1+\alpha)\mathbf{R}^I_{k+1} - \alpha\mathbf{R}^I_k = (1+\alpha)\mathbf{R}^E_{k+1} - \alpha\mathbf{R}^E_k. \tag{3.16}$$

Here $\mathbf{M}$ is the mass matrix, $\mathbf{C}$ the damping matrix, $\mathbf{R}^I$ the internal force vector and $\mathbf{R}^E$ the external force vector. Subscript $k+1$ refers to the next time step and subscript k to the current time step.

The total damping matrix includes both Rayleigh damping and a diagonal damping matrix,

$$\mathbf{C} = \mathbf{C}_0 + \zeta_1\mathbf{M} + \zeta_2\mathbf{K}_T, \tag{3.17}$$

where $\mathbf{K}_T$ is the global tangent stiffness matrix.

The acceleration and velocity at time step $k+1$ are found by the same formulas as in the Newmark-β method,

$$\Delta\ddot{\mathbf{r}}_{k+1} = \ddot{\mathbf{r}}_{k+1} - \ddot{\mathbf{r}}_k = \frac{1}{\Delta t^2\beta}\Delta\mathbf{r}_{k+1} - \frac{1}{\Delta t\beta}\dot{\mathbf{r}}_k - \frac{1}{2\beta}\ddot{\mathbf{r}}_k, \tag{3.18}$$

$$\Delta\dot{\mathbf{r}}_{k+1} = \dot{\mathbf{r}}_{k+1} - \dot{\mathbf{r}}_k = \frac{\gamma}{\Delta t\beta}\Delta\mathbf{r}_{k+1} - \frac{\gamma}{\beta}\dot{\mathbf{r}}_k - \Delta t\left(\frac{\gamma}{2\beta} - 1\right)\ddot{\mathbf{r}}_k. \tag{3.19}$$

By subtracting the equilibrium equation at time step k from (3.16) the following relation can be found,

$$\hat{\mathbf{K}}_k\Delta\mathbf{r}_{k+1} = \Delta\hat{\mathbf{R}}_{k+1}. \tag{3.20}$$

Here the effective stiffness matrix $\hat{\mathbf{K}}_k$ is

$$\hat{\mathbf{K}}_k = a_0\mathbf{M} + c_0\mathbf{C} + b_0\mathbf{K}_{T,k}, \tag{3.21}$$

$$a_0 = \frac{1}{\Delta t^2\beta} + (1+\alpha)\frac{\zeta_1\gamma}{\Delta t\beta}, \tag{3.22}$$

$$c_0 = (1+\alpha)\frac{\gamma}{\Delta t\beta}, \tag{3.23}$$

$$b_0 = (1+\alpha)\left(1 + \frac{\zeta_2\gamma}{\Delta t\beta}\right). \tag{3.24}$$

The effective load increment vector,

$$\Delta\hat{\mathbf{R}}_{k+1} = (1+\alpha)[\mathbf{R}^E_{k+1} - \mathbf{R}^E_k + \mathbf{C}\mathbf{b}_k] + \mathbf{M}\mathbf{a}_k + \mathbf{R}^E_k - \mathbf{R}^I_k - \mathbf{C}_k\dot{\mathbf{r}}_k, \tag{3.25}$$

$$\mathbf{a}_k = \frac{1}{\Delta t\beta}\dot{\mathbf{r}}_k + \left(\frac{1}{2\beta} - 1\right)\ddot{\mathbf{r}}_k, \tag{3.26}$$

$$\mathbf{b}_k = \frac{\gamma}{\beta}\dot{\mathbf{r}}_k + \Delta t\left(\frac{\gamma}{2\beta} - 1\right)\dot{\mathbf{r}}_k. \tag{3.27}$$

$$\tag{3.28}$$

By solving (3.20) the displacements at time step $k+1$ are found. Thereafter accelerations and velocities are calculated by (3.18) and (3.19).

(3.25) accounts for unbalanced forces at time step k such that unbalance in (3.16) will not be accumulated. It should also be noted that the HHT-α method will coincide with the Newmark-β method if $\alpha = 0$. When the HHT-α method is formulated for a linear undamped system in free oscillations, it will be unconditionally stable for the following values of α, β and γ [12],

$$-\frac{1}{3} < \alpha < 0, \tag{3.29}$$

$$\gamma = \frac{1}{2}(1-2\alpha), \tag{3.30}$$

$$\beta = \frac{1}{4}(1-\alpha)^2. \tag{3.31}$$

3.6.2 Equilibrium Iteration Scheme

The solution obtained in the time integration scheme in Section 3.6.1 will in general not fulfill (3.16). Therefore it is necessary to perform equilibrium iterations before the time step is increased. The equilibrium iterations can be formulated as a Newton-Raphson iteration scheme. Then the governing equation is given as [20]

$$\hat{\mathbf{K}}^i_k\,\delta\mathbf{r}^{i+1}_{k+1} = (1+\alpha)[\mathbf{R}^E_{k+1} - \mathbf{R}^{I,i}_{k+1} - \mathbf{C}\dot{\mathbf{r}}^i_{k+1}] - \mathbf{M}\ddot{\mathbf{r}}^i_{k+1} - \alpha(\mathbf{R}^E_k - \mathbf{R}^I_k - \mathbf{C}\dot{\mathbf{r}}_k). \tag{3.32}$$

$\hat{\mathbf{K}}$ is the effective stiffness matrix given in (3.21). The right-hand side of (3.32) accounts for unbalance in inertia, damping and internal forces. The increment in the acceleration and velocity vectors are found through the contributing terms in (3.18) and (3.19). The updating process can hence be summarized as [20],

$$\Delta\mathbf{r}^{i+1}_{k+1} = \Delta\mathbf{r}^i_{k+1} + \delta\mathbf{r}^{i+1}_{k+1}, \tag{3.33}$$

$$\Delta\dot{\mathbf{r}}^{i+1}_{k+1} = \Delta\dot{\mathbf{r}}^i_{k+1} + \frac{\gamma}{\Delta t\beta}\,\delta\mathbf{r}^{i+1}_{k+1}, \tag{3.34}$$

$$\Delta\ddot{\mathbf{r}}^{i+1}_{k+1} = \Delta\ddot{\mathbf{r}}^i_{k+1} + \frac{1}{\Delta t^2\beta}\,\delta\mathbf{r}^{i+1}_{k+1}. \tag{3.35}$$

In addition the tangent stiffness matrix contained in $\hat{\mathbf{K}}$ should be updated after each iteration such that the convergence rate is improved. If the tangent stiffness is not updated the iteration process is called modified Newton-Raphson.

When equilibrium is achieved the right-hand side of (3.32) will vanish. The iteration algorithm is terminated by means of a vector norm when equilibrium at a given tolerance level is achieved. Such a norm can for instance be based on total displacements as given in (3.36) – (3.38) [11],

$$\left|\left|\delta \mathbf{r}_{k+1}^{i+1}\right|\right| < \epsilon_D \left|\left|\mathbf{r}_{k+1}^{i+1}\right|\right|, \tag{3.36}$$

$$\left|\left|\mathbf{r}_{k+1}^{i+1}\right|\right| = \frac{1}{N}\sqrt{\sum_{j=1}^{N}(r_j^{i+1})^2}, \tag{3.37}$$

$$\left|\left|\delta \mathbf{r}_{k+1}^{i+1}\right|\right| = \left|\left|\mathbf{r}_{k+1}^{i+1}\right|\right| - \left|\left|\mathbf{r}_{k+1}^{i}\right|\right|. \tag{3.38}$$

The accuracy of the solution is governed by the ϵ_D-parameter in (3.36). Reasonable values for the ϵ_D-parameter is usually in the order of 10^{-2} to 10^{-6} [11]. In SIMLA a predefined number of iterations will be performed, and if equilibrium is not achieved, the time step will be divided before a new trial is initiated. It is also possible to use norms in terms of energy or forces in SIMLA.

Chapter 4

DNV-RP-F111

4.1 Trawl Gear Interference

A collision between a trawl gear and a pipeline is divided into three parts in the DNV-RP-F111 code [3]. The first part is called impact calculation and focus on denting deformations of the steel wall. The impact calculation covers a time interval in the order of 10^{-1} s. The subsequent part is called the pull-over stage and covers the time interval where the trawl gear is pulled over the pipeline. For high temperature pipelines the design is often governed by the pull-over calculations. The third stage which is a rarely occurring event is called the hooking part. Here the trawl gear is assumed to get stuck beneath the pipeline such that the load level in the most extreme case will be equal to the warpline breaking strength. In this thesis the focus will be on the response during the pull-over phase.

4.2 DNV Pull-over Analysis Method

The pull-over loads in the DNV-RP-F111 code are valid when the flexibility of the potential free span is low and the pipeline diameter is between 250 mm and 1000 mm. The pipeline response during pull-over must be evaluated by means of a dynamic analysis which takes the following nonlinearities into account [3],

- Nonlinear material behaviour,
- Geometrical stiffness due to large displacements,
- Soil resistance,
- Buckling effects.

In case of buckling the pipeline model must be adequately long such that possible buckling modes can be represented. Alternatively, the boundary conditions must allow the buckled part to be exposed to potential axial feed-in. The pull-over forces from the trawl board act at a small area and are therefore applied as horizontal and vertical point loads.

4.2.1 Maximum Pull-over Loads for a Polyvalent Board

One of the objectives in this thesis was to investigate the effect of a rectangular trawl board geometry. It should be mentioned that the DNV-RP-F111 code gives no information of the pull-over loading from a rectangular trawl board. In the following the pull-over loads for a polyvalent board as given in the DNV code will be presented. The pull-over loads are expressed by means of the dimensionless parameters C_F and $\overline{H}$. As seen in (4.1) and (4.2) they are functions of purely geometrical quantities.

$$C_F = 8.0(1 - \mathrm{e}^{-0.8\overline{H}}) \tag{4.1}$$

$$\overline{H} = \frac{2h_{sp} + D_o + 0.4}{h} \tag{4.2}$$

In (4.2) the span height h_{sp} is measured as the seabed to pipeline gap, h is the trawl board height and D_o is the outer diameter of the pipeline including coating. The maximum lateral and downward force applied to the pipe is given respectively by

$$F_x = C_F V \sqrt{m_t k_w}, \tag{4.3}$$

$$F_z = F_x(0.2 + 0.8\mathrm{e}^{-2.5\overline{H}}). \tag{4.4}$$

In (4.3) the steel mass is denoted m_t, the trawling velocity as V and the stiffness of the warpline as k_w. According to the DNV code k_w can be estimated as the elastic stiffness of a straight warpline. Alternatively, a catenary-shaped warpline which include both elastic and geometric stiffness can be used to calculate k_w. This will result in a lower stiffness and is therefore less conservative.

One of the objectives in this thesis was to investigate the effect of hit angle. It can be seen from (4.1) – (4.4) that the hit angle is not explicitly taken into account in the DNV code.

The hydrodynamic mass is not present in (4.3) and (4.4). Based on the trawl board geometry it is sensible that the added mass in the lateral direction will be several times larger than the structural mass. The trawl board will have a heading angle of approximately 30° and the lateral added mass will hence give a significant contribution. Therefore it is reasonable that the hydrodynamic mass is incorporated in the C_F-coefficient.

A submerged pipeline is exposed to both external and internal pressure. Compared to an empty pipeline without external pressure the equilibrium equations will be modified. In the equilibrium equations for submerged pipelines a quantity called effective axial force will appear instead of the true axial force in the pipeline wall. The effective axial force must be accounted for and is given by (4.5) where T_e is positive in tension.

$$T_e = T_w - p_i A_i + p_e A_e \tag{4.5}$$

4.2.2 Time History of the Pull-over Force for a Polyvalent Board

The duration of the pull-over forces are given by the expression in (4.6).

$$T_p = 2 \cdot C_F \sqrt{\frac{m_t}{k_w}} + \frac{\delta_p}{V} \tag{4.6}$$

The parameter δ_p is the maximum global pipeline deflection at the point of trawl board pull-over. In advance the deflection is unknown and must be obtained by running the analysis several times and updating the value. According to DNV the response is rather insensitive to realistic values of δ_p.

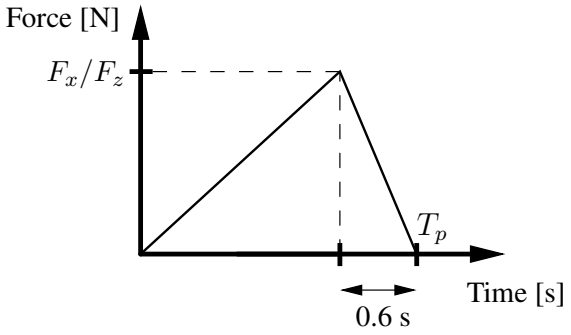

Figure 4.1: Pull-over force history [3]

For a polyvalent board the time history in Figure 4.1 applies for both the vertical and the horizontal pull-over load.

DNV-RP-F111 states that for shorter durations than 0.6 s, a rise time of 0.1 s can be used together with a fall time which is equal to the total time, but still allowing for a 0.1 s force build-up. In case of short pull-over times a sensitivity check with respect to the duration should be executed. This is especially important if the duration is equal to half the natural period of the spanning pipe.

4.3 Applied Pull-over Loading

The pull-over forces for a span height of 0 m and 1 m was determined from the trawl board and warpline data presented in Chapter 5. Thereafter several analysis runs were executed to determine the pull-over duration. The pull-over loading in Tables 4.1 and 4.2 are applied to the midnode of the SIMLA pipeline model presented in Chapter 5.

Name	**Symbol**	**Value**	**unit**
Horizontal pull-over force	F_x	47.5	kN
Downward pull-over force	F_z	30.5	kN
Pull-over duration	T_p	1.27	s

Table 4.1: Pull-over loading for 0 m span height

Name	**Symbol**	**Value**	**unit**
Horizontal pull-over force	F_x	130.9	kN
Downward pull-over force	F_z	40.1	kN
Pull-over duration	T_p	4.08	s

Table 4.2: Loading for 1 m span height, DNV-RP-F111

Chapter 5

SIMLA Model

5.1 Trawl Gear Configuration

The trawl gear configuration used in the SIMLA analyses is depicted in Figures 5.1 and 5.2. According to DNV [3] the warpline length is 2.5 to 3.5 times the water depth. The pipeline in this thesis is assumed to be located at the Skarv field where the depth is 400 m. In a report by Havforskningsinstituttet [7] from 2004 a standard codfish trawl net with two 3500 kg trawl boards were used aboard the factory trawler F/T Havstrand. The report states that this specific trawl net requires a trawl board spreading distance of 170 m when sweeplines of length 140 m are used.

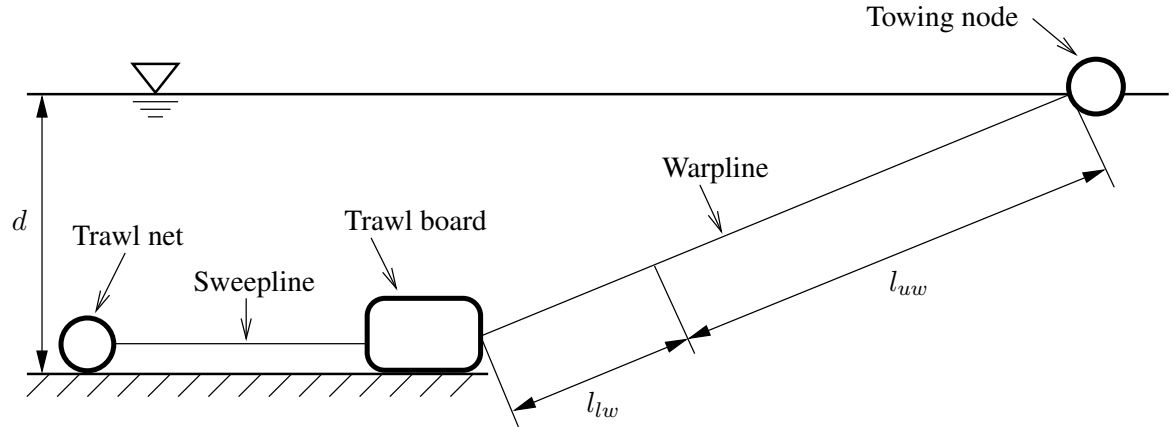

Figure 5.1: Trawl gear in the vertical plane

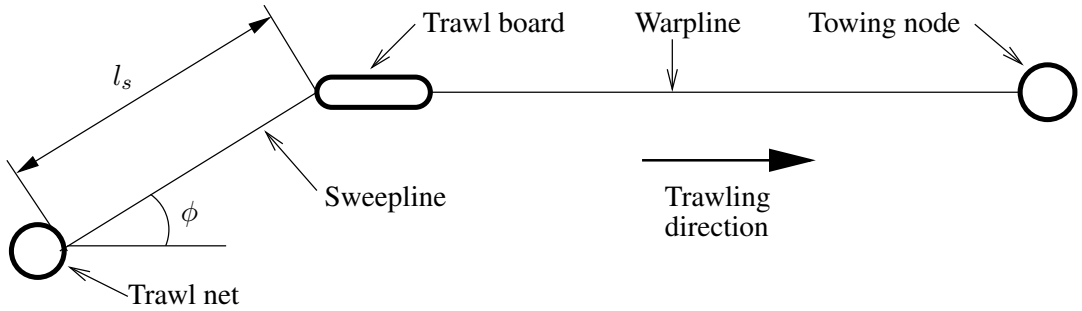

Figure 5.2: Trawl gear in the horizontal plane

The maximum trawling velocity is according to DNV [3] equal to 3.0 m/s. Resistance plots of some common trawl nets used in cod fishery can be found in a textbook of Ludvig Karlsen [9]. The trawl net resistance was estimated to 150 kN by extrapolation in these plots. The simulations in this report include only the port side trawl board and therefore a drag coefficient which corresponds to a towing resistance of 75 kN should be used.

Quantity	**Symbol**	**Value**	**Unit**
Water depth	d	400	m
Sweepline angle	ϕ	37	deg
Trawling velocity	V	3.0	m/s
Optimal trawl net drag coefficient[1]	C_D	16.2	m^2
Trawl net mass	m	0.0	kg

Table 5.1: Trawl gear data

The sweepline will be close to straight during the trawl board acceleration phase and is therefore modelled by one single cable element and a linear material. The cable element in SIMLA coincides with the bar element formulation and the sweepline can hence take compressive forces. In a realistic situation the inertia force from the trawl net will may give a slack sweepline during pipeline interference. To exclude the possibility of a compressive sweepline force the trawl net is modelled with zero mass.

Quantity	**Symbol**	**Value**	**Unit**
Length	l_s	140	m
Axial stiffness	EA	35	MN
Drag coefficient	C_D	1.0	
Added mass coefficient	C_a	1.0	
Structural mass	m	4.0	kg/m
Submerged weight	w_s	0.0	N/m

Table 5.2: Sweepline properties

The warpline is modelled as a straight cable and includes hence no contribution from the geometric stiffness. By setting the submerged warpline weight equal to zero the line will become close to straight. This configuration represents an upper bound of the warpline stiffness. According to the DNV [3] the stiffness of a straight warpline can conservatively be calculated as

$$k_w = \frac{3.5 \cdot 10^7}{l_{lw} + l_{uw}} \quad \text{N/m.} \tag{5.1}$$

During pipeline interference about 50 m of the lower warpline will be excited. The lower part is therefore modelled with realistic dynamic properties and twenty cable elements is used to capture the behaviour. The remaining 1150 m of the warpline is modelled without dynamic properties and consists of one single element such that it will function as a pure spring. A linear material model is applied for both upper and lower warpline.

[1] In SIMLA the reference area is included in the drag coefficient for body elements

Quantity	Symbol	Value	Unit
Length	l_{lw}	50	m
Axial stiffness	EA	35	MN
Drag coefficient	C_D	1.0	
Added mass coefficient	C_a	1.0	
Structural mass	m	4.8	kg/m
Submerged weight	w_s	0.0	N/m

Table 5.3: Lower warpline properties

Quantity	Symbol	Value	Unit
Length	l_{uw}	1150	m
Axial stiffness	EA	35	MN
Drag coefficient	C_D	0.0	
Added mass coefficient	C_a	0.0	
Structural mass	m	0.0	kg/m
Submerged weight	w_s	0.0	N/m

Table 5.4: Upper warpline properties

5.2 Trawl Board Models

In a realistic pipeline interference the kinetic trawl board energy will dissipate as strain energy in the steel pipeline, trawl board deformation, coating deformation, seabed frictional work and deformation of the soil [3]. In this report the amount of strain energy related to the trawl board is assumed to be neglectable. The pipe elements which define the contact geometry of the board are therefore modelled with a very high bending stiffness and a linear material. In Section 5.8 these elements are referred to as slave elements when they interact with the pipeline. It should be noted that the trawl board thickness is not represented since the pipe elements have a diameter of 20 mm and are located in the same plane.

5.2.1 Polyvalent Trawl Board

The model of the polyvalent trawl board in Figure 5.3 consists of a flat pate part and a heavy ski at the edge which rests on the seafloor. An important purpose of the ski is to lower the centre of gravity such that the lateral stability is improved. This stability effect is included by setting the total mass of the ski elements equal to 900 kg. The mass of the flat plate part is for simplicity assumed to be located at the origin in Figure 5.3 and is set equal to 3600 kg. The warpline is attached 665 mm in front of the origin in Figure 5.3 and the sweepline is attached at the aft end.

5.2.2 Rectangular Trawl Board

The trawl board in Figure 5.4 was used to study the effect of a more rectangular trawl board geometry. Compared to the polyvalent board it is reasonable that the elongated ski and modified front will give a different location of the centre of gravity. This has been neglected in order to isolate the effect of an alternative geometry. In addition the sweepline and warpline connection points are located at the

same positions and the hydrodynamic coefficients are chosen to be identical for the two boards. The rectangular board has therefore the same dynamic properties as the polyvalent board.

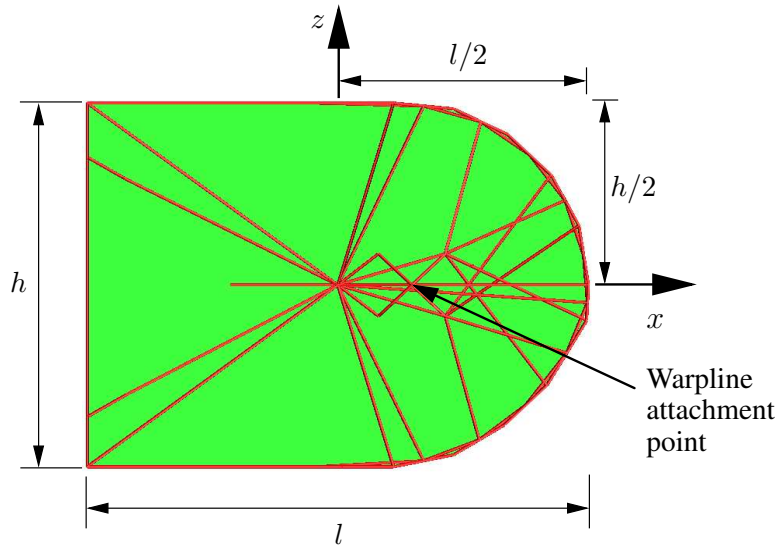

Figure 5.3: Polyvalent trawl board model

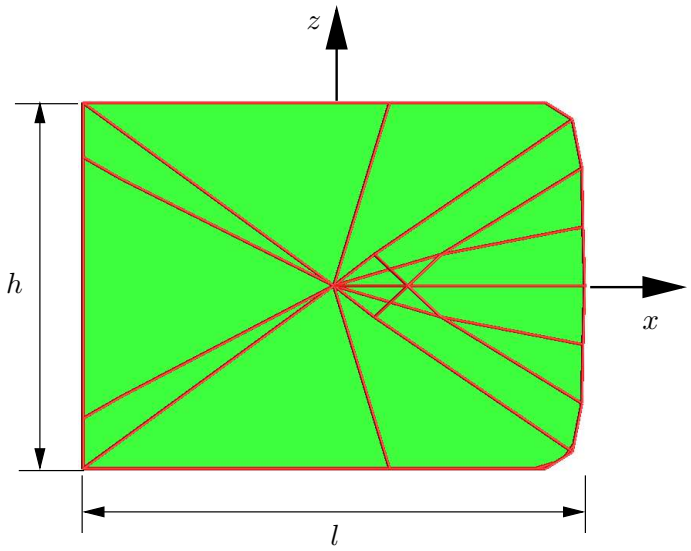

Figure 5.4: Rectangular trawl board model

Quantity	**Symbol**	**Value**	**Unit**
Mass of trawl board plate	m_p	3600	kg
Mass of trawl board ski	m_s	900	kg
Submerged weight	w_s	33.5	kN
Length	l	4.5	m
Height	h	3.5	m
Thickness[2]	t	0.4	m

Table 5.5: Trawl board data

5.3 The Standard Hydrodynamic Load Model

The hydrodynamic load model used in the majority of the simulations includes diagonal hydrodynamic mass, diagonal quadratic damping and excitation for all 6 degrees of freedom. In the surge, sway and heave degrees of freedom a Froude-Krylov excitation term is included. The expression for the Froude-Krylov term is valid when the body is wetted on all surfaces and small such that the undisturbed fluid acceleration is approximately constant over the body volume. The hydrodynamic load model in (5.2) is given on the same format as the one implemented in SIMLA. In Section 5.4 estimates of the matrix entries in (5.2) are presented.

$$
\begin{bmatrix}
m+\rho m_{a11} & & & & & \\
0 & m+\rho m_{a22} & & & \text{SYM.} & \\
0 & 0 & m+\rho m_{a33} & & & \\
0 & 0 & 0 & m_{44}+\rho m_{a44} & & \\
0 & 0 & 0 & 0 & m_{55}+\rho m_{a55} & \\
0 & 0 & 0 & 0 & 0 & m_{66}+\rho m_{a66}
\end{bmatrix}
\begin{bmatrix} \ddot{u}_x \\ \ddot{u}_y \\ \ddot{u}_z \\ \ddot{\theta}_x \\ \ddot{\theta}_y \\ \ddot{\theta}_z \end{bmatrix} =
$$

$$
\frac{1}{2}\rho
\begin{bmatrix}
C_{11} & & & & & \\
0 & C_{22} & & & \text{SYM.} & \\
0 & 0 & C_{33} & & & \\
0 & 0 & 0 & C_{44} & & \\
0 & 0 & 0 & 0 & C_{55} & \\
0 & 0 & 0 & 0 & 0 & C_{66}
\end{bmatrix}
\begin{bmatrix}
|\dot{w}_x-\dot{u}_x|(\dot{w}_x-\dot{u}_x) \\
|\dot{w}_y-\dot{u}_y|(\dot{w}_y-\dot{u}_y) \\
|\dot{w}_z-\dot{u}_z|(\dot{w}_z-\dot{u}_z) \\
|\dot{\theta}_x|\dot{\theta}_x \\
|\dot{\theta}_y|\dot{\theta}_y \\
|\dot{\theta}_z|\dot{\theta}_z
\end{bmatrix}
+\rho\nabla
\begin{bmatrix} \ddot{w}_x \\ \ddot{w}_y \\ \ddot{w}_z \\ 0 \\ 0 \\ 0 \end{bmatrix}
\tag{5.2}
$$

In (5.2) the water particle displacements are denoted w_x, w_y and w_z. With reference to Figure 5.5 the body motions along the x-axis, y-axis and z-axis are denoted respectively u_x, u_y and u_z. The rotational motions about the same axes are denoted respectively θ_x, θ_y and θ_z. (5.2) refers to a body-fixed coordinate system which is located at the centre of gravity because no coupling entries related to structural mass are present. Strictly speaking it is also assumed that the coordinate system orientation coincide with the principal axes because the mass product of inertia entries are set equal to zero. The hydrodynamic inertia coefficients are denoted m_{aii} and coupling entries cannot be given as input by the user. This implies that the hydrodynamic center is assumed to be located at the centre of gravity. Viscous effects are included by the diagonal drag coefficients which are denoted C_{ii}.

5.4 Estimation of Trawl Board Dynamic Properties

A simplified approach for estimation of the hydrodynamic coefficients in (5.2) will be described in this section. The two main assumptions in the simplified approach is that the polyvalent board can be modelled as a rectangular flat plate and that principles of slender-body hydrodynamic theory can be used. The latter assumption is however not fulfilled since the flow will be 3-dimensional around the trawl board. The 2-dimensional flow assumption would have been reasonable if the length was much larger than the height in Figure 5.5. Even though the slender-body approximation does not hold it must be accepted such that simple estimates can be obtained.

[2]The thickness is not represented in the SIMLA model

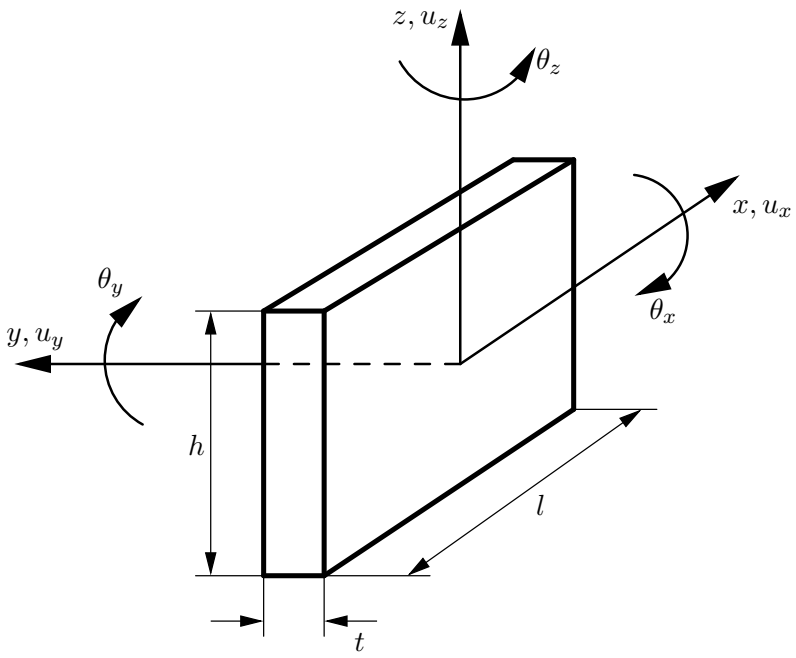

Figure 5.5: Hydrodynamic model of trawl board

The hydrodynamic inertia coefficients are derived one by one of force and moment considerations when the trawl board has forced oscillations in the six degrees of freedom. The surge, sway and heave drag coefficients are found by assuming a stationary trawl board velocity in the relevant degree of freedom. Very uncertain estimates are obtained for the rotational drag coefficients because a 2-dimensional approach based on considerations of the transverse and in-plane forces of a plate is used. It should also be noted that the effect of lift is not taken into account in the drag coefficients.

In the sway degree of freedom the added mass of a flat plate and the drag coefficient for a 90° inclined plate in a stationary current are utilized. These coefficients are given in the DNV-RP-H103 code [4]. Here the 3-dimensional flow effects are taken into account and the plate is assumed to be located in an infinite fluid, i.e. an evident seabed to trawl board gap must be present. The sway hydrodynamic coefficients can then be expressed as

$$m_{a22} = C_a l h^2 \qquad C_a = 0.51, \tag{5.3}$$

$$C_{22} = C_D l h \qquad C_D = 1.16. \tag{5.4}$$

When the trawl board has a forced yaw motion the flow is assumed to be 2-dimensional in planes which are perpendicular to the longitudinal axis, i.e. the yz-planes in Figure 5.5. With this assumption the yaw added moment of inertia can be found by considerations of the 2-dimensional sway added mass forces. The forced yaw acceleration will result in a local sway acceleration along the trawl board which introduces local sway added mass forces that in turn will induce a yaw moment. The 2-dimensional sway added mass will not be constant along the trawl board, but for simplicity this is neglected and it is found by dividing the sway added mass in (5.3) by the trawl board length. By integration of moment contributions from the local sway forces the yaw added moment of inertia becomes

$$m_{a66} = \frac{1}{12} m_{a22} l^2. \tag{5.5}$$

The yaw drag coefficient can be estimated by considerations of the local sway velocity induced by the yaw motion. By assuming that the flow is 2-dimensional in the yz-planes in Figure 5.5, the yaw

moment can be found by integration of the sectional drag forces multiplied by the torque arm along the longitudinal axis. In that case a reasonable 2-dimensional sway drag coefficient must be determined as a function of longitudinal position. The longitudinal dependency is for simplicity neglected and a constant sectional drag coefficient along the whole length is used instead. The drag coefficient for the sections located close to the origin in Figure 5.5 will not give a large contribution to the yaw moment because the torque arm and sway velocity is small here. Contrary, the sections located at the aft and front will give a large contribution to the yaw moment, and hence flow conditions at these locations should be emphasized when the constant sectional drag coefficient is determined. According to DNV-RP-H103 [4] the drag coefficient for an infinitely long plate is 1.9 and if the aspect ratio is equal to 1.0 the drag coefficient will be 1.16. The latter coefficient takes the 3-dimensional effects of four plate edges into account and is thus believed to give a more reasonable estimate for the trawl board. It must be emphasized that this drag coefficient gives no information about the pressure distribution, but it can be used to predict the upper bound of the sectional drag coefficient at the ends. Since the approach described here introduces large uncertainties it was however decided to use a sectional drag coefficient of 1.5. This will give a yaw drag coefficient which can be expressed as

$$C_{66} = \frac{1}{32} C_d h l^4 \qquad C_D = 1.5. \tag{5.6}$$

The roll drag coefficient is calculated by the same considerations used in the previous paragraph. For this case the flow is assumed to be 2-dimensional in the xy-planes in Figure 5.5. The 2-dimensional flow assumption will be even more violated for the roll degree of freedom than in the yaw degree of freedom, but in order to obtain simple estimates this must be accepted. The roll added moment of inertia can be found from the 2-dimensional added moment for a rectangular box in DNV-RP-H103 [4] with edges corresponding to the trawl board height and thickness, i.e. the flow is assumed to be 2-dimensional in the yz-planes in Figure 5.5. With these assumptions the roll hydrodynamic coefficients become

$$C_{44} = \frac{1}{32} C_D l h^4 \qquad C_D = 1.5, \tag{5.7}$$

$$m_{a44} = C_a h^4 l \qquad C_a = 0.0289. \tag{5.8}$$

In the surge degree of freedom the drag coefficient is estimated by a formula used for resistance prediction of foil-shaped bodies. This formula assumes that skin friction is the dominant resistance component while the viscous pressure resistance is accounted for by a form factor which depends on the thickness and body length in the flow direction [13]. The formula is given as

$$R_D = 0.075 \rho h l \frac{\left(1 + 2\frac{t}{l}\right)}{\left[log(R_e) - 2\right]^2} V^2 \qquad R_e = \frac{Vl}{\nu}. \tag{5.9}$$

The Reynolds number which corresponds to a trawling velocity of 3 m/s is used when the surge drag coefficient is estimated. (5.9) can also be used to predict the heave drag coefficient, but the trawl board is less streamlined in the vertical direction and the heave velocity will be much smaller than 3 m/s during pipeline interference. The heave drag coefficient is expected to be small and for simplicity it is set equal to the surge drag coefficient. With this assumption the surge and yaw drag coefficients become

$$C_{11} = C_D l h \qquad C_D = 0.0072, \tag{5.10}$$

$$C_{33} = C_D l h \qquad C_D = 0.0072. \tag{5.11}$$

The added mass in heave and surge is determined by the 2-dimensional added mass for a rectangular box found in the DNV-RP-H103 code [4]. This approach gives a poor approximation for the surge added

mass since the trawlboard height is smaller than the length. The added mass coefficients can then be written as

$$m_{a11} = C_a t^2 h \qquad C_a = 1.77, \tag{5.12}$$

$$m_{a33} = C_a t^2 l \qquad C_a = 1.72. \tag{5.13}$$

In the pitch degree of freedom the hydrodynamic coefficients are estimated by the same approach which was used for the yaw coefficients. Now it is assumed that the 2-dimensional heave added mass and damping force can be found by dividing the heave coefficients given (5.11) and (5.13) by the trawl board length. It should be noted that the surge forces are neglected due to the over-simplified estimation approach. Thereafter the moment induced by the 2-dimensional heave forces is found by integration in the longitudinal direction. This approach results in the following estimates,

$$m_{a55} = \frac{1}{12} m_{a33} l^2, \tag{5.14}$$

$$C_{55} = \frac{1}{32} C_D h l^4 \qquad C_D = 0.0072. \tag{5.15}$$

The trawl board is modelled as a flat plate with a heavy steel ski mounted at the edge which rests on the seafloor. Only the flat plate part is represented by the SIMLA body element and hence the ski mass must not be included when the mass moments of inertia are calculated. The mass of the steel plate, m_p, is equal to 3600 kg and since it is thin and has a nearly uniform mass distribution the mass moments of inertia are calculated by the following formulas,

$$m_{44} = \frac{1}{12} m_p h^2, \tag{5.16}$$

$$m_{55} = \frac{1}{12} m_p (h^2 + l^2), \tag{5.17}$$

$$m_{66} = \frac{1}{12} m_p l^2. \tag{5.18}$$

Several shortcomings are included in the simplified estimations given in this section. The effect of forward speed will induce a lift force in the sway degree of freedom which was not taken into account. For a high-aspect foil the lift force will attack about one quarter length from the leading edge and a yaw moment will therefore arise. Since the trawl board slides along the seabed an unsymmetric vertical pressure distribution will appear and a roll moment is induced as well. The moments related to lift effects are not included in the estimates given in Table 5.6 simply because the hydrodynamic load model in Section 5.3 cannot handle moments related to forward speed. The sway lift force can however be included, but since it depends strongly on the yaw angle it is convenient to exclude it. This may be accepted since the lift force will be reduced when forward velocity and body orientation changes abruptly [13]. Such an abrupt change must be expected to occur when the trawl board collides with the pipeline. It should also be noted that 2-dimensional slender-body theory was used to estimate coefficients for cases where the flow conditions in reality will be 3-dimensional.

One of the objectives in this thesis was to investigate the effect of increasing added mass due to seabed proximity. This effect can be understood by considerations of a submerged body which accelerates close to a wall. The dynamic pressure around the body will change due to the wall proximity and compared to the infinite fluid case the added mass will increase. The hydrodynamic inertia coefficients given in Table 5.6 should therefore be multiplied by a correction factor to include the effect of seabed proximity. In Section 5.5 an advanced hydrodynamic load model which takes the seabed proximity effect into account is presented. From the coefficients used in this load model it can be observed that

Quantity	Symbol	Value	Unit
Roll mass moment of inertia	m_{44}	3675	kgm^2
Pitch mass moment of inertia	m_{55}	9750	kgm^2
Yaw mass moment of inertia	m_{66}	6075	kgm^2
Surge added mass coefficient	m_{a11}	0.99	m^3
Sway added mass coefficient	m_{a22}	28.10	m^3
Heave added mass coefficient	m_{a33}	1.24	m^3
Roll added moment of inertia coefficient	m_{a44}	19.50	m^5
Pitch added moment of inertia coefficient	m_{a55}	2.09	m^5
Yaw added moment of inertia coefficient	m_{a66}	47.40	m^5
Surge drag coefficient	C_{11}	0.11	m^2
Sway drag coefficient	C_{22}	18.30	m^2
Heave drag coefficient	C_{33}	0.11	m^2
Roll drag coefficient	C_{44}	31.70	m^5
Pitch drag coefficient	C_{55}	0.32	m^5
Yaw drag coefficient	C_{66}	67.30	m^5

Table 5.6: Dynamic properties of the trawl board

the hydrodynamic inertia coefficients depend on the roll angle and the trawl board to seabed gap[3]. The correction factors are found as the ratio of the hydrodynamic inertia coefficients at 0.1 m seabed gap and at 5.25 m seabed gap for a roll angle of 10°, i.e. it is assumed that a 5.25 m seabed gap represents the infinite fluid case. The goodness of this assumption can be evaluated by the coefficients at seabed gaps of 1.75 m and 5.25 m. For these gaps the maximum relative increase of the hydrodynamic inertia coefficients is equal to 1.6 % and occurs in the sway degree of freedom. Therefore it is reasonable that a seabed gap of 5.25 m represents the infinite fluid case. The hydrodynamic inertia coefficients which take the seabed proximity into account are given in Table 5.7.

Degree of Freedom	Symbol	Value	unit	Relative increase
Surge	$\hat{m}_{a11}$	1.04	m^3	1.05
Sway	$\hat{m}_{a22}$	30.90	m^3	1.10
Heave	$\hat{m}_{a33}$	1.47	m^3	1.18
Roll	$\hat{m}_{a44}$	20.70	m^5	1.06
Pitch	$\hat{m}_{a55}$	2.28	m^5	1.09
Yaw	$\hat{m}_{a66}$	48.80	m^5	1.03

Table 5.7: Seabed proximity hydrodynamic inertia coefficients

[3]The hydrodynamic inertia coefficients are not tabulated in this thesis due to restrictions imposed by Statoil

5.5 The Advanced Hydrodynamic Load Model

The main advantage of the advanced hydrodynamic load model given in (5.19) is that effects related to forward speed and seabed proximity can be described more consistently. In the following only differences from the standard hydrodynamic load model in Section 5.3 will be described.

$$
\begin{bmatrix}
m+\rho m_{a11} & & & & & \\
0 & m+\rho m_{a22} & & & \text{SYM.} & \\
0 & 0 & m+\rho m_{a33} & & & \\
0 & 0 & 0 & m_{44}+\rho m_{a44} & & \\
0 & 0 & 0 & 0 & m_{55}+\rho m_{a55} & \\
0 & 0 & 0 & 0 & 0 & m_{66}+\rho m_{a66}
\end{bmatrix}
\begin{bmatrix} \ddot{u}_x \\ \ddot{u}_y \\ \ddot{u}_z \\ \ddot{\theta}_x \\ \ddot{\theta}_y \\ \ddot{\theta}_z \end{bmatrix} +
$$

$$
\rho
\begin{bmatrix}
0 & & & & & \\
0 & 0 & & & \text{SYM.} & \\
0 & 0 & 0 & & & \\
0 & -z_M m_{a22} & y_M m_{a33} & y_M^2 m_{a33}+z_M^2 m_{a22} & & \\
z_M m_{a11} & 0 & -x_M m_{a33} & -x_M y_M m_{a33} & x_M^2 m_{a33}+z_M^2 m_{a11} & \\
-y_M m_{a11} & x_M m_{a33} & 0 & -x_M z_M m_{a22} & -y_M z_M m_{a11} & x_M^2 m_{a22}+y_M^2 m_{a11}
\end{bmatrix}
\begin{bmatrix} \ddot{u}_x \\ \ddot{u}_y \\ \ddot{u}_z \\ \ddot{\theta}_x \\ \ddot{\theta}_y \\ \ddot{\theta}_z \end{bmatrix}
$$

$$
= \frac{1}{2}\rho
\begin{bmatrix}
\tilde{C}_{11} \\
\tilde{C}_{22} \\
\tilde{C}_{33} \\
\tilde{C}_{44}+y_D\tilde{C}_{33}-z_D\tilde{C}_{22} \\
\tilde{C}_{55}+z_D\tilde{C}_{11}-x_D\tilde{C}_{33} \\
\tilde{C}_{66}+x_D\tilde{C}_{22}-y_D\tilde{C}_{11}
\end{bmatrix}
V_R^2 + \frac{1}{2}\rho
\begin{bmatrix}
C_{11}|\dot{w}_x-\dot{u}_x|(\dot{w}_x-\dot{u}_x) \\
C_{22}|\dot{w}_y-\dot{u}_y|(\dot{w}_y-\dot{u}_y) \\
C_{33}|\dot{w}_z-\dot{u}_z|(\dot{w}_z-\dot{u}_z) \\
C_{44}|\dot{\theta}_x|\dot{\theta}_x \\
C_{55}|\dot{\theta}_y|\dot{\theta}_y \\
C_{66}|\dot{\theta}_z|\dot{\theta}_z
\end{bmatrix}
+ \rho\nabla
\begin{bmatrix} \ddot{w}_x \\ \ddot{w}_y \\ \ddot{w}_z \\ 0 \\ 0 \\ 0 \end{bmatrix}
\qquad
\begin{matrix} m_{aii} = m_{aii}(\Delta,\Phi,\Psi) \\ \tilde{C}_{ii} = \tilde{C}_{ii}(\Delta,\Phi,\Psi) \end{matrix}
\tag{5.19}
$$

(5.19) refers to a coordinate system which is located at the centre of gravity. The position where the hydrodynamic mass matrix becomes diagonal is called hydrodynamic center and is located at (x_M, y_M, z_M). The $\tilde{C}_{ii}$-coefficients refers to the drag center which is located at (x_D, y_D, z_D). It should be noted that the input hydrodynamic inertia coefficients in (5.19) must refer to the hydrodynamic center. The hydrodynamic center will have a small offset relative to the centre of gravity when the seabed gap is close to zero. This offset was neglected by Statoil who calculated the coefficients. In all simulations the hydrodynamic center and the drag center are positioned at the centre of gravity, i.e. matrix number two and the offset moment contributions in the drag vector which contains the $\tilde{C}_{ii}$-coefficients will vanish.

Seabed proximity is taken into account by expressing the hydrodynamic inertia and drag coefficients as a function of Δ, Φ and Ψ. Here Δ denotes the trawl board to seabed gap, Φ is the roll angle and Ψ is the heading angle illustrated in Figure 5.6. The seabed gap is measured as the minimum seabed distance from the trawl board ski. The hydrodynamic inertia and drag coefficients are given as input by the user at several data points in terms of Δ, Φ and Ψ. Thereafter interpolation is performed by SIMLA such that the coefficients are described on intervals between the user-defined data points. The hydrodynamic coefficients applied in the simulations cannot be tabulated in this thesis due to restrictions imposed by Statoil. Only general features of the hydrodynamic coefficients will therefore be described in the following. To ease the understanding of this paragraph a set of censored coefficients are included in Appendix A with identical data points compared to the one used in the simulations.

The hydrodynamic inertia coefficients which were used in connection with (5.19) are based on calculations performed by Statoil for two different trawl board aspect ratios. The coefficients which are valid

for the aspect ratio in this thesis was calculated by linear interpolation. The interpolation introduces neglectable uncertainties since one of the original aspect ratios were close to the aspect ratio used in the simulations. It should also be mentioned that the coefficents experience only a slight increase due to seabed proximity and that they are independent of the heading angle.

The effect of forward speed is included by the vector which contains the $\tilde{C}_{ii}$-coefficients in (5.19). In the SIMLA code these drag coefficients are multiplied with the relative velocity such that a possible current velocity is included, see Figure 5.6. The drag coefficients should be established by a model test which measure the forces and moments in terms of Δ, Φ and Ψ in a body-fixed coordinate system. In this thesis the applied drag coefficients were received from Statoil who had performed a model test of a trawl board in a steady current of 0.6 m/s. The length of the board was 0.79 m and the height was 0.6 m. The essential assumption in the model test is that the dimensionless drag coefficients are independent of the Reynolds number, i.e. they are identical in model- and full-scale. A full-scale velocity of 3.0 m/s gives a Reynolds number which is about 20 times larger than the one used in the model test. According to a textbook in foil theory [1] both drag and maximum lift force of a wing section will depend on the Reynolds number. If the model trawl board can be simplified to a flat plate it should be noted that the model-scale Reynolds number correspond to the transition regime between laminar and turbulent flow [14]. Therefore it must be expected that the full-scale coefficients might deviate somewhat from the true ones. It should also be mentioned that the aspect ratio of the boards presented in Section 5.2 are equal to 0.78, while the model trawl board had an aspect ratio of 0.76.

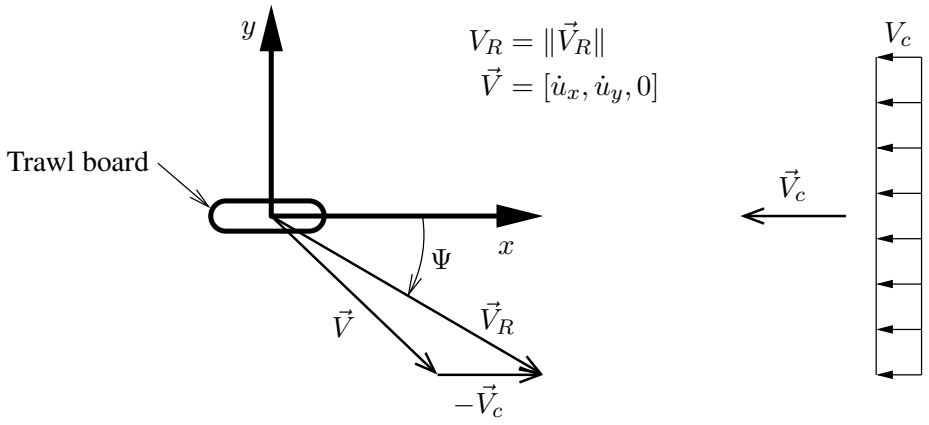

Figure 5.6: Definition of relative velocity and heading angle

Since the $\tilde{C}_{ii}$-coefficients are established from a model test with constant current velocity they are strictly speaking only valid for a stationary trawl board motion. It is known from foil theory that the lift force will decrease when the forward velocity or the orientation of the foil changes abruptly [13]. There is no doubt that there to some extent will be a transient flow around the trawl board when it collides into the pipeline. Therefore it can be questionable to claim that the $\tilde{C}_{ii}$-coefficients completely represent the drag forces and moments during pipeline interference.

In Section 5.4 the C_{11}- and C_{22}-coefficients were estimated one at a time by assuming a stationary velocity in the relevant degree of freedom. These coefficients must be set equal to zero in (5.19) because their contributions are included by the corresponding $\tilde{C}_{ii}$-coefficients. The same argument cannot be used when it comes to the other C_{ii}-coefficients. The rotational drag coefficients were however estimated on questionable assumptions and they should therefore be used with caution. In order to avoid uncertainties related to the rotational C_{ii}-coefficents they are simply set equal to zero when the advanced hydrodynamic load model is used. The C_{33}-coefficient was poorly estimated and is also set equal to zero.

5.6 The Pipeline Model

The modelled pipeline has a total length of 420 m and is assumed to be restrained against horizontal displacements at the end nodes due to rock dumping. The pull-over forces result in significant displacements for approximately 60 m of the midpart. In order to reduce the computational effort, element lengths of 1.0 m are used for the part of the pipeline which remains at rest and element lengths of 0.33 m for the part that moves.

The coating diameter is set equal to 429.5 mm and is conservatively assumed to give no stiffness contribution. Elastoplastic pipe elements are used to model the steel part of the pipeline which has a diameter of 255.1 mm. The stress-strain curve obeys the kinematic hardening feature and has a smooth transition from the onset of yield and into the plastic range where a fairly constant tangent modulus is applied. The effective axial force is assumed to be -220 kN in all elements of the modelled pipeline. This is obtained by using a fictitious temperature load which together with seabed friction adjust the axial force to the correct magnitude. Relevant properties of the pipeline are given in Table 5.8.

Quantity	**Symbol**	**Value**	**unit**
Coating diameter	D_o	429.5	mm
Mean steel diameter	D_m	255.1	mm
Wall thickness steel pipe	t_w	18	mm
Structural mass	m	170	kg/m
Submerged weight	w	579	N/m
Length of pipeline model	L	420	m
Drag coefficient	C_D	1.0	
Added mass coefficient at seabed	C_a	2.29	
Added mass coefficient at free span	C_a	1.12	
Rayleigh damping mass factor	ζ_1	0.0	s^{-1}
Rayleigh damping stiffness factor	ζ_2	0.05	s
Length of free span	l_{fs}	20	m
Height of free span	h_{sp}	1.0	m
Internal pressure	p_i	11.3	MPa
Effective axial force	T_e	-220	kN
Offset yield strength	$\sigma_{0.2}$	408	MPa
Young's modulus	E	210	GPa
Mean tangent modulus	E_T	1.0	GPa
Hardening parameter	κ	1.0	

Table 5.8: Pipeline properties

One of the objectives in this thesis was to investigate the effect of oblique trawl board crossings. In this connection analysis models for hit angles of $-20°$, $-10°$, $0°$ $10°$, $20°$ and $30°$ were established. In Figure 5.7 the positive direction of the hit angle ψ is defined.

At the midpoint of the modelled pipeline a free span is included, see Figure 5.7. The length of the free span is measured in the direction of the pipeline and is set equal to 20 m. Simulations were executed for two different span heights, 0 m and 1 m. The height is measured as the seabed to pipeline gap after the static loads are applied, i.e. in case of 0 m span height the whole pipeline rests on the seabed.

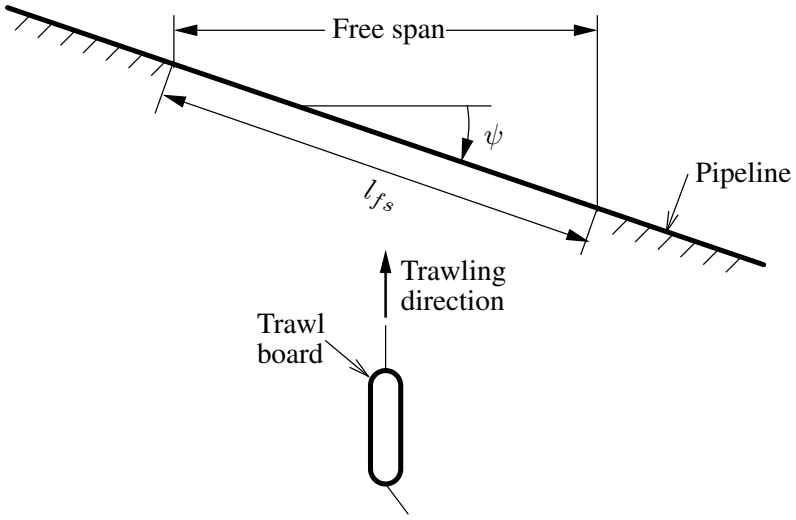

Figure 5.7: Pipeline midsection in the horizontal plane

5.7 Seabed Interaction

5.7.1 Pipeline

The modelled seafloor is completely flat at all positions along the pipeline. Interaction with the seafloor is taken care of by seabed contact elements which are attached to all nodal points of the pipeline. In the vertical direction the contact force is defined by a force-displacement curve which has a constant steep slope as depicted in Figure 5.10, i.e. stiff linear springs are attached vertically to the pipeline.

The frictional forces due to displacements in the horizontal plane are taken care of by user-specified curves of a unit horizontal force per unit contact length. Thereafter the curves are scaled in SIMLA by a coulomb friction factor times the product of the vertical distributed reaction force and the actual contact length. The horizontal interaction curves in Figures 5.8, 5.9 and 5.11 are based on data from the Master thesis of Martin Møller [15] where similar pull-over simulations were performed. The coulomb friction factors which scale these curves are all set equal to 1.0. The additional lateral interaction curve in Figure 5.9 is included to describe the soil resistance before pipeline outbreak correctly and is not scaled by the coulomb factor and the vertical contact force.

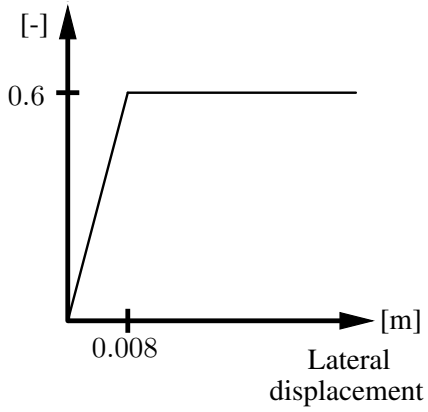

Figure 5.8: Seabed lateral interaction curve

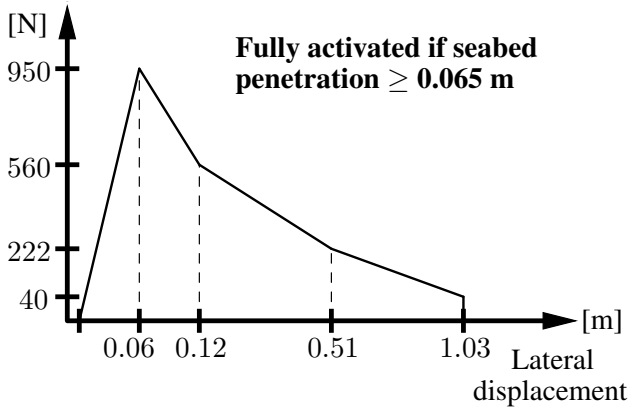

Figure 5.9: Additional lateral interaction curve

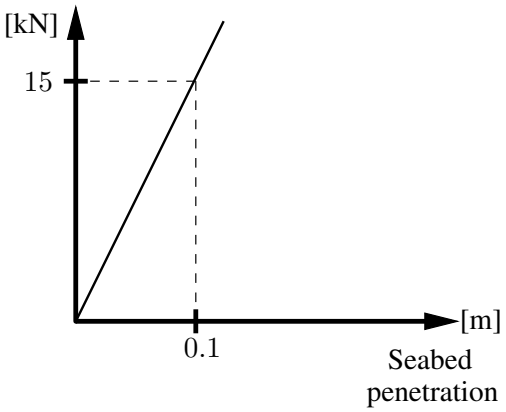

Figure 5.10: Seabed vertical interaction curve

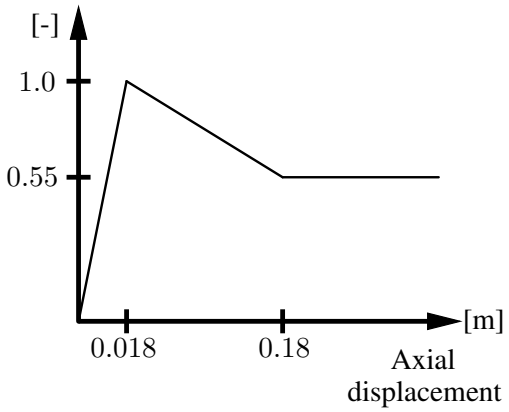

Figure 5.11: Seabed axial interaction curve

5.7.2 Trawl Board

The trawl board has six seabed contact elements attached to nodes at the four corners, the midpoint and in the front. With this contact element configuration it is possible for the trawl board to lay flat on the seabed. Contact forces in the vertical direction are described by the seabed interaction curve in Figure 5.10. The horizontal seabed interaction curves caused problems during the acceleration phase of the trawl board and they were therefore deactivated. This deactivation will result in a decrease of the warpline tension. In a real situation the seabed will not be completely flat and the trawl board will thus bounce up and down during the trawling process. In addition the seabed proximity will result in an upward pressure-induced force which also reduces the seabed frictional force in the towing direction. Based on these arguments it is reasonable that a realistic pull-over simulation can be obtained without seabed frictional forces on the trawl board.

5.8 Trawl Board and Pipeline Interaction

During pipeline interference the forces from the trawl board are transferred to the pipeline via rigid master elements which are attached to the midnode of the free span. The number of master elements is governed by the number of slave element groups on the trawl board which are expected to obtain contact with the pipeline. All master elements have the geometry of a roller with a diameter equal to 429.5 mm and a length of 9 m, see Figure 5.12. The minimal distance between the master rollers and the slave elements on the trawl board is calculated at every equilibrium iteration. Contact is defined to occur when the minimal distance becomes negative [17]. It should also be mentioned that bending moments are transferred to the pipeline if the trawl board slave elements have an axial offset relative to the midnode. In a real situation there will not be transferred any bending moments during pipeline interference. The acceptable offset distance in the simulations is therefore taken to be such that the sampled shear forces at each side of the midnode are approximately equal.

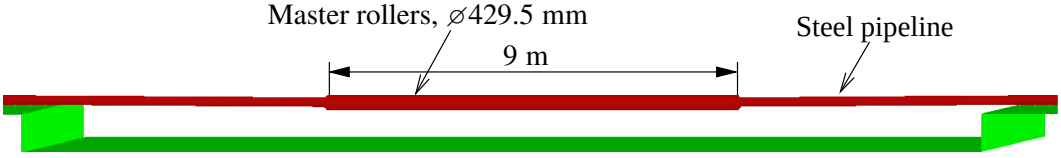

Figure 5.12: Master rollers attached to midnode

As depicted in Figure 5.13 the master rollers are assigned a constant normal stiffness. In order to obtain reasonable pull-over simulations it was necessary to modify the roller normal stiffness stepwise during interference as mentioned in Chapter 6. In this connection the upper and lower bound of the applied roller material curves are depicted in Figure 5.13. The axial and circumferential interaction curves are given in Figure 5.14 and assumes that the frictional forces will gradually increase if the trawl board slides along the pipeline. The curve in Figure 5.14 is scaled in SIMLA by the contact force and a user-defined friction coefficient which was set equal to 0.2.

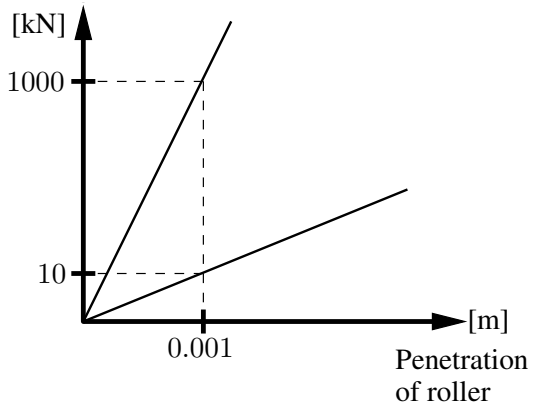

Figure 5.13: Material curve of master roller (1)

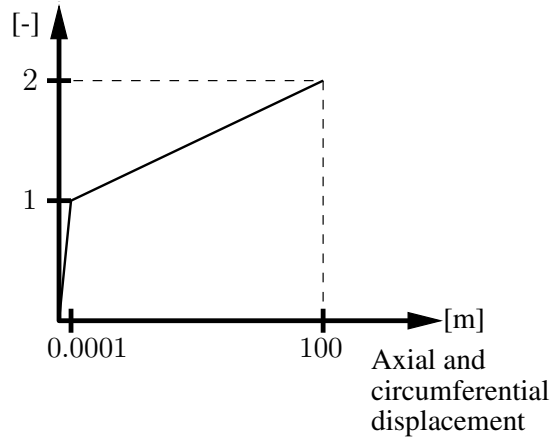

Figure 5.14: Material curve of master roller (2)

5.9 Estimation of Contact Damping

The concentrated damping of the contact elements are estimated by considerations of the local eigenfrequency. In connection with pipeline and trawl board interaction the added mass which contributes to the local eigenfrequency is found by decomposing the acceleration in the trawling direction into the trawl board coordinate system. Here the pipeline inertia is neglected and the trawl board angle of attack is set equal to 30°. With these assumptions the master rollers at the pipeline are assigned a damping constant equal to

$$c_c = 2\lambda \left[(m_s + m_p + \rho m_{a11} \cos^2 \theta_z + \rho m_{a33} \sin^2 \theta_z) k_c \right]^{\frac{1}{2}} . \qquad \begin{matrix} \theta_z \approx 30 \text{ deg} \\ \lambda \approx 0.05 \end{matrix} \tag{5.20}$$

In (5.20) the damping ratio is denoted λ and is set equal to 0.05. The contact stiffness is denoted k_c and is found from the material curve in Figure 5.13. Based on data from Tables 5.5 and 5.6 the contributing trawl board mass is approximately 12500 kg. The damping is chosen to be identical in all simulations.

The damping of the seabed contact elements located at the trawl board and the pipeline is found by the same principles as outlined above. Here the stiffness is found from the seabed vertical interaction curve in Figure 5.10 and the relevant mass is lumped to the nodes where the seabed contact elements are attached.

5.10 Pull-over Convergence Test

As explained in Section 5.8 the pull-over force is transferred from the master contact element via the midnode and into the pipeline. In SIMLA there is no simple way to measure this force and therefore the vertical and horizontal shear force at the two nodes next to the midspan node must be sampled instead. The pull-over force can then be calculated as the sum of the shear force at these nodes corrected for pipeline inertia and damping forces. If the element length is sufficiently short the inertia and drag forces can conveniently be neglected.

By executing a convergence test with respect to the shear forces the element length which gives neglectable contributions from the pipeline inertia and drag forces can be determined. Since the trawl board pull-over forces were unknown in advance, the DNV-RP-F111 [3] pull-over forces for a span height of 1 m have been applied in the convergence test. According to Section 4.3 the downward pull-over force is 40.1 kN and the horizontal force is 130.9 kN for a span height of 1 m. The pull-over forces are combined with the load factor time history shown in Figure 5.15 which is very conservative compared to the one recommended by DNV in Section 4.2.2. To isolate the pipeline inertia and drag force contributions the convergence test was executed without structural and numerical damping.

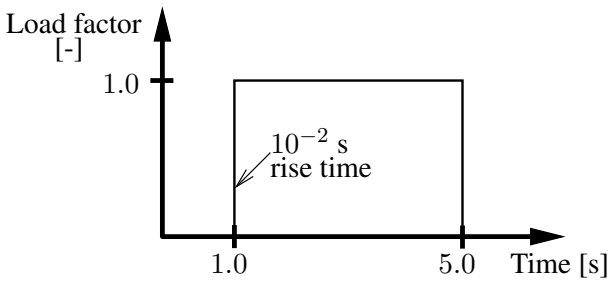

Figure 5.15: Load factor in the convergence test

Maximum horizontal shear force was observed to occur after 1.11 s. The horizontal acceleration of the midnode at this time instant was 13.6 m/s^2 while the nodal velocity had a value of 3.0 m/s. Thus a significant contribution from both inertia and drag forces were included. Convergence in terms of pipeline displacement was achieved for an element length of 0.5 m. According to Table 5.9 an element length of 0.33 m gives only a deviation of 1.1 kN from the applied horizontal pull-over force. Since the pull-over loading was conservatively selected it can be concluded that the pipeline double shear force at midspan can be set approximately equal to the pull-over force when an element length of 0.33 m is applied[4].

Element length [m]	**Double horizontal shear force [kN]**	**Double vertical shear force [kN]**
1.00	127.7	39.5
0.50	129.1	40.0
0.33	129.8	40.0
0.25	130.0	40.0

Table 5.9: Maximum pipeline shear forces at midspan

[4]The axial force will also contribute to the horizontal equilibrium. This is not taken into account, see Chapter 6 for further details.

5.11 Description of the Simulations

At analysis start the distance between the pipeline and the trawl board is 60 m. The static loads which consists of gravity, temperature load, internal pressure and external pressure are applied during the first second of the simulation in static mode. When the static load factors have approached unit values the analysis switches into dynamic mode and the trawl board boundary conditions are released. A constant acceleration of 0.2 m/s^2 is applied at the towing node in Figure 5.1 until the velocity reaches 3.0 m/s. Thereafter the board travels with constant velocity in further 15 s such that transient rotations are damped out. In this connection artificially large drag coefficients are applied in the roll and yaw degrees of freedom to reduce the damping time. About 6-7 s before pipeline interference most of the transient motion is damped out and the real drag coefficients are applied. To obtain an appropriate number of equilibrium iterations it was necessary to use time steps of 10^{-1} s before pipeline interference when the standard hydrodynamic load model was applied. Time steps of 10^{-2} s were needed in the advanced hydrodynamic load model due to the interpolation scheme for the hydrodynamic coefficients.

The optimal trawl net drag coefficient in Table 5.1 resulted in a significant lateral velocity. To obtain zero lateral velocity it was necessary to reduce the trawl net resistance with approximately 50 %. The mean yaw angle is from experience known to be approximately 30° at normal operation conditions. This angle was calibrated by the offset of the sweepline connection point in Figure 5.16 which is denoted d. To obtain a yaw angle of 30° the offset in the negative sway direction was set equal to 300 mm when the standard hydrodynamic load model was used, while the offset was 500 mm for the advanced hydrodynamic load model. The mean roll angle was adjusted by the offset of the warpline attachment point relative to the trawl board surface. Here an offset of 100 mm in the positive sway direction gave a mean roll angle of $-6°$ for the standard hydrodynamic model, while a mean roll angle of $-22°$ appeared when the advanced hydrodynamic load model was used.

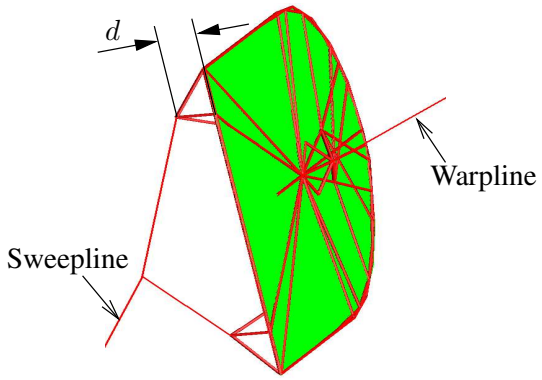

Figure 5.16: Sweepline connection points

The applied drag coefficients in the advanced hydrodynamic load model are only valid for roll angles up to $-20°$. When the original coefficients were used the mean yaw angle was approximately $-40°$. The input format of the roll drag coefficients was therefore modified such that the mean yaw angle before interference became equal to $-22°$, see Appendix A. It should also be mentioned that the roll angle did not exceed $-20°$ during pipeline interference.

The selected time steps during pipeline interference should be able to represent the local period by about 15 points. The local period was found from the contributing trawl board mass in (5.20) and the contact element stiffness given in Figure 5.13. Based on the local period and some test runs in SIMLA it was seen that time steps of 10^{-3} s gave a reasonable number of equilibrium iterations.

The convergence criteria used in the equilibrium iterations was based on an energy norm and the recommended tolerance in the SIMLA user manual of 10^{-5} was applied. Numerical damping was included in the time integration scheme with an α-parameter of -0.05. The tangent stiffness matrices in the elasto-plastic pipeline elements were calculated by a 16-point numerical integration over the cross-section. A consistent mass representation was selected for all structural elements.

Quantity	**Symbol**	**Value**	**Unit**
Trawling velocity	V	3.0	m/s
Mean yaw angle	$\overline{\theta}_z$	30	deg
Mean roll angle, std. hydro model	$\overline{\theta}_x$	-6	deg
Mean roll angle, adv. hydro model	$\overline{\theta}_x$	-22	deg
Trawl net drag coefficient, std. hydro model	C_D	7.7	m^2
Trawl net drag coefficient, adv. hydro model	C_D	9.0	m^2
Numerical damping factor	α	-0.05	
Energy convergence tolerance	ϵ_E	10^{-5}	

Table 5.10: Simulation data

Chapter 6

Results

This chapter contains all results from the trawl board simulations and the DNV-RP-F111 analysis. The results are supplemented with comments and in specific cases the observed trawl board behaviour is also described. Amendments which have been made to the trawl board models in Section 5.2 will also be mentioned. It should be noted that screenshots of a limited number of simulations are presented in Appendix D.

The horizontal displacement time histories in this chapter refer to the midnode of the free span. The horizontal pull-over force refers to the local pipe element coordinate system, while the output horizontal displacement in SIMLA refers to a global coordinate system. In the analyses with varying hit angle these coordinate systems will not coincide. To obtain coherence all horizontal pipeline displacements in this chapter have therefore been transformed to the local pipe element coordinate system, i.e. the horizontal displacement refers to the direction which is perpendicular to the pipeline.

The vertical pull-over forces in this chapter are defined to be positive upwards. It was seen that the vertical pipeline displacements were small in all simulations and they are therefore not included in the following sections. It can however be mentioned that maximum seabed penetration at the midnode was 40 mm for the simulation cases where the whole pipeline model rests on the seabed.

As explained in Section 5.10 the horizontal and vertical pull-over forces must be found from the pipeline shear forces. In the DNV-RP-F111 analysis for a span height of 1 m the maximum horizontal pull-over force is 123.3 kN while the applied load is 130.9 kN, see Figure 6.38. This discrepancy can be explained by the effective axial force which is equal to 754 kN at the instant of maximum applied horizontal pull-over force. On basis of the global rotation at the shear force sampling nodes the axial force contributes with 7 kN in the direction of the applied horizontal pull-over load. The axial force contribution was first realised after completion of all simulations. In order to correct for the axial force contribution it would have been necessary to repeat every single simulation. Due to a large time-consumption in many of the simulations this option was rejected. This can be justified since the axial force contribution is of approximately the same magnitude in the simulations which are of interest to compare against each other.

For comparison purposes the impulse of the pull-over loading is also presented in this chapter. The impulse is based on the resultant of the sampled pull-over forces and is given by

$$I = \int_0^{T_p} \sqrt{\hat{F}_x^2 + \hat{F}_z^2}\, \mathrm{d}t. \tag{6.1}$$

6.1 Polyvalent Trawl Board

The objective in these simulations was to investigate the effect of hit angle for increasing trawl board added mass. In total six different hit angles which varied from $-20°$ to $30°$ were examined. In Figure 5.7 the positive direction of the hit angle ψ is defined. The simulations can be divided into two parts in terms of the trawl board added mass properties. In the first part the added mass properties are based on an infinite fluid assumption, while in the second part the increase due to seabed proximity is taken into account. The applied hydrodynamic inertia coefficients are given in Tables 5.6 and 5.7. The trawl board is represented by the standard hydrodynamic load model and the polyvalent board in Figure 5.3.

6.1.1 Span Height of 0 m

In these analyses the trawl board ski slides over the pipeline at the end of pull-over. Due to the sliding behaviour it was very difficult to avoid pipeline penetration with subsequent spurious behaviour of both board and pipeline. Violent peaks in the vertical force time history emerged when the master element normal stiffness was increased. The violent peaks can be related to the high vertical stiffness which was applied for the seabed contact elements. In order to avoid unphysical peaks in the time histories it was decided to accept partial pipeline penetration and use an unnatural low master element stiffness. The low master stiffness was applied when the trawl board slides over the pipeline as shown in Figure 6.1 and is not believed to influence the results significantly. Some minor peaks in the pull-over force time histories occurred at the end of the pull-over even when the stiffness was set unnatural low. It should be mentioned that the lower bound stiffness in Figure 5.13 was applied at the beginning of contact.

Contact problems related to an insufficient description of the trawl board geometry occurred in all simulations. Typically pipeline contact was lost and thereafter violent peaks emerged in the pull-over force time history when contact was restored. The problem was solved by increasing the number of elements in the lower part of the trawl board front. This is further explained in Appendix C.

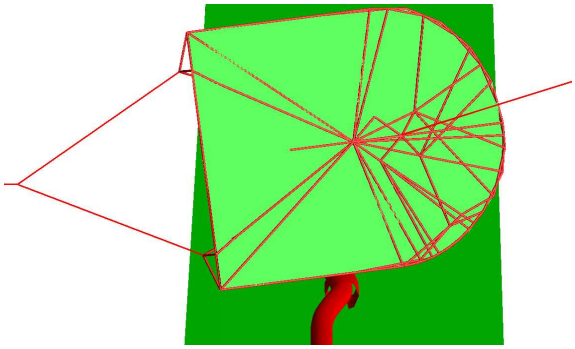

Figure 6.1: Trawl board sliding on pipeline

According to the horizontal pull-over forces in Figures 6.2 – 6.5 there is no effect of increased trawl board added mass. Here it should be noted that the hit angles of $10°$, $20°$ and $30°$ give a horizontal pull-over force which is 5-10 kN larger than what the other hit angles predict.

The vertical pull-over forces in Figures 6.6 – 6.9 indicate no effect from increased trawl board added mass. The case with $30°$ hit angle has a vertical pull-over force which is about 30 % lower than the other hit angles. This is related to the trawl board sliding motion along the pipeline which causes a reduced vertical contact force component.

Figures 6.10 and 6.11 clearly indicate that the horizontal displacements depend on the hit angle. There is no significant effect from the increase of trawl board added mass. In the case with 30° hit angle the horizontal displacement is twice as large compared to the other simulations. This can be explained from the vertical pull-over force in Figures 6.8 and 6.9 which is 30 % lower than the other cases and gives thus a reduced seabed frictional force. In addition the horizontal force peak at beginning of contact in Figures 6.4 and 6.5 is somewhat wider for the 30° case.

It can also be observed that the hit angles of $-10°$ and $-20°$ results in very small horizontal displacements. The longitudinal trawl board axis was almost perpendicular to the pipeline for these hit angles. In combination with the circular-shaped front the board slid over the pipeline rather than pushing it away as for the other hit angles.

As mentioned above the trawl board ski was allowed to penetrate the pipeline at the end of pull-over. Even with this approach some peaks are present in the time histories of the pull-over loading. The impulses in Tables 6.1 and 6.2 should therefore not be used to assess the simulations.

ψ **[deg]**	**Impulse [kNs]**
30	41.8
20	36.5
10	34.3
0	33.5
-10	28.1
-20	26.4

Table 6.1: Impulse of pull-over load, infinite fluid added mass

ψ **[deg]**	**Impulse [kNs]**
-20	36.9
30	35.8
-10	33.5
0	33.3
10	32.0
20	25.0

Table 6.2: Impulse of pull-over load, seabed added mass

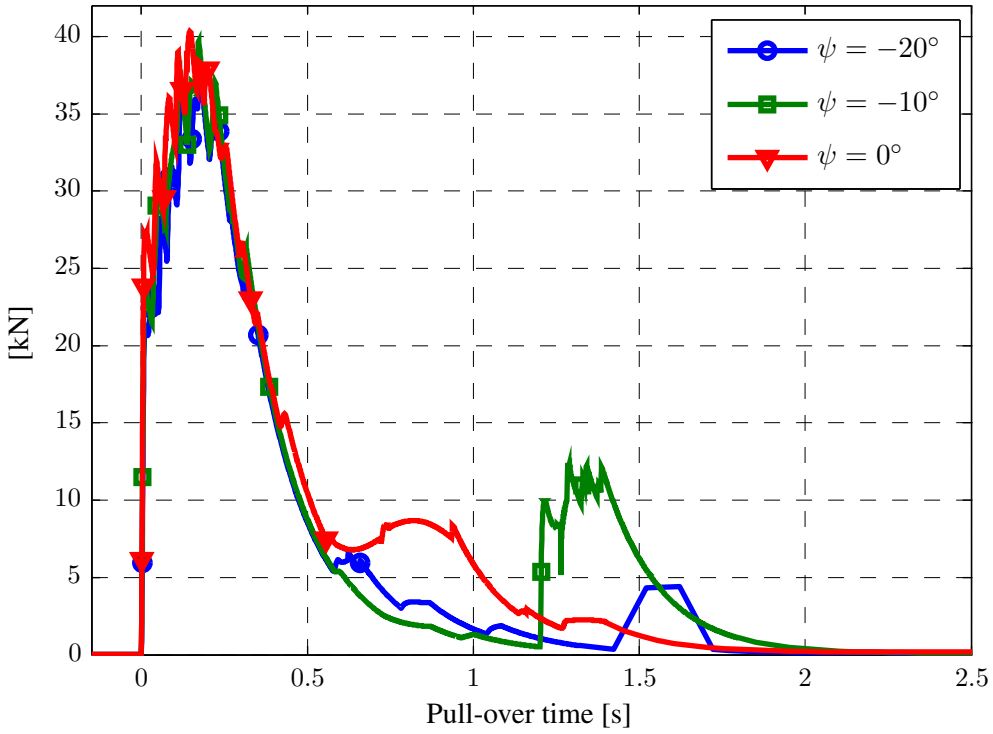

Figure 6.2: Horizontal pull-over force, infinite fluid added mass

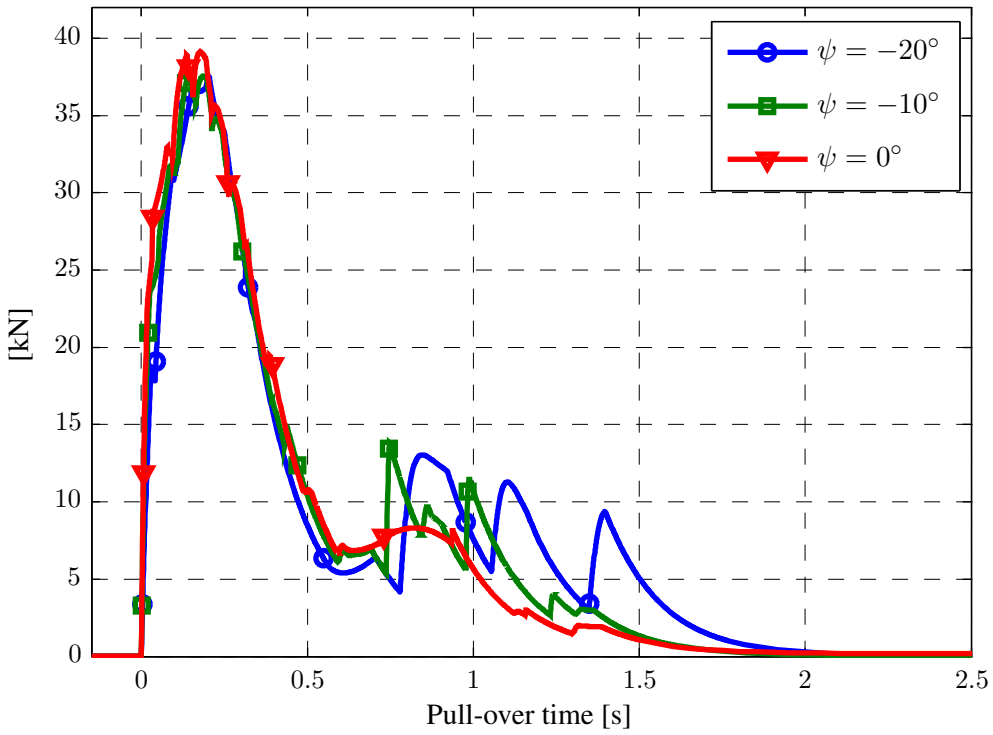

Figure 6.3: Horizontal pull-over force, seabed added mass

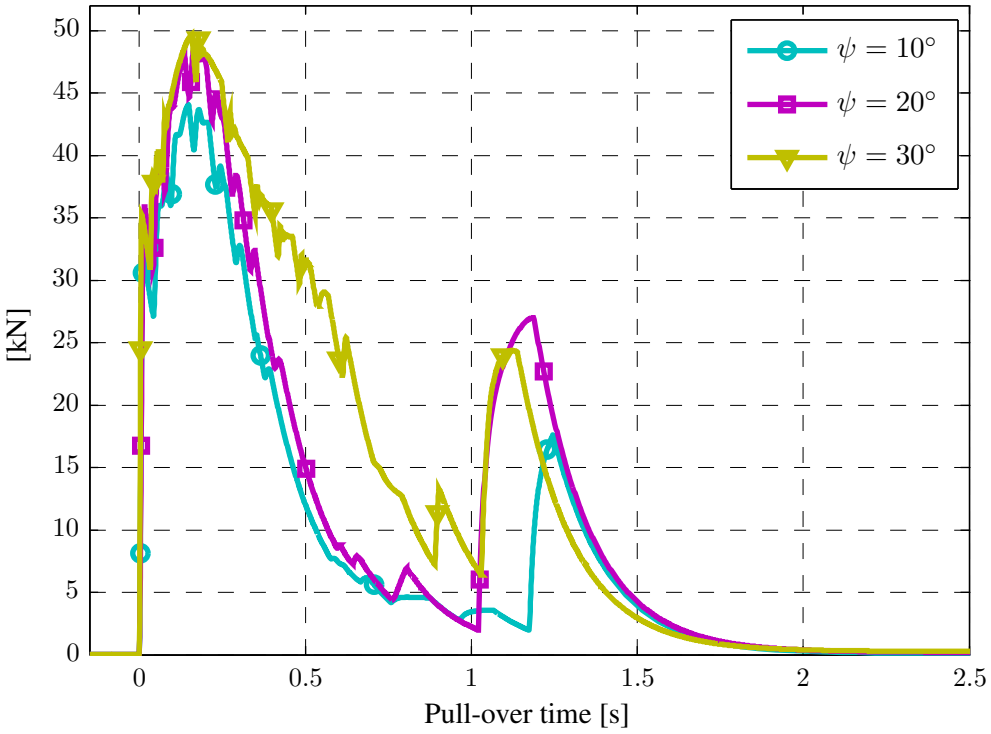

Figure 6.4: Horizontal pull-over force, infinite fluid added mass

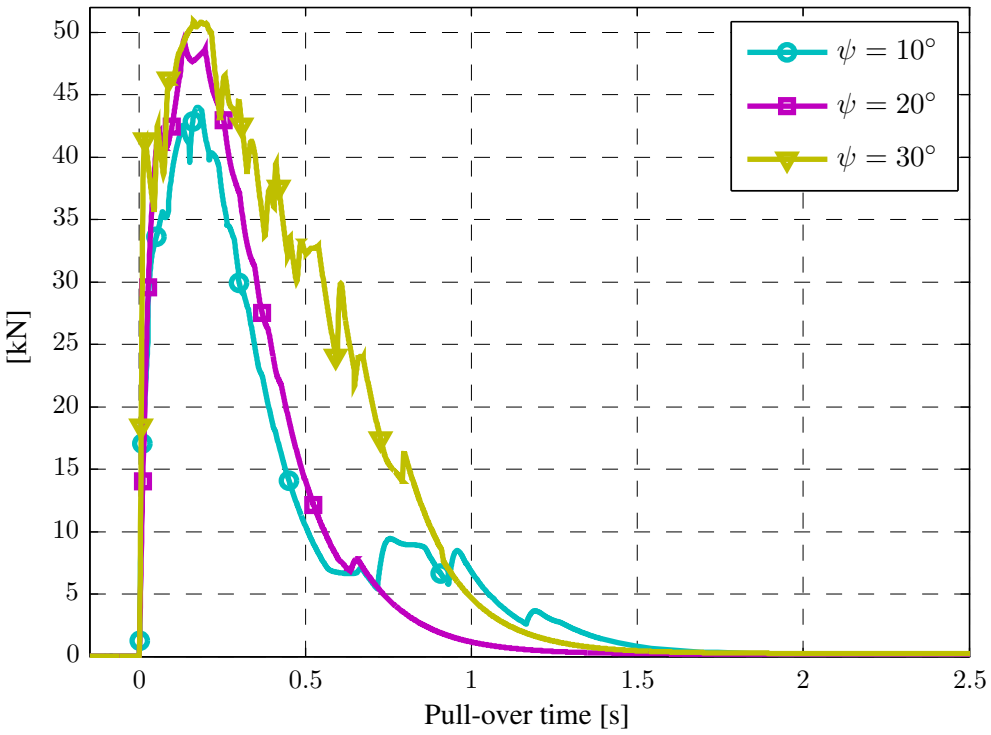

Figure 6.5: Horizontal pull-over force, seabed added mass

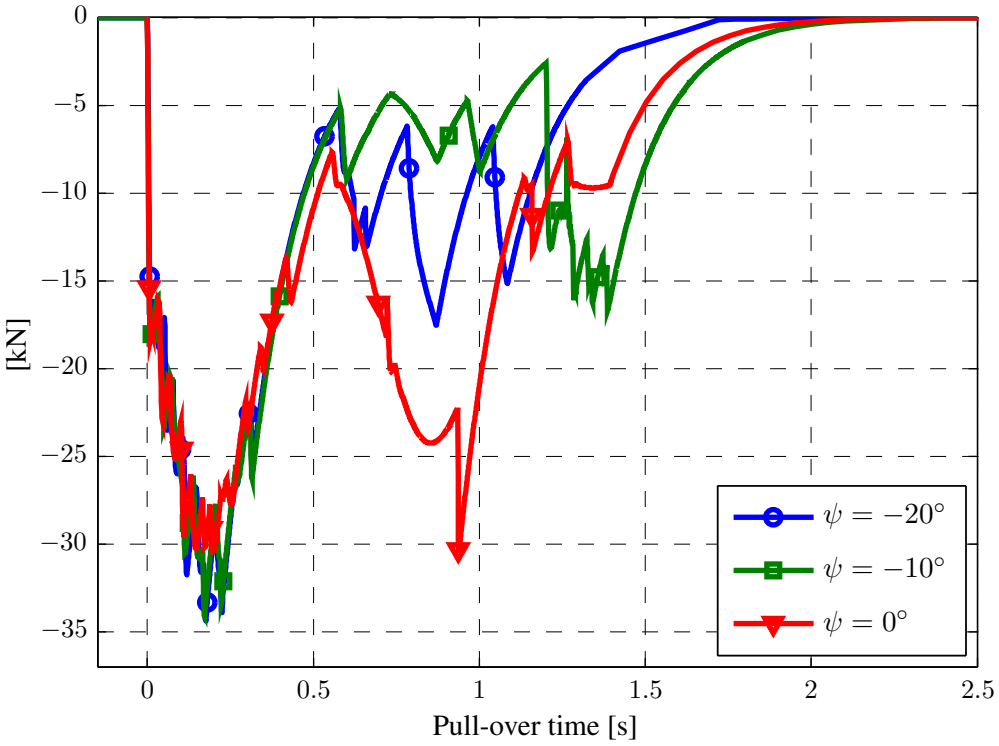

Figure 6.6: Vertical pull-over force, infinite fluid added mass

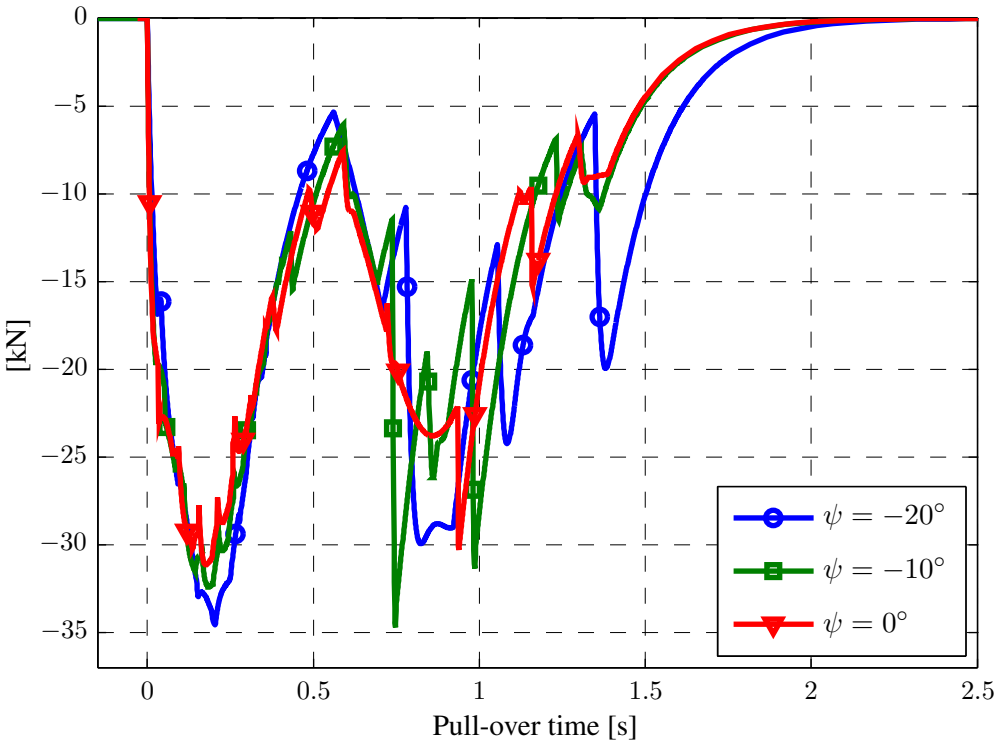

Figure 6.7: Vertical pull-over force, seabed added mass

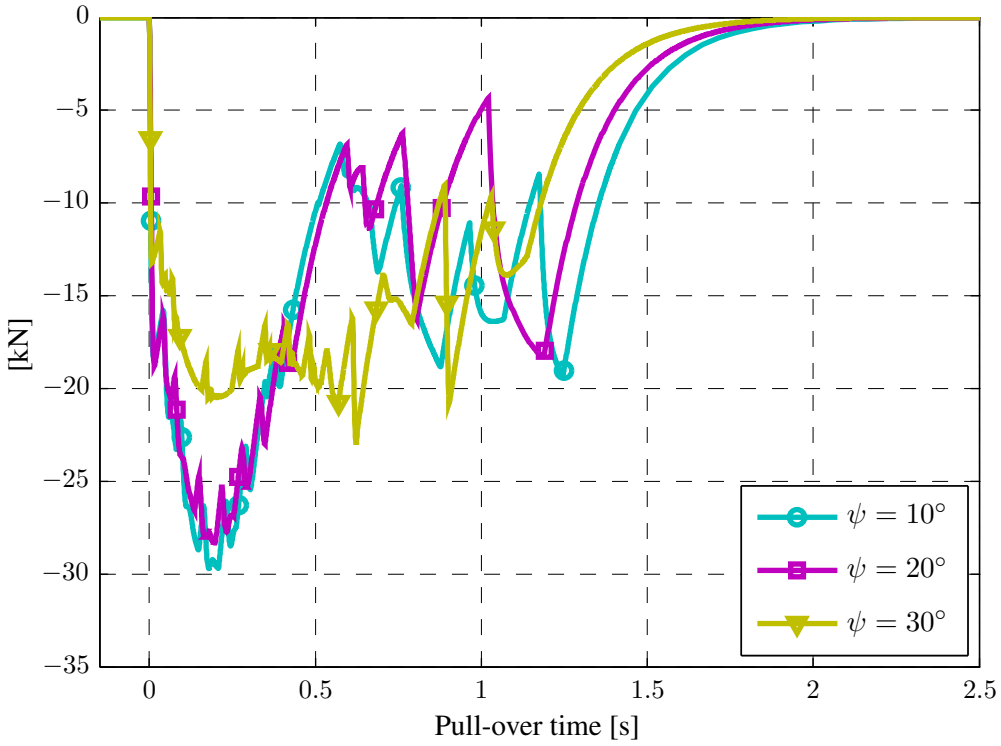

Figure 6.8: Vertical pull-over force, infinite fluid added mass

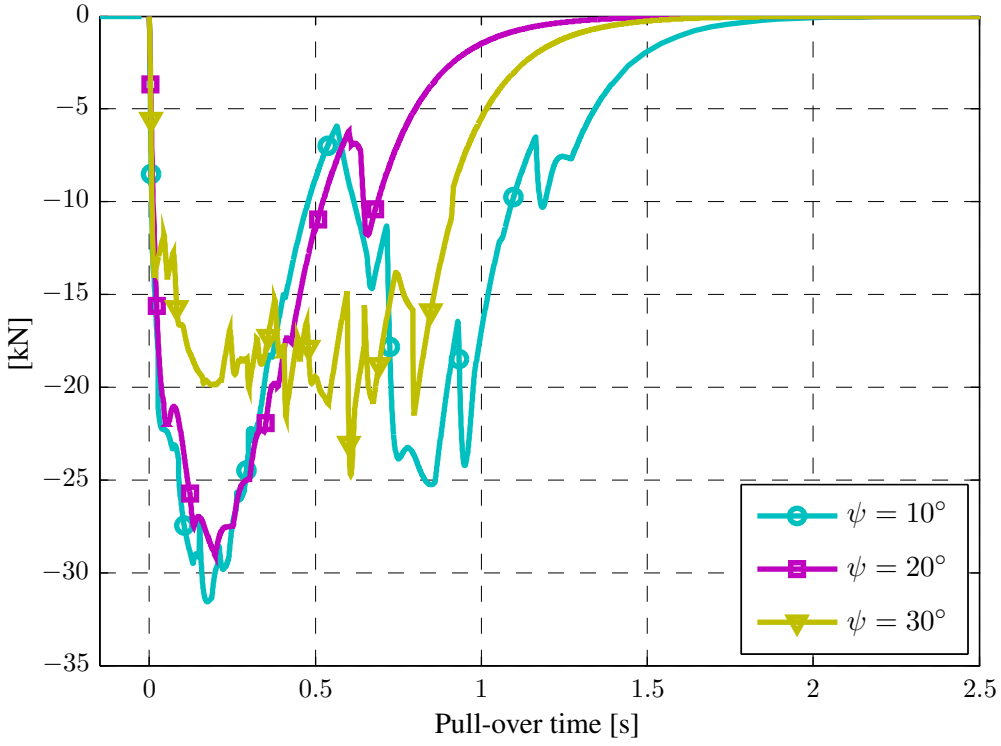

Figure 6.9: Vertical pull-over force, seabed added mass

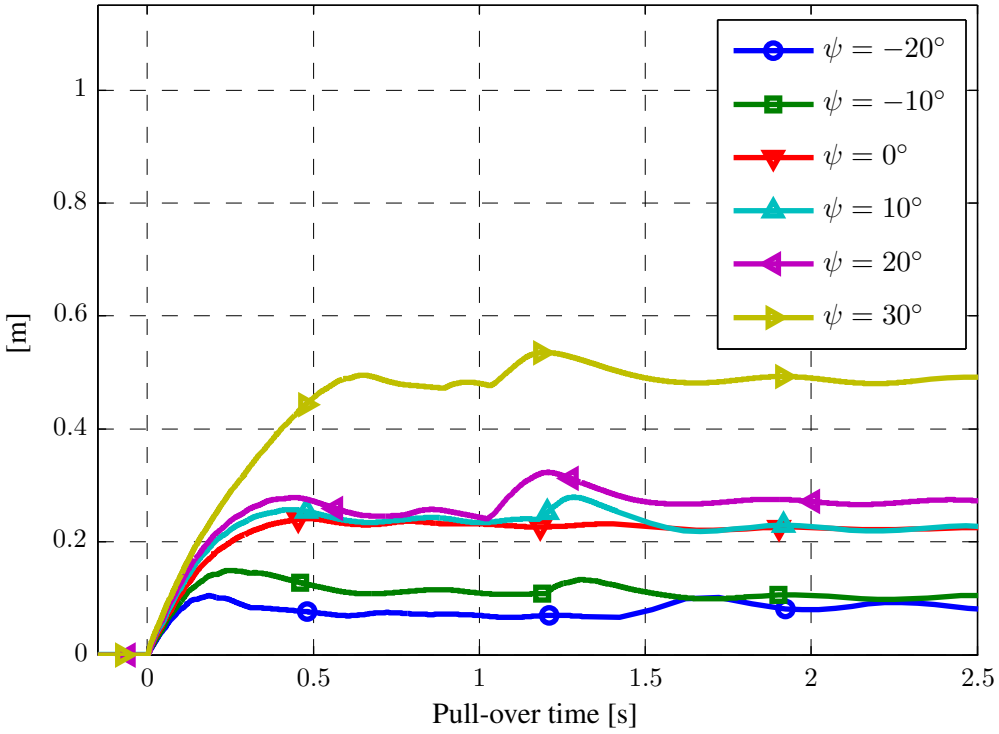

Figure 6.10: Horizontal displacement, infinite fluid added mass

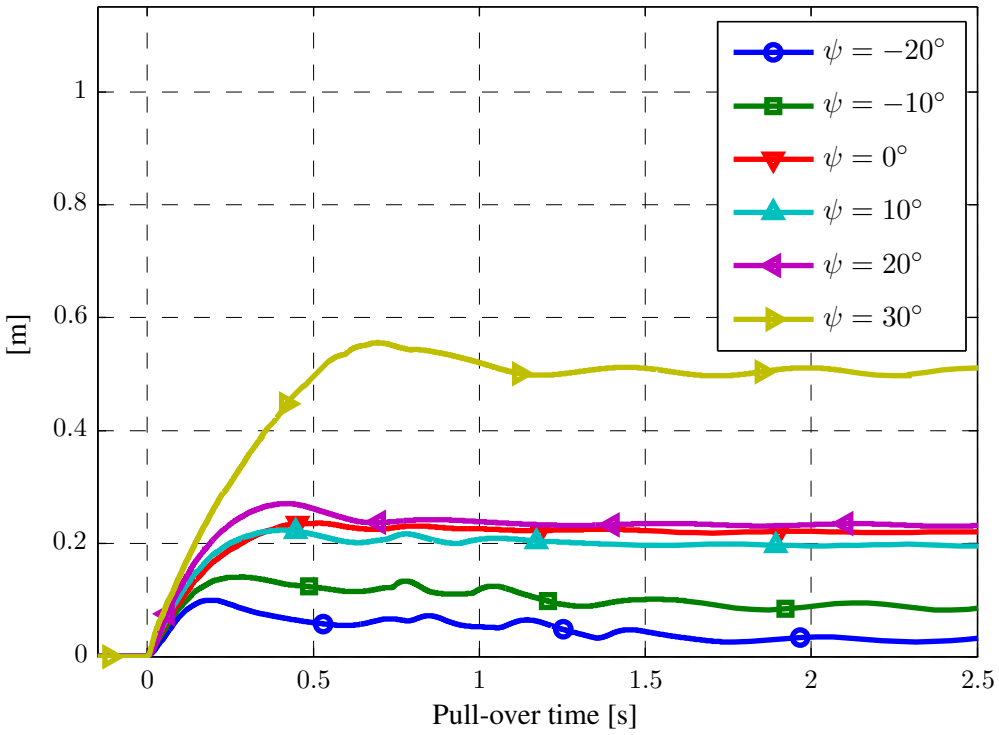

Figure 6.11: Horizontal displacement, seabed added mass

6.1.2 Span Height of 1 m

In these analyses it was necessary to adjust the normal stiffness of the master elements several times during interference. Typically a low stiffness had to be applied at beginning of pipeline contact to avoid violent peaks in the time histories. Thereafter the stiffness was stepwise increased such that penetration was avoided when the board was lifted upwards and away from the pipeline. The upper and lower bound of the applied stiffness are given in Figure 5.13. A material curve which gave a low stiffness for small penetrations and a high stiffness for larger penetrations was used for the 30° case. This is also the reason of the small offset at beginning of contact which can be observed for the horizontal displacement and the horizontal pull-over force for this hit angle.

According to the pull-over forces in Figure 6.14 – 6.21 there is no significant effect from increased trawl board added mass. Figures 6.14 – 6.17 indicate that the horizontal pull-over force depends strongly on the pipeline hit angle. A major peak emerge in the horizontal force at 2.0 s pull-over time for hit angles of 10°, 20° and 30°. These peaks occur when the trawl board aft end hits into the pipeline as shown in Figure 6.12. In the cases with hit angles of $-20°$, $-10°$ and 0° this trawl board behaviour did not appear. A snapshot of the trawl board just before it moves upwards and away from the pipeline is shown for a hit angle of 0° in Figure 6.13.

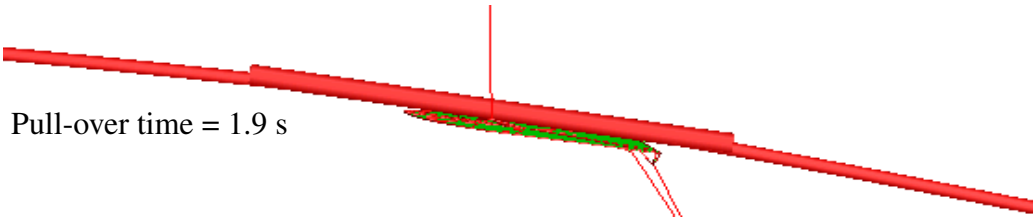

Figure 6.12: Trawl board behaviour for $\psi = 10°$

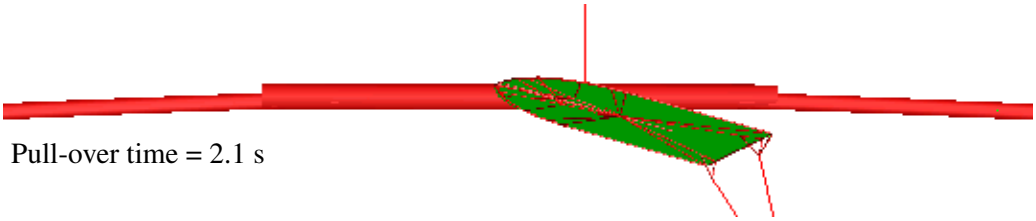

Figure 6.13: Trawl board behaviour for $\psi = 0°$

The horizontal pull-over force in the $-20°$ case has a steeper slope and a larger maximum value than the hit angles of $-10°$ and 0°. During interference the warpline tension increase was approximately equal in all three cases. Therefore the steep slope must be explained by considerations of the hydrodynamic forces on the trawl board. When the hit angle is $-20°$ it was observed that the trawl board slides along the pipeline without any significant yaw motion, i.e. the angle of attack is kept nearly constant during interference. Since the yaw angle is almost constant the sway drag force will not contribute to the same extent as in the $-10°$ case where the angle of attack gradually increases. In turn this will result in a steeper slope and a larger maximum value for the hit angle of $-20°$.

In Figures 6.22 and 6.23 the largest hit angles, both negative and positive ones, result in slightly larger horizontal displacements than the 0° case. Here it is not possible to observe a clear trend of the increased trawl board added mass. Some of the time histories indicate also that an increase of trawl board added mass results in reduced horizontal pipeline displacements. These unreasonable observations can be related to the stepwise increase of the master element stiffness. During one single analysis run it was

necessary to perform restarts and modify the master stiffness several times. The magnitude of the stiffness modifications were roughly the same for corresponding hit angles, but the restarts were not executed at exactly the same time instants in the infinite fluid case and the seabed proximity case. It is therefore plausible that the unexpected results can be related to the time instants of the stiffness modifications.

The impulses of the pull-over loading are given in Tables 6.3 and 6.4. Here it seen that some hit angles predict a lower impulse when the trawl board added mass is increased. As explained above this can be related to the time instants of the master element stiffness modifications. The impulses can however be used to assess general trends of the simulations. In this connection it is seen that large hit angles, both negative and positive ones, predict the largest impulses.

ψ **[deg]**	**Impulse [kNs]**
-20	154.2
20	140.7
30	130.7
0	130.3
-10	119.2
10	117.1

Table 6.3: Impulse of pull-over load, infinite fluid added mass

ψ **[deg]**	**Impulse [kNs]**
-20	148.1
30	139.5
20	125.6
10	120.1
-10	119.0
0	114.4

Table 6.4: Impulse of pull-over load, seabed added mass

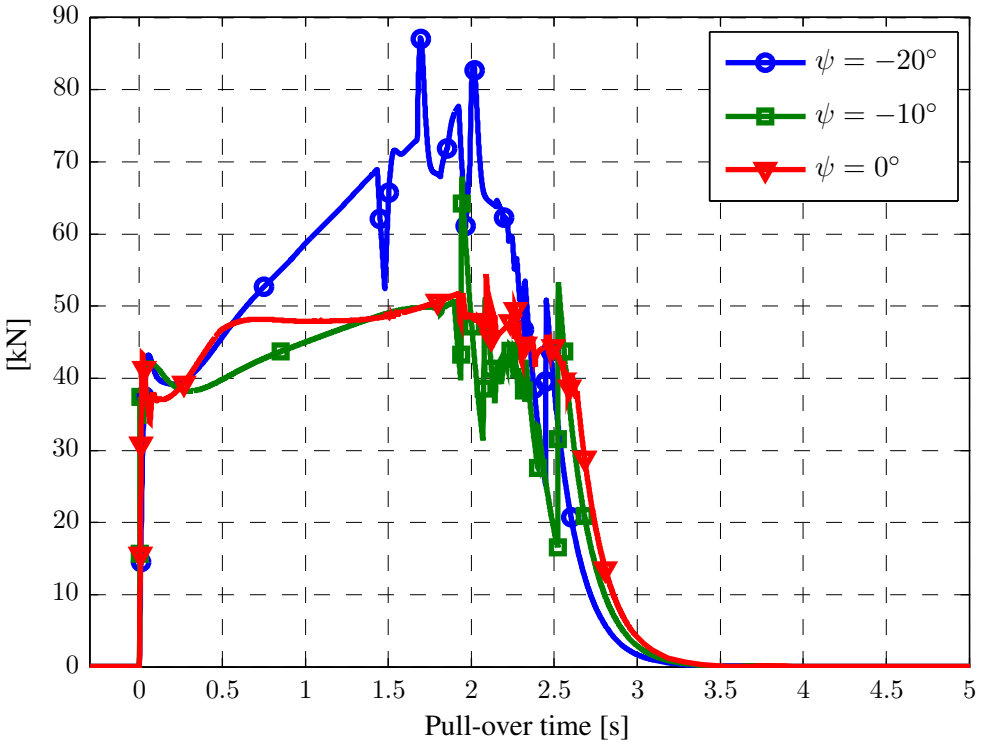

Figure 6.14: Horizontal pull-over force, infinite fluid added mass

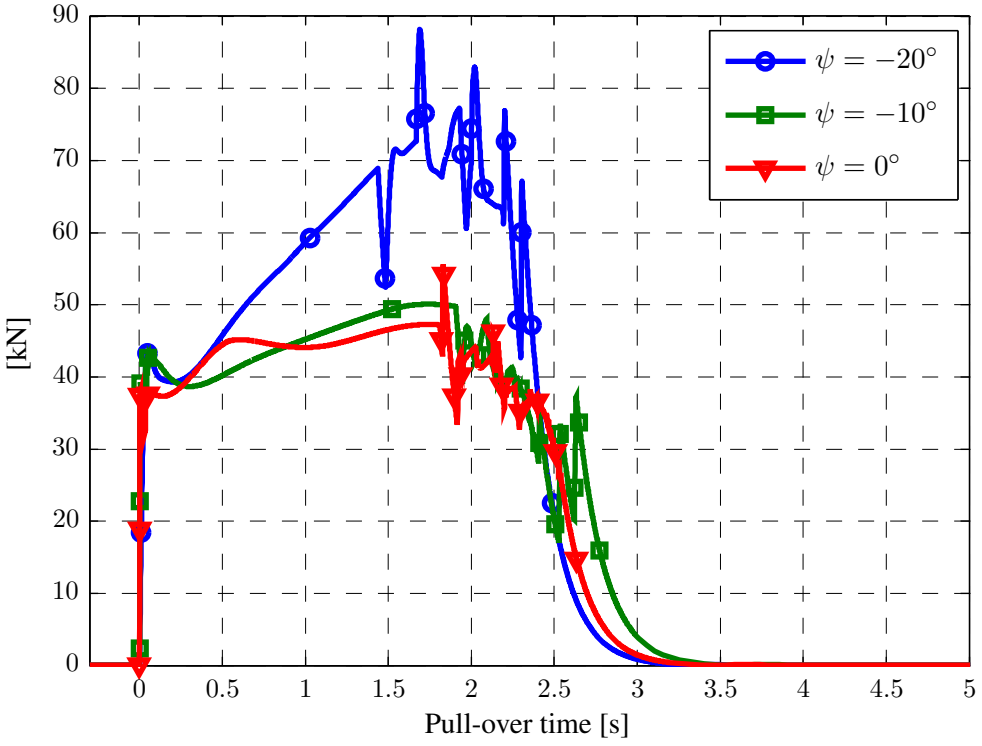

Figure 6.15: Horizontal pull-over force, seabed added mass

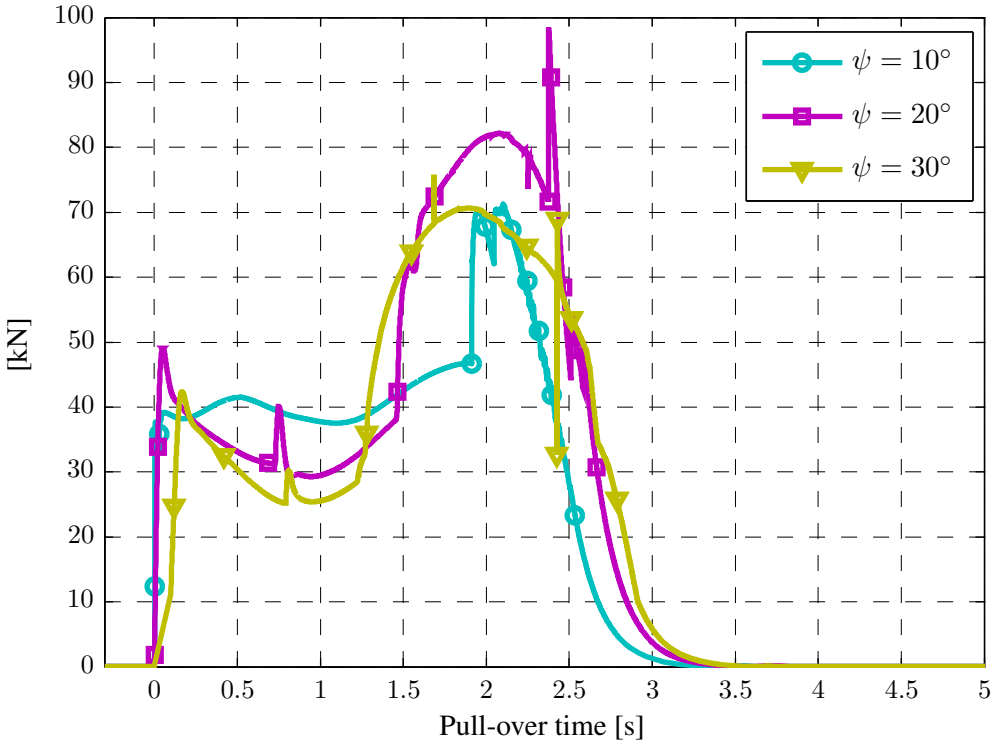

Figure 6.16: Horizontal pull-over force, infinite fluid added mass

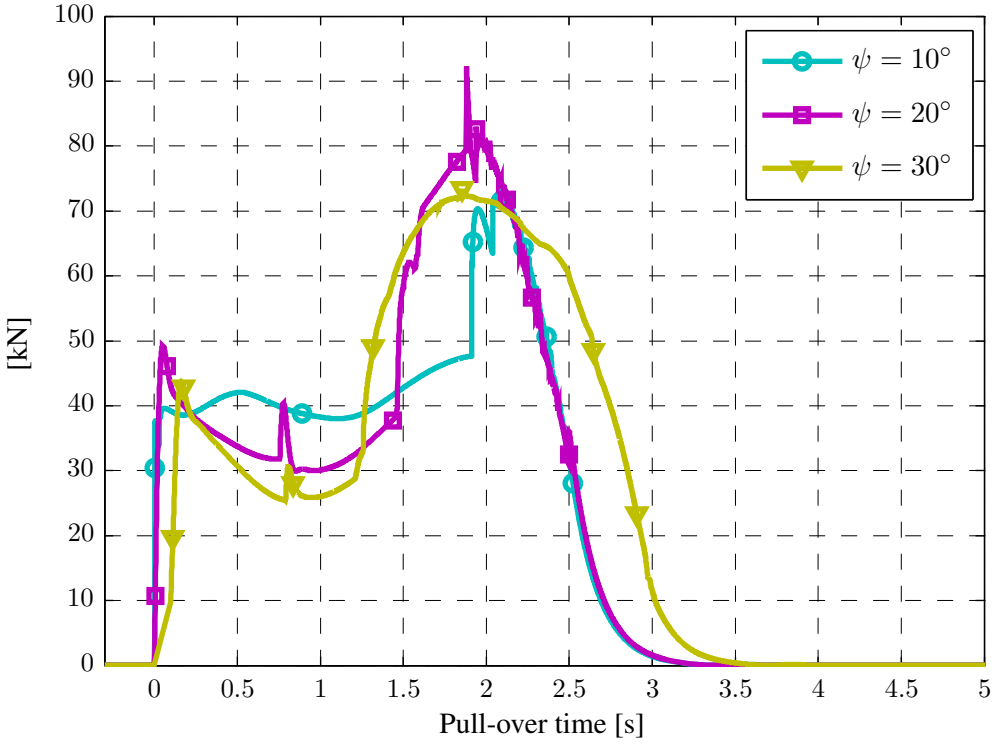

Figure 6.17: Horizontal pull-over force, seabed added mass

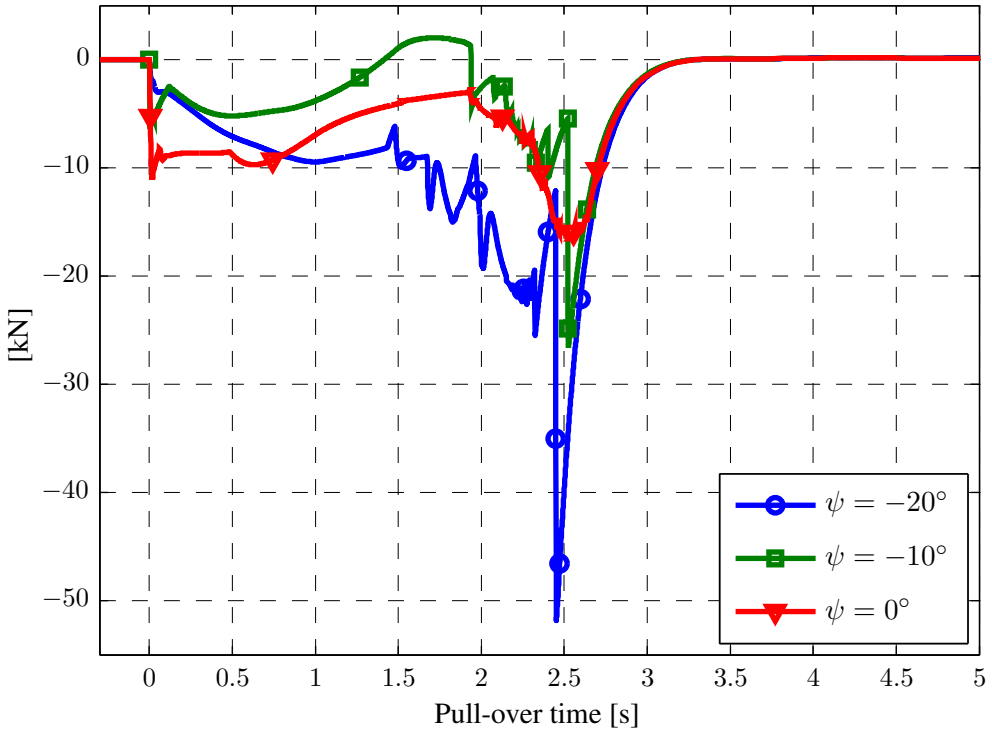

Figure 6.18: Vertical pull-over force, infinite fluid added mass

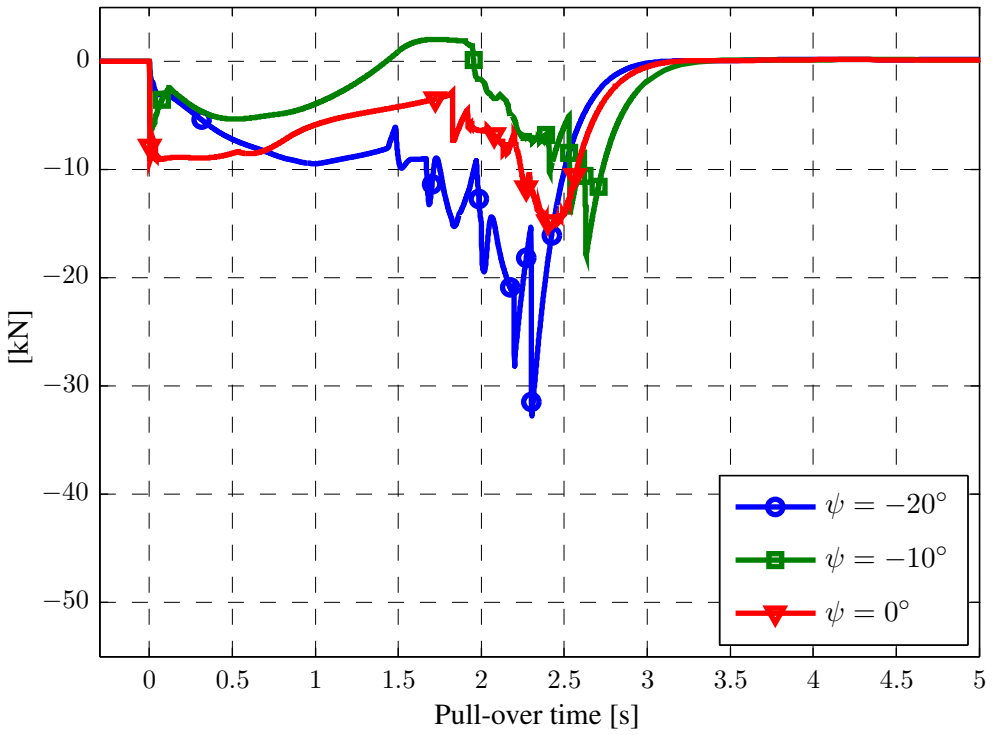

Figure 6.19: Vertical pull-over force, seabed added mass

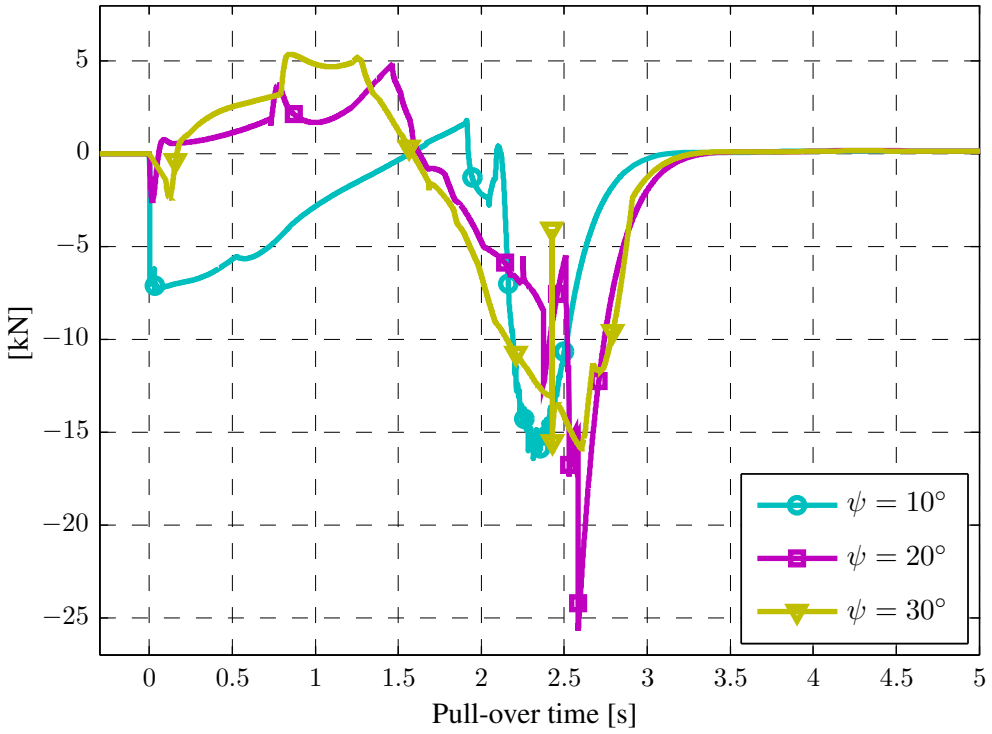

Figure 6.20: Vertical pull-over force, infinite fluid added mass

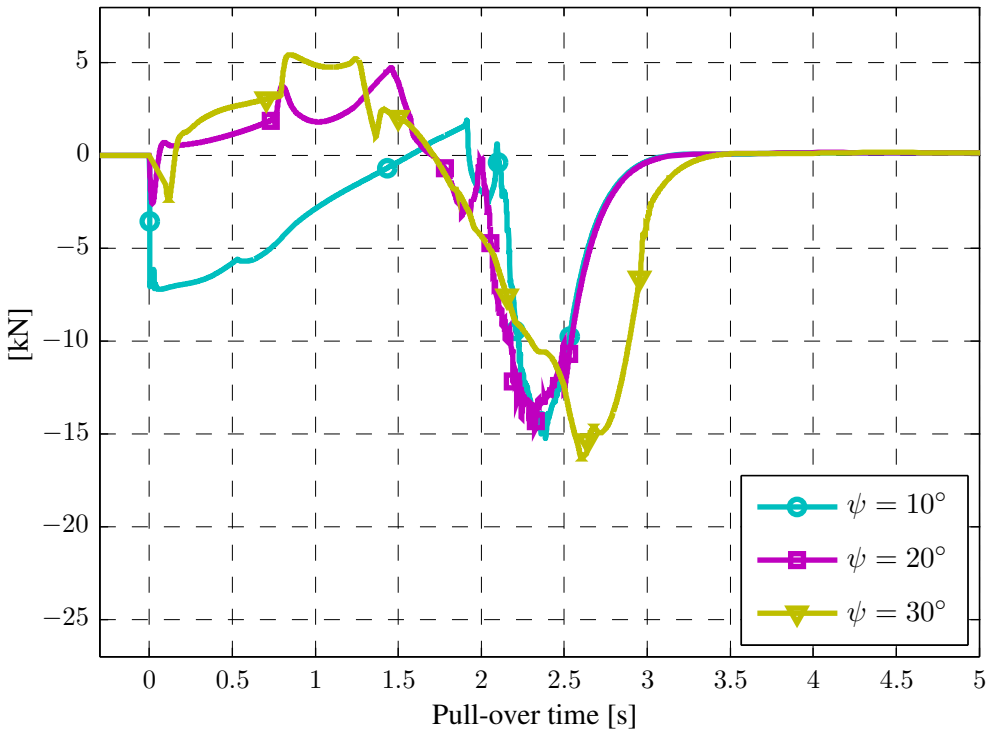

Figure 6.21: Vertical pull-over force, seabed added mass

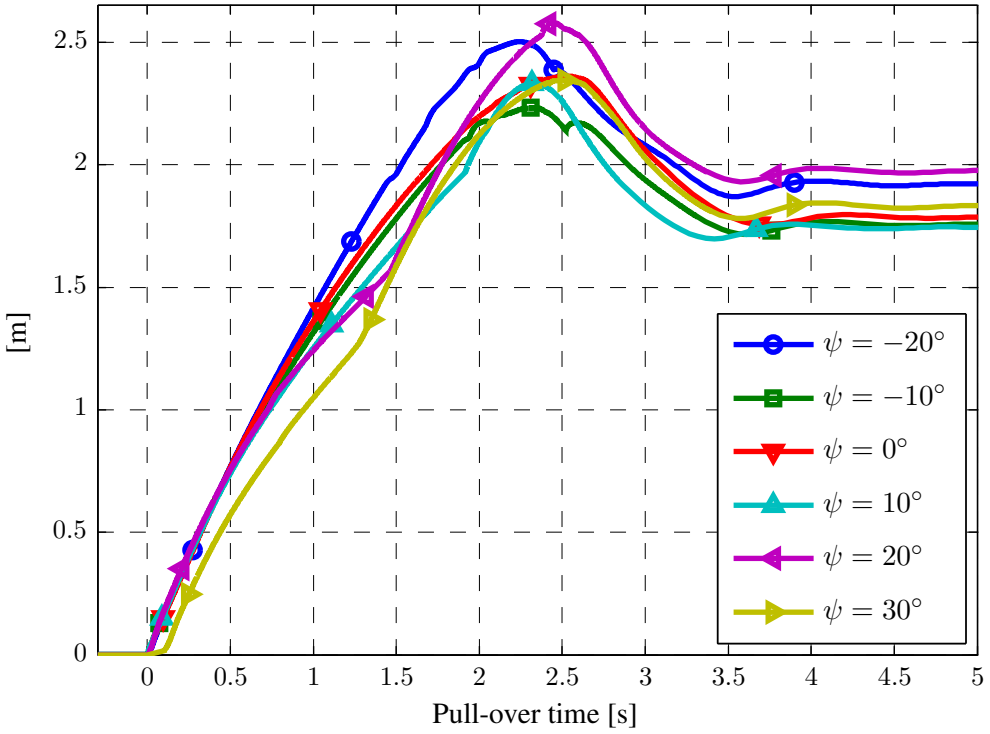

Figure 6.22: Horizontal displacement, infinite fluid added mass

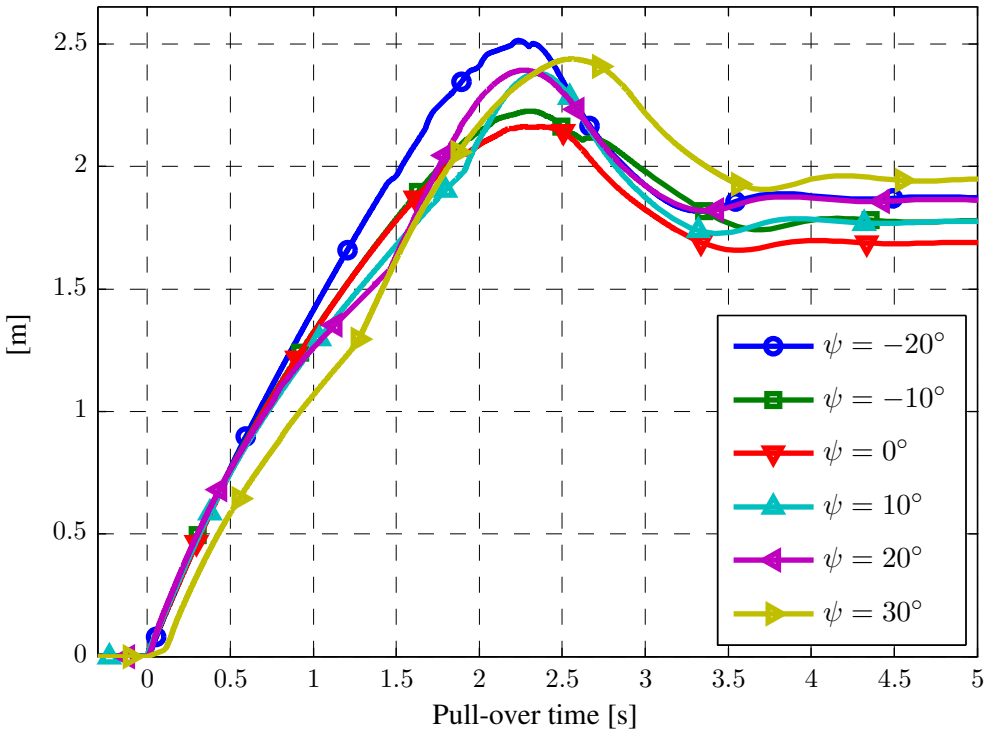

Figure 6.23: Horizontal displacement, seabed added mass

6.2 Rectangular Trawl Board

The trawl board is represented by the rectangular board in Figure 5.4 and the standard hydrodynamic load model with the dynamic properties in Table 5.6. Conclusions regarding the effect of a more rectangular geometry must be based on several analysis runs such that the uncertainty level is reduced. The simulations are therefore executed for the same hit angles used for the polyvalent board in Section 6.1.

6.2.1 Span Height of 0 m

The lower bound stiffness in Figure 5.13 was applied at the beginning of contact and thereafter it was adjusted somewhat if contact problems emerged. As explained in Section 6.1.1 the polyvalent board was allowed to partly penetrate the pipeline at the end of pull-over. This approach was not necessary for the rectangular board because the warpline tension increased 2-3 times more than in the polyvalent board simulations. Due to the large warpline tension the rectangular board was lifted upwards at the end of pull-over such that the ski did not interact with the pipeline. Contact problems emerged however for the rectangular board due to an insufficient description of the trawl board geometry. This problem was solved by increasing the number of elements in the lower corner of the front. See Appendix C for further details.

The horizontal pull-over forces for the polyvalent board had a dominant peak at beginning of contact. This is in contrast to Figures 6.24 and 6.25 which indicate a rectangular-shaped time history and a duration increase of 0.5 s. It can be observed that the mean horizontal pull-over forces for hit angles of 10°, 20° and 30° are 5-15 kN lower than for the other hit angles. It should also be noted that the maximum horizontal pull-over load for hit angles of -20°, -10° and 0° are 6-10 kN larger than in the corresponding simulations for the polyvalent board.

The vertical pull-over forces in Figures 6.26 and 6.27 are reduced compared to the polyvalent board. This is related to the large warpline tension which prevented the board from sliding over the pipeline.

As seen in Figure 6.28 the rectangular-shaped horizontal force results in much larger horizontal displacements than the polyvalent board. Here the hit angles of -10° and 0° give the largest displacements. This is solely related to the duration and load level of the horizontal pull-over force.

It can also be observed that the hit angle of -20° has a shorter pull-over duration than the other cases. This can be explained from the trawl board behaviour during interference. The simulations clearly show that the trawl board has minor yaw rotations and slides a small distance along the pipeline. This enforces the trawl board front to slide earlier over the pipeline.

The impulses in Tables 6.5 and 6.6 are considerably larger compared to the polyvalent board impulses. This is a direct consequence of the rectangular-shaped time history of the horizontal pull-over forces.

ψ [deg]	Impulse [kNs]
-10	80.7
0	67.8
-20	67.7
20	58.2
30	56.5
10	56.3

Table 6.5: Impulse of pull-over load

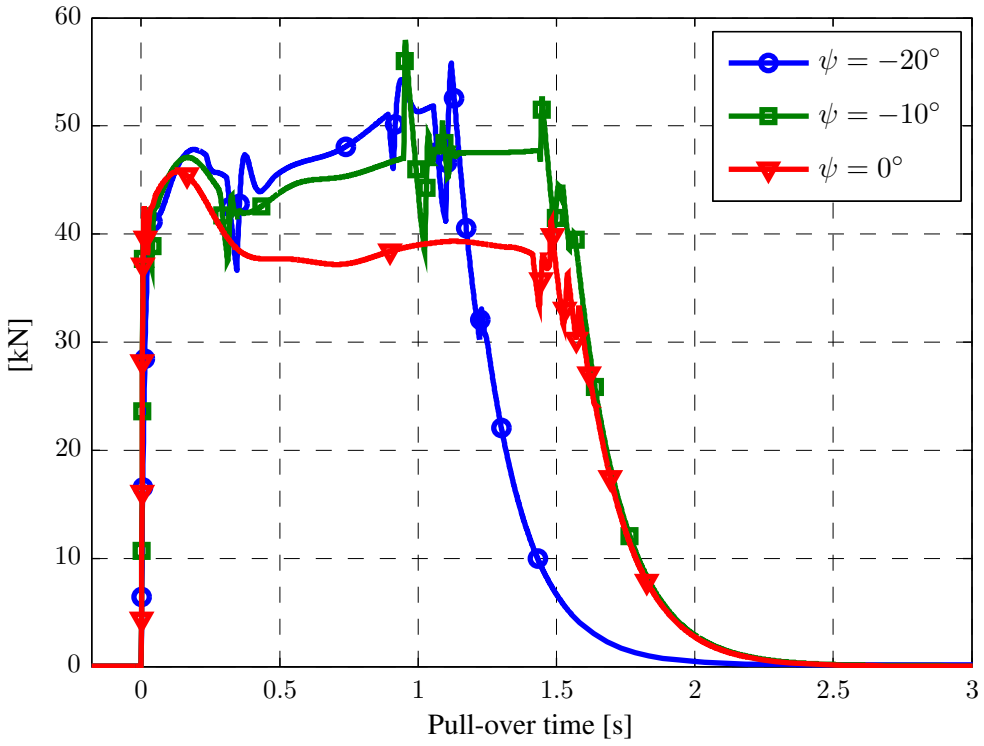

Figure 6.24: Horizontal pull-over force, rectangular trawl board

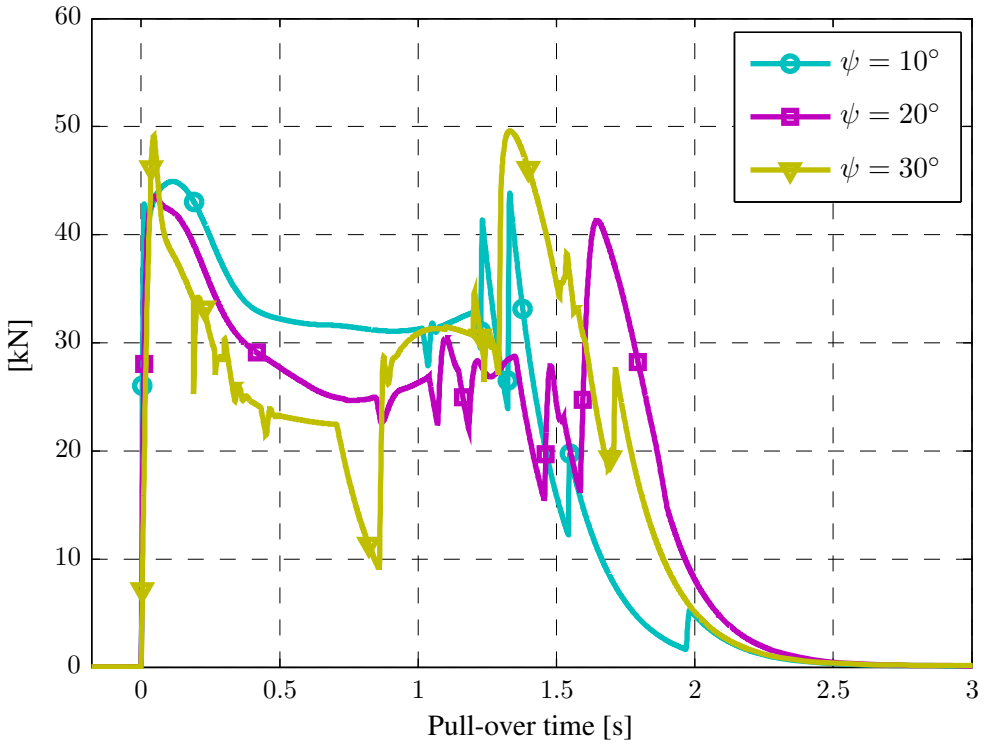

Figure 6.25: Horizontal pull-over force, rectangular trawl board

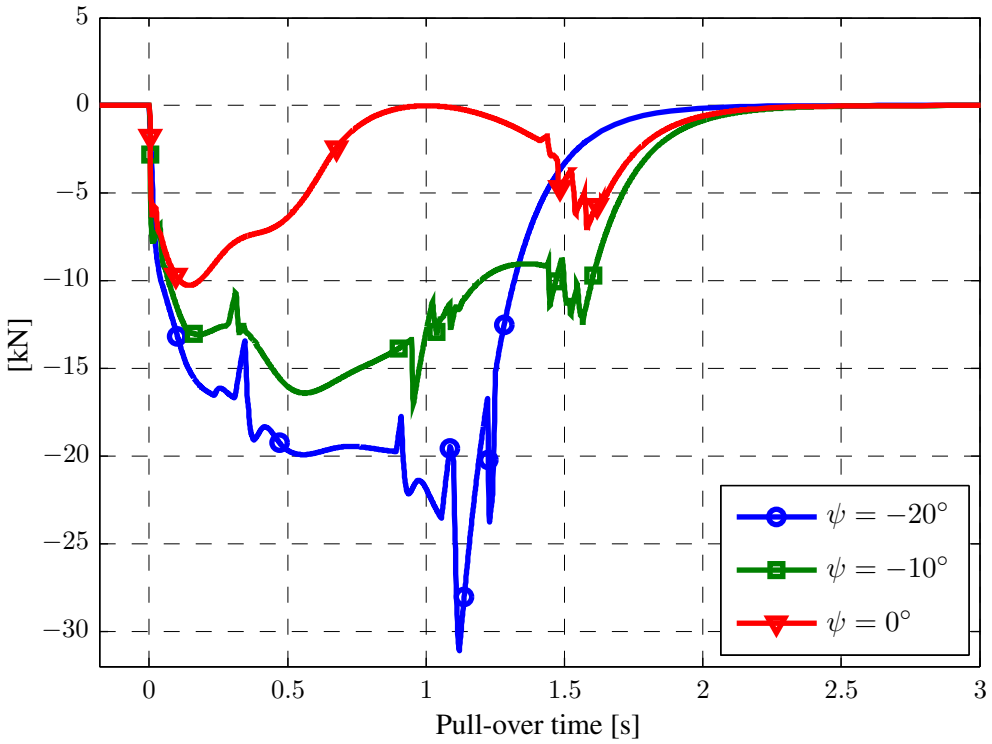

Figure 6.26: Vertical pull-over force, rectangular trawl board

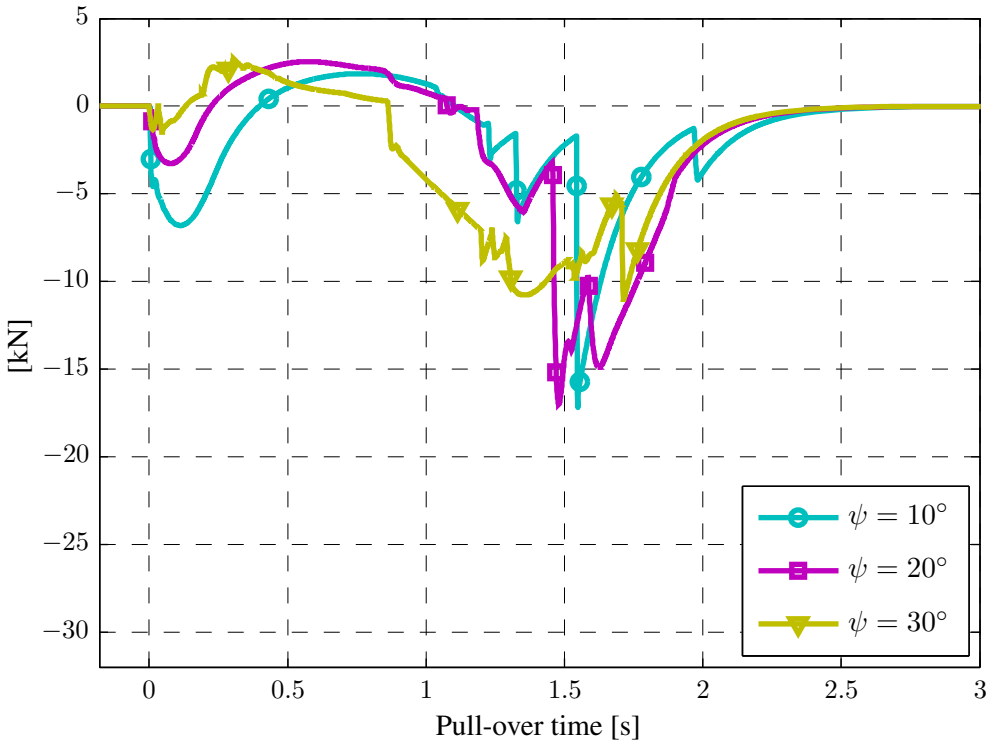

Figure 6.27: Vertical pull-over force, rectangular trawl board

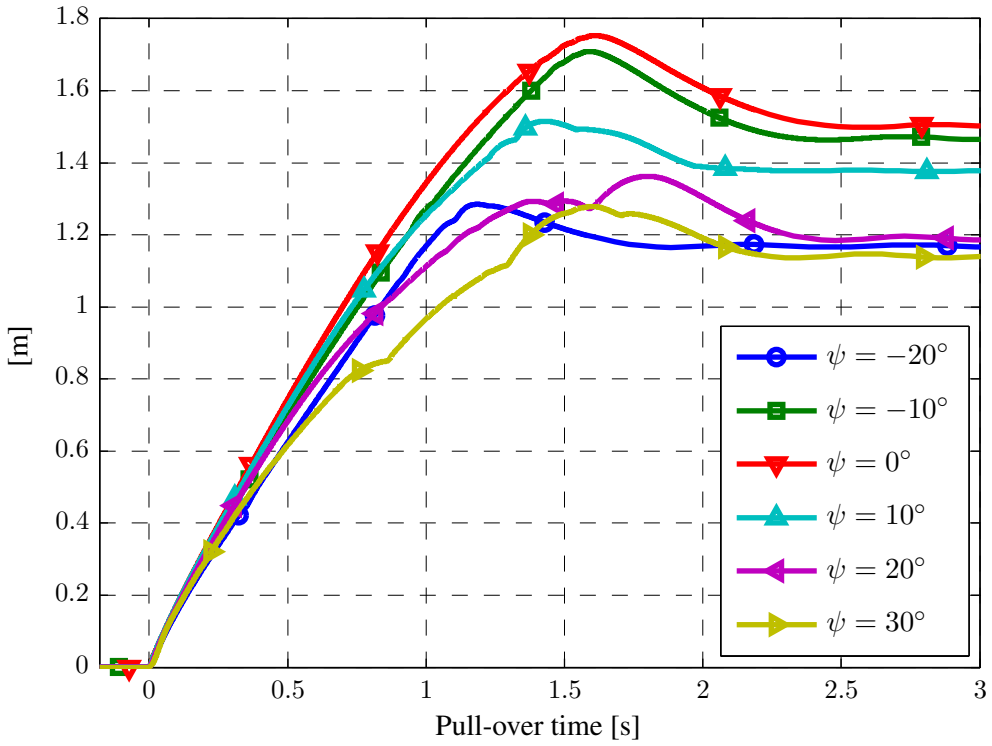

Figure 6.28: Horizontal displacement, rectangular trawl board

6.2.2 Span Height of 1 m

In these simulations it was necessary to modify the contact element stiffness several times during pipeline interference to avoid violent peaks in the time histories. The lower bound material curve in Figure 5.13 was used at beginning of pipeline contact. Thereafter the stiffness was increased stepwise to the upper bound stiffness in Figure 5.13 such that pipeline penetration at the end of pull-over was avoided.

The lower corner in the front of the trawl board was slightly modified due to a contact problem which emerged for hit angles of $-10°$, $10°$ and $30°$. The modifications are not believed to influence the pull-over results. See Appendix C for further details.

The pull-over forces in Figures 6.29 – 6.32 indicate similarity with the polyvalent trawl board results in Section 6.1.2. The trawl board behaviour illustrated in Figures 6.12 and 6.13 was observed for the rectangular board as well. This explains why the dominant peak at 2.0-2.3 s analysis time occurs only for hit angles of $10°$, $20°$ and $30°$.

Compared to the polyvalent board the hit angle of $10°$ predicts a 15 kN increase of maximum horizontal pull-over force, while the $0°$ case predicts a horizontal pull-over force which is 5-10 kN lower during the first 2.0 s of the pull-over. In these cases neither the warpline tension histories nor the trawl board motion indicate any evident differences. These hit angles are therefore not emphasized in the following.

The effect of a rectangular geometry comes into view for the hit angles of $-20°$ and $-10°$ which experience a 0.5 s increase of pull-over duration.

The increased pull-over duration for the $-20°$ case is clearly seen in Figure 6.33 where the maximum horizontal displacement becomes equal to 3.1 m. Apart from the $0°$ case, the horizontal displacement for the other hit angles have increased with 0.2-0.3 m compared to the polyvalent board simulations.

Table 6.6 indicates that the hit angles of $-20°$ and $-10°$ have increased their impulses by 40-50 kNs compared to polyvalent board simulations. The other hit angles experiences insignificant changes of the pull-over impulses. Here it must be reminded that hit angles of $0°$ and $10°$ should not be emphasized.

ψ **[deg]**	**Impulse [kNs]**
-20	201.1
-10	150.2
10	148.7
20	145.1
30	143.3
0	109.5

Table 6.6: Impulse of pull-over load

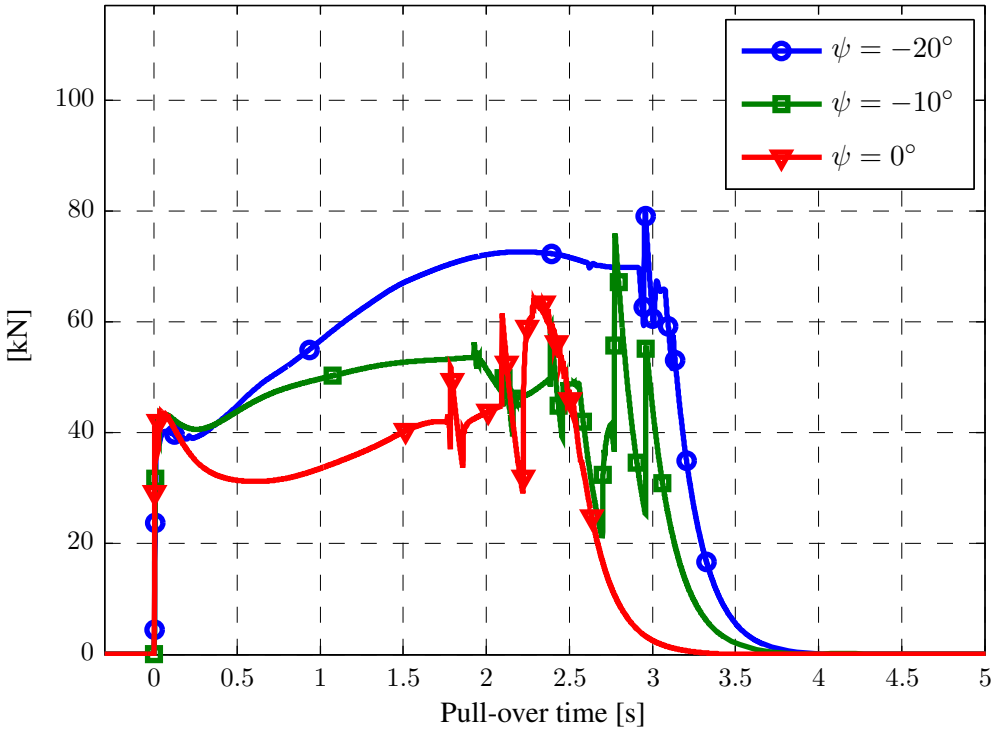

Figure 6.29: Horizontal pull-over force, rectangular trawl board

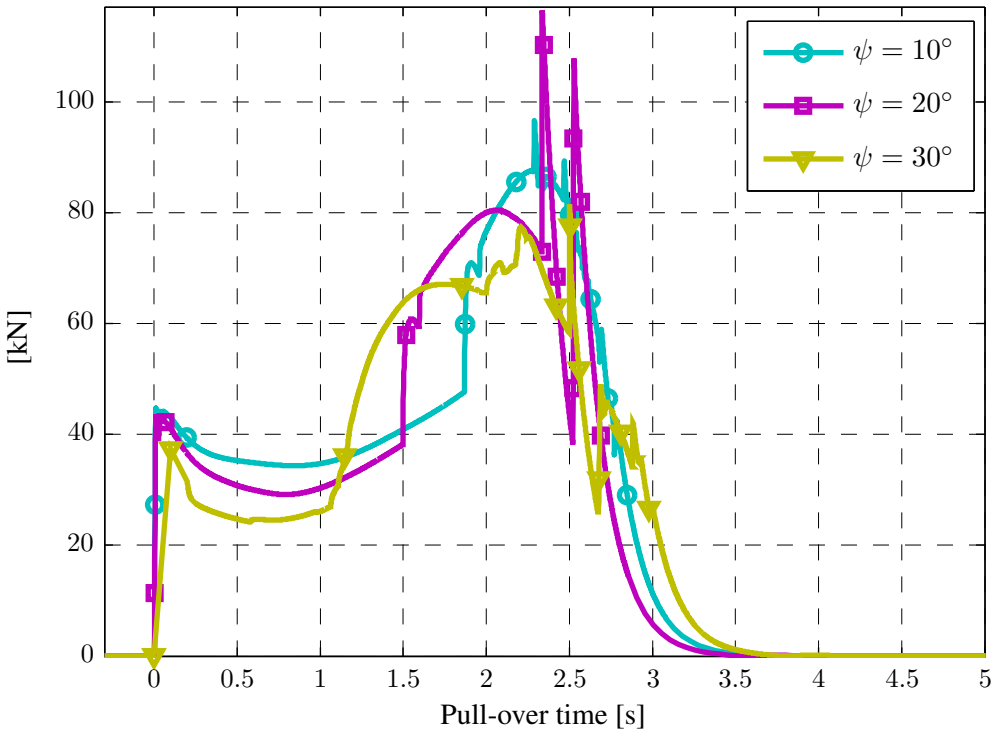

Figure 6.30: Horizontal pull-over force, rectangular trawl board

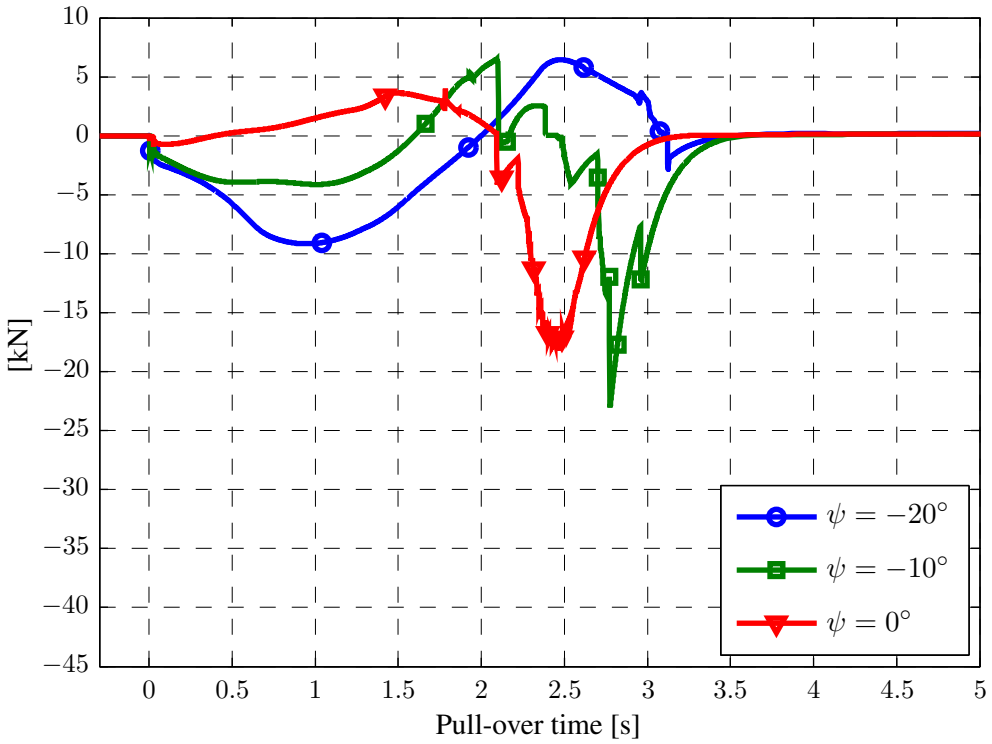

Figure 6.31: Vertical pull-over force, rectangular trawl board

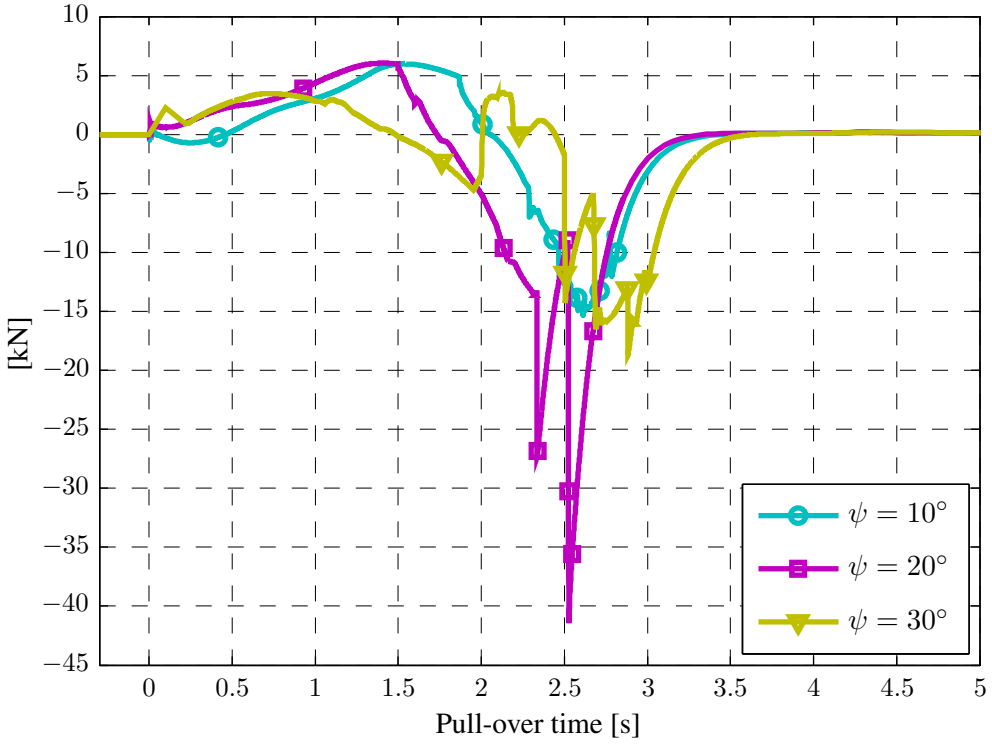

Figure 6.32: Vertical pull-over force, rectangular trawl board

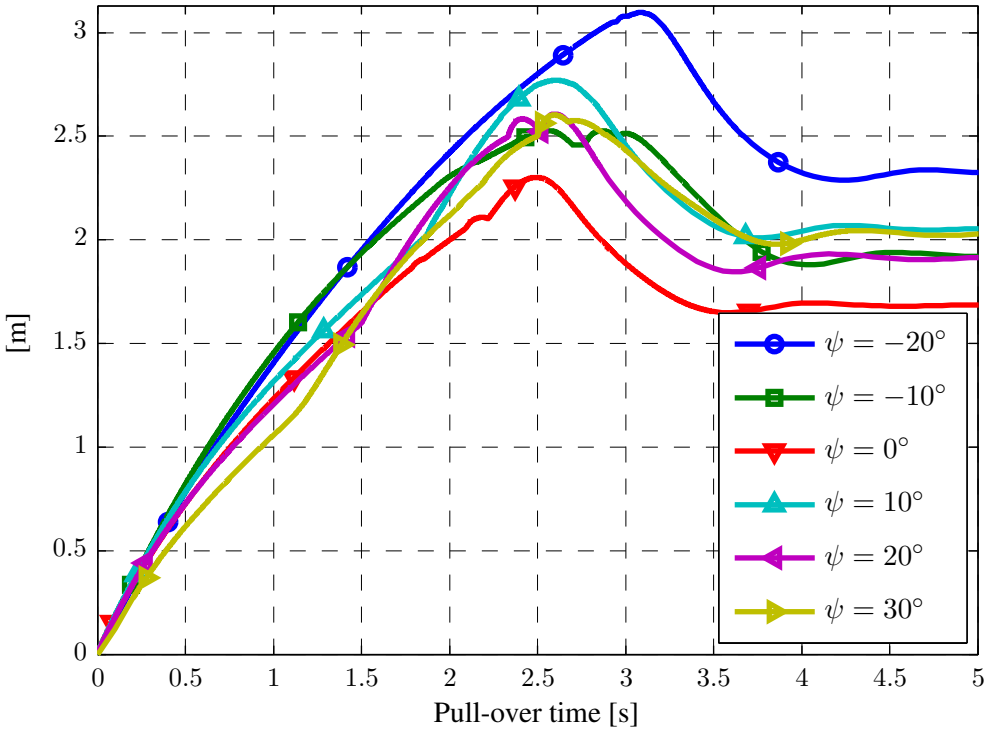

Figure 6.33: Horizontal displacement, rectangular trawl board

6.3 Advanced Hydrodynamic Load Model and DNV-RP-F111

Two trawl board simulations with a hit angle of 0° were executed for span heights of 0 m and 1 m. Here the trawl board was represented by the polyvalent board in Figure 5.3 and the advanced hydrodynamic load model.

The applied drag coefficients in the advanced hydrodynamic load model are only valid for roll angles up to -20°. When the original coefficients were used the mean yaw angle was approximately -40° before pipeline interference. The input format of the roll drag coefficients was therefore modified such that the mean yaw angle became equal to -22°. See Appendix A for further details.

According to the verification test in Appendix B there are some errors present in the advanced hydrodynamic load model. The errors occurred in the degrees of freedom which are not of major importance during pipeline interference.

The results obtained by the DNV-RP-F111 approach for a span height of 0 m and 1 m are also presented in this chapter. All observations and remarks in Sections 6.3.1 and 6.3.2 refer however to the advanced hydrodynamic load model.

6.3.1 Span Height of 0 m

In Section 6.1.1 it was mentioned that contact problems emerged when the polyvalent trawl board ski slid over the pipeline. This problem did not appear when the advanced hydrodynamic load model was used. Contact problems related to an insufficient description of the trawl board geometry did however occur. The problem was solved by increasing the number of elements in the lower part of the trawl board front, see Appendix C.

It was necessary to apply the lower bound master element stiffness in Figure 5.13 at beginning of contact in order to reduce a violent peak in the horizontal pull-over force. As seen in Figure 6.34 the peak at beginning of contact is still rather violent. An even more violent peak emerged if the stiffness was increased. Throughout the simulation the master stiffness was stepwise increased to a level in between the upper and lower bound stiffness in Figure 5.9.

The horizontal pull-over force in Figure 6.34 has a large peak of 99 kN at the beginning of contact and thereafter it decreases as the trawl board slides over the pipeline. Contrary, the DNV-RP-F111 code predicts a linear increase up to the maximum value of 44 kN. A less dominant peak at beginning of contact is observed for the vertical pull-over force in Figure 6.35. The vertical force is approximately 15-25 kN larger than the DNV-RP-F111 predictions throughout the pull-over.

The maximum horizontal pipeline displacements in Figure 6.36 agrees fairly well with the DNV-RP-F111 code. The time histories deviates however in the two approaches. This is related to the large horizontal force peak which occured at beginning of contact in the trawl board simulation.

Table 6.7 indicates that the trawl board simulation predicts a significantly larger impulse than the DNV approach. It should be noted that the pull-over duration is in good agreement in the two approaches.

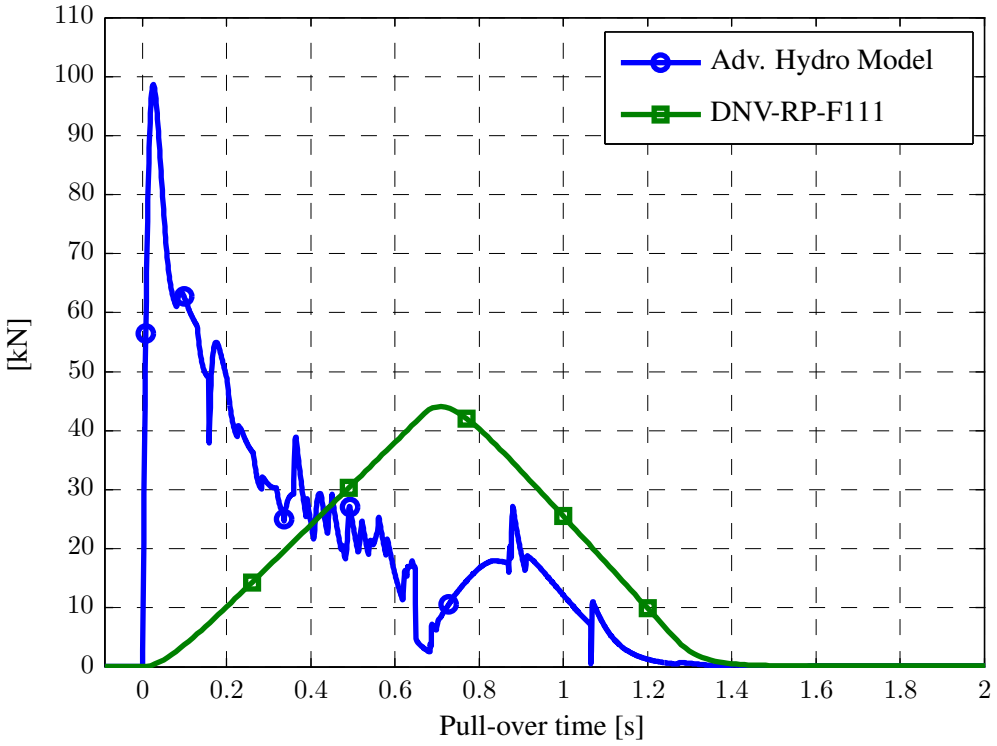

Figure 6.34: Horizontal pull-over force, DNV-RP-F111 vs. Advanced hydrodynamic model

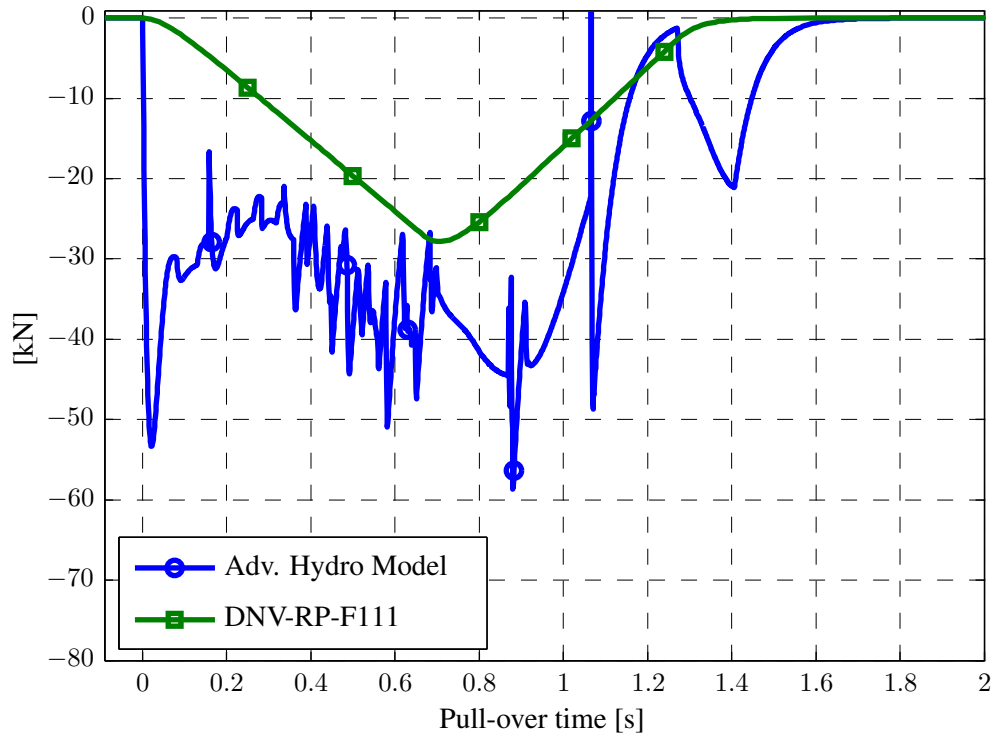

Figure 6.35: Vertical pull-over force, DNV-RP-F111 vs. Advanced hydrodynamic model

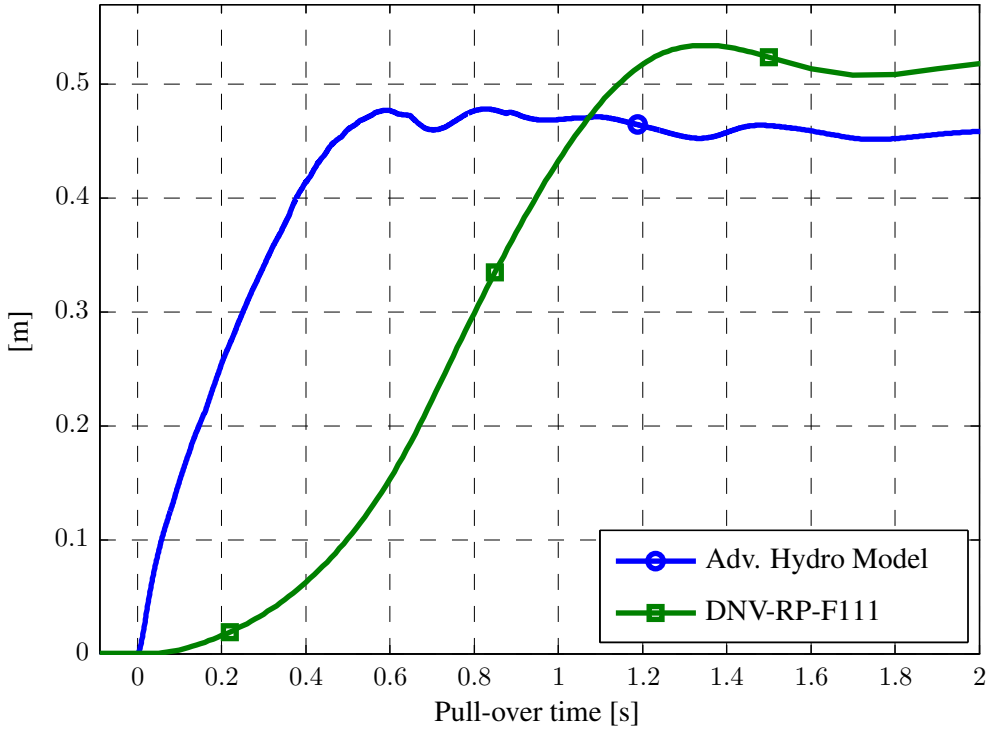

Figure 6.36: Horizontal displacement, DNV-RP-F111 vs. Advanced hydrodynamic model

Simulation	**Impulse [kNs]**
Advanced hydrodynamic model	57.0
DNV-RP-F111	35.3

Table 6.7: Impulse of pull-over load

6.3.2 Span Height of 1 m

In order to avoid violent peaks in the time histories the master element stiffness was adjusted during pipeline interference. A low stiffness was applied at the instant of first contact and thereafter the stiffness was stepwise increased throughout the analysis. The upper and lower bound of the applied stiffness is depicted in Figure 5.13.

The trawl board behaviour illustrated in Figure 6.13 which emerged for the standard hydrodynamic load model was suppressed. Instead the trawl board rotates such that the aft end hits into the pipeline as shown in Figure 6.37. In this trawl board position the drag force induces a large moment which counteracts the moment contribution from the warpline. Therefore the trawl board will not roll over the pipeline and be pulled upwards as rapidly as in the simulations with the standard hydrodynamic load model. This behaviour extends the pull-over duration by 0.7 s. The trawl board is kept in the position in Figure 6.37 until the warpline tension overcomes the roll drag moment at the end of pull-over.

It should be noted that the seabed frictional force on the trawl board is deactivated, see Section 5.7.2. Based on simple hand calculations the frictional force would have induced a roll moment of approximately the same order as the warpline moment contribution. This would have resulted in a reduction of the pull-over duration. The results presented in this section should therefore be considered as conservative in terms of load level and duration.

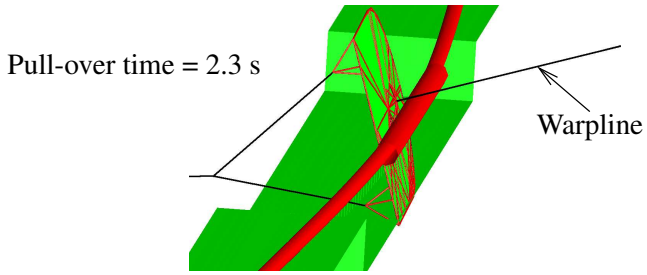

Figure 6.37: Trawl board behaviour in the advanced hydrodynamic model

The horizontal pull-over force in Figure 6.38 is in very good agreement with the DNV-RP-F111 predictions in terms of maximum value, shape and duration. A large peak occurs at the beginning of pipeline contact, but since the duration is relatively large the peak will not be so dominant as in the 0 m span height case. It should also be mentioned that the maximum warpline tension increased by about 70 % compared to the simulations which used the standard hydrodynamic load model.

In Figure 6.39 the vertical pull-over force acts upwards. This is in contrast to the DNV-RP-F111 code which predicts a downward force. It should however be noted that the maximum value of the vertical forces have approximately the same magnitude. The reason for the upward force can be explained from the screenshot in Figure 6.37. In this trawl board position the contact force will give an upward acting force on the pipeline.

In Figure 6.40 the horizontal displacement is 0.5 m larger than the DNV-RP-F111 prediction. This must be seen in connection with the upward pull-over force which reduces the horizontal frictional forces at the span shoulders.

The impulses in Table 6.8 indicate that there is a good accordance between the trawl board simulation and the DNV-RP-F111 code. This is mainly related to the good agreement of the horizontal pull-over forces in the two approaches.

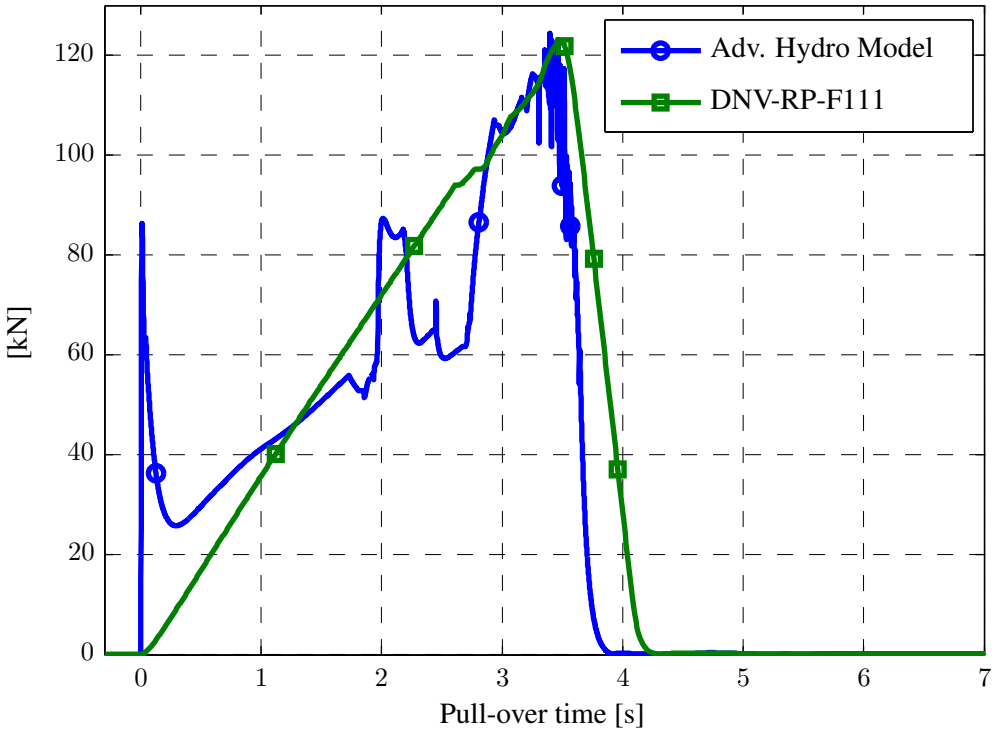

Figure 6.38: Horizontal pull-over force, DNV-RP-F111 vs. Advanced hydrodynamic model

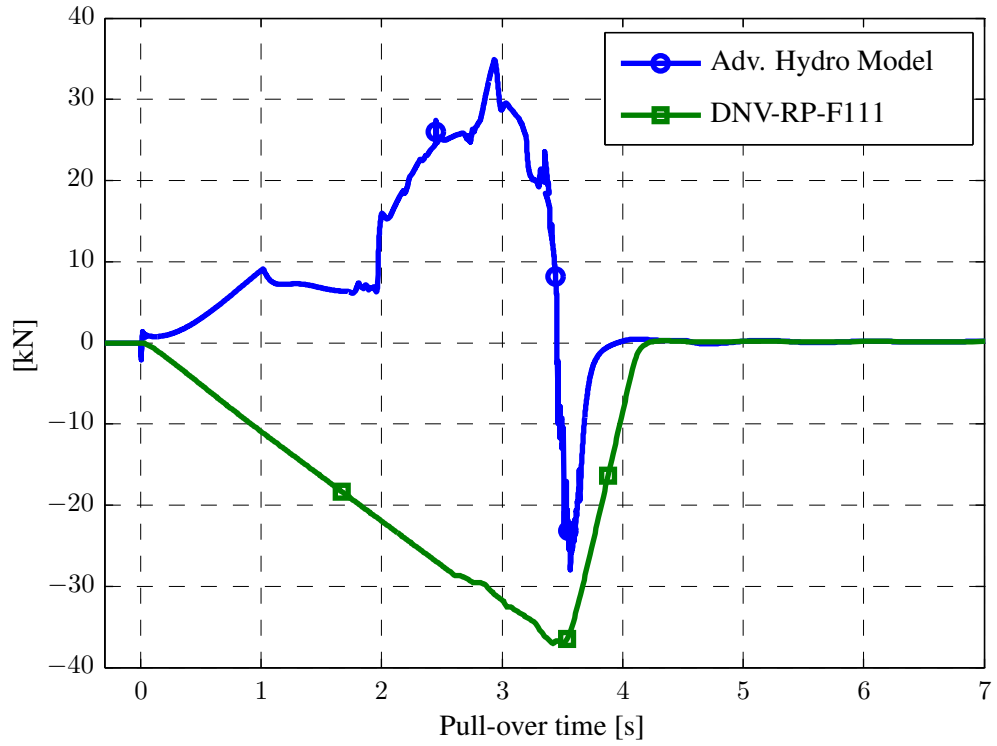

Figure 6.39: Vertical pull-over force, DNV-RP-F111 vs. Advanced hydrodynamic model

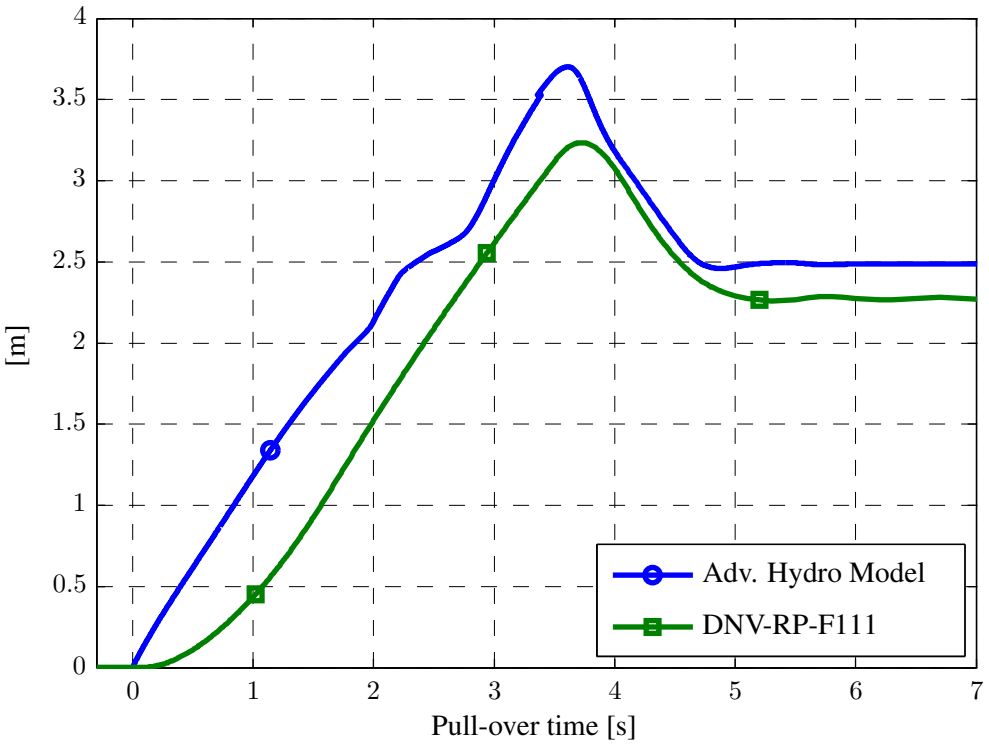

Figure 6.40: Horizontal displacement, DNV-RP-F111 vs. Advanced hydrodynamic model

Simulation	**Impulse [kNs]**
DNV-RP-F111	270.6
Advanced hydrodynamic model	239.1

Table 6.8: Impulse of pull-over load

Chapter 7

Conclusions and Recommendations for Future Work

7.1 Effect of Increasing Added Mass for the Polyvalent Board

Based on the results presented in Section 6.1 it is not possible to observe any effect of increased trawl board added mass due to seabed proximity. As explained in Section 5.4 the added mass correction factors due to seabed proximity were estimated by data received from Statoil. Here it was assumed that the added mass coefficients at a seabed gap of 5.25 m were identical with the ones from an infinite fluid case. The coefficients at a seabed gap of 1.75 m indicates that this assumption is reasonable. Therefore it must be concluded that added mass increase due to seabed proximity has no significant effect on the pull-over loading.

7.2 Effect of Hit Angle for the Polyvalent Board

Span Height of 0 m

The effect of hit angle was most pronounced for the horizontal pipeline displacement. The hit angle of 30° has a reduced vertical force and achieves therefore a horizontal displacement which is more than 50 % larger than the other cases. Negative hit angles predict neglectable horizontal displacements. This trend is also observed to some extent in the maximum horizontal pull-over loads. Here a hit angle of 30° gives a horizontal force of 50 kN while the -20° case results in a horizontal load of 40 kN. From these observations it must be concluded that the largest utilization of pipeline capacity will occur for large positive hit angles.

Span Height of 1 m

The simulations clearly indicate that large hit angles result in the largest horizontal pull-over forces. This tendency is confirmed by the pull-over impulses and horizontal displacements for hit angles of -20°, 20° and 30°. The cases with hit angles of 0° and -10° predicts significantly lower pull-over loads. Therefore it must be stated that the most extreme loading occurs for large hit angles, both positive and negative ones. It should however be noted that the advanced hydrodynamic load model predicts a completely

different pull-over in the 0° case. This indicates that the standard hydrodynamic load model does not represent the forces and moments on the trawl board during interference correctly and the statement made here regarding the hit angle is therefore uncertain.

7.3 Effect of Hit Angle for the Rectangular Board

Span Height of 0 m

The shape of the horizontal force time histories resembles a rectangle and therefore the mean forces are considered in the following. The general trend is that hit angles of $-20°$, $-10°$ and $0°$ have a mean force which is 5-15 kN larger than the other hit angles. This results in 20-30 % larger horizontal displacements for the two last-named hit angles. It must therefore be concluded that hit angles of $-10°$ and $0°$ will give the largest pipeline utilization factors.

Span Height of 1 m

The lowest pull-over load occured for the hit angle of 0°. A stepwise increase in terms of horizontal pull-over load and horizontal displacement is observed for the hit angles of $-10°$ and $-20°$. The horizontal pull-over force is larger for the positive hit angles as well, but they indicate a more mutual resembling behaviour. In total it must therefore be stated that large hit angles, both positive and negative ones, give the most extreme pull-over loading. As mentioned in Section 7.2 the standard hydrodynamic load model seems to give an insufficient description of the pull-over and a high degree of uncertainty is therefore associated with the statement made here.

7.4 Effect of a Rectangular Trawl Board

Span Height of 0 m

The horizontal pull-over forces experience a rapid increase up to approximately the same maximum values as in the polyvalent board simulations, but the load level is in contrast kept more or less constant throughout the pull-over. It was also seen that the duration increased by 0.5 s. The downward forces are reduced because the rectangular board did not slide over the pipeline during interference. The loading results in horizontal displacements which are 0.7-1.2 m larger than in the polyvalent board simulations. Based on these observation it must be stated that the rectangular board will result in a larger utilization of the pipeline capacity compared to the polyvalent trawl board.

Span Height of 1 m

The simulations indicate that there are small differences between the rectangular and polyvalent board. The most noticeable effect was that the rectangular geometry extends the pull-over duration by 0.5 s for hit angles of $-20°$ and $-10°$. On a general basis the other hit angles experience an increase in horizontal displacement of 0.2-0.3 m. Therefore it must be concluded that a rectangular trawl board geometry will give a slightly larger pull-over loading than the polyvalent board.

7.5 The Standard Hydrodynamic Load Model versus DNV-RP-F111

The DNV-RP-F111 code gives no information about the pull-over loading from a rectangular board. In the following the DNV predictions are therefore compared against the results from the polyvalent trawl board simulations.

Span Height of 0 m

The DNV-RP-F111 code predicts a maximum pull-over load which is 10 % below the largest values obtained in the trawl board simulations with varying hit angle. The maximum horizontal displacement agrees well with the largest value obtained in the trawl board simulation. In terms of maximum values the DNV code is hence in fairly good agreement with the simulations. The time instant where maximum pull-over load occur is however significantly delayed in the DNV recommendations. It must therefore be concluded that the DNV-RP-F111 code and the trawl board simulations with the standard hydrodynamic load model are not in complete agreement for a span height of 0 m.

Span Height of 1 m

Compared to the DNV-RP-F111 code it is seen that pull-over forces, duration and horizontal displacement are significantly smaller in the trawl board simulations. In addition the shape of the pull-over force time histories for hit angles of -10° and 0° disagrees completely with the triangular shape in the DNV code. Based on the findings with the advanced hydrodynamic load model it is probable that the discrepancies are related to the simple hydrodynamic load model which was used. Therefore it is rational to conclude that the DNV-RP-F111 code and the trawl board simulations with the standard hydrodynamic load model are not in accordance for a span height of 1 m.

7.6 The Advanced Hydrodynamic Load Model versus DNV-RP-F111

First it should be noted that the advanced hydrodynamic load model failed the drag force verification test in Appendix B. The errors occurred for a seabed gap and in the degrees of freedom which are of minor importance during pipeline interference. Therefore it is maybe possible to obtain reasonable results even with the errors present.

Span Height of 0 m

The horizontal pull-over force has a peak of 99 kN at the beginning of pipeline contact and thereafter it decays throughout the simulation. This is in contrast to the DNV-RP-F111 code which predicts a linear increase up to the maximum pull-over load of 44 kN and thereafter a linear decay. The shape of the vertical force time history is in better agreement, but here DNV underpredicts the magnitude with 15-25 kN.

The time histories of the horizontal pull-over forces are not in accordance in the two approaches. It should be noted that also the standard hydrodynamic load model gave a dominant peak at the beginning of pipeline contact. Therefore it is tempting to claim that the DNV code should reduce the rise time of the horizontal pull-over load for cases where the whole pipeline rests on the seabed. Due to the discrepancies

in the pull-over forces it must be concluded that the trawl board simulation and the DNV-RP-F111 code are not in agreement for a span height of 0 m.

Span Height of 1 m

The maximum value, shape and duration of the horizontal pull-over forces indicate no significant differences between the DNV-RP-F111 approach and the trawlboard simulations. The good accordance of the horizontal forces is confirmed by the pull-over impulses of the two approaches.

The direction of the vertical pull-over force is however not in agreement with the DNV-RP-F111 code. Here the trawl board simulations clearly indicate an upward pull-over force until the time instant where the board is lifted upwards and rolls over the pipeline. The upward force also reduces the seabed friction force and hence the horizontal displacement becomes 0.5 m larger than the DNV prediction.

In advance it was expected that the DNV-RP-F111 code would overpredict the pull-over loading due to implicitly included safety factors in the pull-over force expressions. The trawl board simulation indicates however that the degree of conservatism is low in the DNV code for span heights of 1 m. Apart from the direction of the vertical force, it must be concluded that the advanced hydrodynamic load model and the DNV-RP-F111 code are in good agreement for this span height.

7.7 Future Work

In Section 5.5 some critical remarks of the advanced hydrodynamic load model were made regarding the model-scale Reynolds number and the incomplete description of reduced lift due to transient effects. These remarks must be rejected based on the results obtained for the 1 m span height case. In future work it is recommended that all simulations are based exclusively on the advanced hydrodynamic load model.

The hit angle of 0° predicted the lowest horizontal pull-over force when oblique crossings were examined for a span height of 1 m. The advanced hydrodynamic load model demonstrated a completely different trawl board behaviour during interference and predicted a horizontal pull-over force which was almost 3 times larger than the 0° case simulation with the standard hydrodynamic load model. A similar discrepancy must be expected for the other hit angles as well. Statements in this thesis regarding the effect of hit angle for a span height of 1 m are therefore uncertain. In order to get results which can be assessed with confidence it is recommended that all analysis runs for the 1 m span height case are executed once more with the advanced hydrodynamic load model.

In Chapter 6 it was explained that the axial force will contribute to the horizontal equilibrium such that the sampled shear forces will deviate somewhat from the applied pull-over load. In future simulations the global rotation of the shear force sampling nodes must be written to the result file such that the axial force contribution can be eliminated. Alternatively, very small element lengths adjacent to the midnode can be used such that the global rotations will be neglectable.

Problems regarding the contact element stiffness during pipeline interference emerged in the majority of the 1 m span height analysis runs. To avoid violent peaks in the time histories it was typically required to use a low stiffness at beginning of pipeline contact and a high stiffness at the end phase when the trawl board is lifted upwards and rolls over the pipeline. The stiffness was modified stepwise with several restarts during one single analysis run. Due to the large number of simulations this approach turned out to be very time-consuming. It should also be mentioned that unsuccessful experiments were

made with a material curve which had a low stiffness for small penetrations and a higher stiffness for large penetrations. Based on observations in the simulations it seems like the low contact stiffness was required only for time instants where a rapid increase of the contact force occurred. This indicates that there is a need of automatic stiffness control in the SIMLA code. Alternatively, more experiments with a new material curve should be carried out.

References

[1] Ira H. Abbott and Albert E. Von Doenhoff. *Theory of Wing Sections*. Dover Publications, Inc, 1959.

[2] Marine Buzz. Accessed: 16.09.09. `http://www.marinebuzz.com/marinebuzzuploads/96d0603f7047_7CFF/typical_trawl.jpg`.

[3] DNV. *Recommended Practice DNV-RP-F111, Interference Between Trawl Gear and Pipelines*, October 2006 edition.

[4] DNV. *Recommended Practice DNV-RP-H103, Modelling and Analysis of Marine Operations*, April 2009 edition.

[5] Crimond Enterprises. Accessed: 16.09.09. `http://www.crimond.com/images/flumetank/Hussey/twin_trawl_diagram.jpg`.

[6] O. Gabriel & K. Lange. *Fish Catching Methods of the World*. Blackwell Publishing Ltd, 2005.

[7] Havforskningsinstituttet. Accessed: 23.02.10. `http://www.imr.no/filarkiv/2004/03/Nr.14_Toktrapport_blaakveite_traal_soer_des_03_9_.pdf/nb-no`.

[8] Ludvig Karlsen. *Redskapsteknologi i fiske*. Universitetsforlaget, 1989.

[9] Ludvig Karlsen. *Redskapslære og fangstteknologi*. Landbruksforlaget, 1997.

[10] Ivar Langen & Ragnar Sigbjørnson. *Dynamisk analyse av konstruksjoner*. Tapir, 1979.

[11] Kjell Magne Mathisen. *Large Displacement Analysis of Flexible and Rigid Systems Considering Displacement-Dependent Loads and Nonlinear Constraints*. PhD thesis, The Norwegian Institute of Technology, Division of Structural Engineering, 1990.

[12] Kjell Magne Mathisen. *Lecture notes in TKT4197 - Nonlinear Finite Element Analysis*. Department of Structural Engineering NTNU, 2009.

[13] Knut Minsaas and Sverre Steen. *TMR4220 - Naval Hydrodynamics, Lecture Notes in Foil Theory*. Department of Marine Technology NTNU, 2008.

[14] Knut Minsaas and Sverre Steen. *TMR4220 - Naval Hydrodynamics, Lecture Notes in Ship Resistance*. Department of Marine Technology NTNU, 2008.

[15] Martin Troels Møller. Simulation of Interference between Trawl Gear and Pipelines. Master's thesis, NTNU, 2009.

[16] Torgeir Moan. *Lecture notes in TMR4190 - Finite Element Modelling and Analysis of Marine Structures*. Department of Marine Technology NTNU, 2003.

[17] Svein Sævik. Description of the modified body502 element. REINERTSEN AS, unpublished, 2009.

[18] Svein Sævik. *SIMLA - Theory Manual*, 2008 edition.

[19] Svein Sævik. *SIMLA - Theory Manual*, 2003 edition.

[20] Jørgen Amdahl & Tore H.Søreide et al. *USFOS - A Computer Program for Progressive Collapse Analysis of Steel Offshore Structures. Theory Manual*, 1993 edition.

[21] Tarek I. Zohdi. *Lecture notes in ME280A - Finite Element Methods: The Basics*. University of California, Berkeley, 2008.

Appendix A

Advanced Hydrodynamic Load Model

Here the input format of the hydrodynamic inertia coefficients used in the advanced hydrodynamic load model is presented. The coefficient values can not be tabulated in this thesis due to restrictions imposed by Statoil.

A.1 Input Format of Hydrodynamic Inertia Coefficients

The hydrodynamic inertia coefficients are given as input to SIMLA in terms of the roll angles in Tables A.1 – A.4 for four different seabed to trawlboard gaps. Only two rows are included since the hydrodynamic inertia coefficients are independent of the heading angle. It should be noted that SIMLA operates with the absolute value of the roll angle such that the coefficients are described for negative roll angles as well.

	Φ [deg]							
Ψ [deg]	**0**	**10**	**20**	**30**	**45**	**60**	**75**	**90**
0	m_1	m_2	m_3	m_4	m_5	m_6	m_7	m_8
90	m_1	m_2	m_3	m_4	m_5	m_6	m_7	m_8

Table A.1: Hydrodynamic inertia coefficients at 0.0 m seabed gap for all DOFs

	Φ [deg]							
Ψ [deg]	**0**	**10**	**20**	**30**	**45**	**60**	**75**	**90**
0	m_1	m_2	m_3	m_4	m_5	m_6	m_7	m_8
90	m_1	m_2	m_3	m_4	m_5	m_6	m_7	m_8

Table A.2: Hydrodynamic inertia coefficients at 0.1 m seabed gap for all DOFs

	Φ [deg]							
Ψ [deg]	**0**	**10**	**20**	**30**	**45**	**60**	**75**	**90**
0	m_9	m_{10}	m_{11}	m_{12}	m_{13}	m_{14}	m_{15}	m_{16}
90	m_9	m_{10}	m_{11}	m_{12}	m_{13}	m_{14}	m_{15}	m_{16}

Table A.3: Hydrodynamic inertia coefficients at 1.75 m seabed gap for all DOFs

	Φ [deg]							
Ψ [deg]	**0**	**10**	**20**	**30**	**45**	**60**	**75**	**90**
0	m_{17}	m_{18}	m_{19}	m_{20}	m_{21}	m_{22}	m_{23}	m_{24}
90	m_{17}	m_{18}	m_{19}	m_{20}	m_{21}	m_{22}	m_{23}	m_{24}

Table A.4: Hydrodynamic inertia coefficients at 5.25 m seabed gap for all DOFs

A.2 Input Format of Drag Coefficients

The model test performed by Statoil included roll angles up to 20°. The drag coefficients for a roll angle of 90° is therefore set equal to the drag coefficients at 20° roll angle. Tables A.5 and A.6 demonstrate the input format which was used for the coefficients in surge, sway, heave, pitch and yaw.

	Φ [deg]			
Ψ [deg]	**0**	**10**	**20**	**90**
0	d_1	d_2	d_3	d_3
10	d_4	d_5	d_6	d_6
20	d_7	d_8	d_9	d_9
25	d_{10}	d_{11}	d_{12}	d_{12}
30	d_{13}	d_{14}	d_{15}	d_{15}
35	d_{16}	d_{17}	d_{18}	d_{18}
40	d_{19}	d_{20}	d_{21}	d_{21}
45	d_{22}	d_{23}	d_{24}	d_{24}
50	d_{25}	d_{26}	d_{27}	d_{27}
60	d_{28}	d_{29}	d_{30}	d_{30}
70	d_{31}	d_{32}	d_{33}	d_{33}
80	d_{34}	d_{35}	d_{36}	d_{36}
90	d_{37}	d_{38}	d_{39}	d_{39}

Table A.5: Drag coefficients at 0 m seabed gap for DOF $= 1, 2, 3, 5, 6$

	Φ [deg]			
Ψ [deg]	**0**	**10**	**20**	**90**
0	d_{40}	d_{41}	d_{42}	d_{42}
10	d_{43}	d_{44}	d_{45}	d_{45}
20	d_{46}	d_{47}	d_{48}	d_{48}
25	d_{49}	d_{50}	d_{51}	d_{51}
30	d_{52}	d_{53}	d_{54}	d_{54}
35	d_{55}	d_{56}	d_{57}	d_{57}
40	d_{58}	d_{59}	d_{60}	d_{60}
45	d_{61}	d_{62}	d_{63}	d_{63}
50	d_{64}	d_{65}	d_{66}	d_{66}
60	d_{67}	d_{68}	d_{69}	d_{69}
70	d_{70}	d_{71}	d_{72}	d_{72}
80	d_{73}	d_{74}	d_{75}	d_{75}
90	d_{76}	d_{77}	d_{78}	d_{78}

Table A.6: Drag coefficients at 1.5 m seabed gap for DOF $= 1, 2, 3, 5, 6$

The mean roll angle before pipeline interference was approximately 40° when the input format in Tables A.5 and A.6 was used for the roll degree of freedom. Since the coefficients are valid only for roll angles up to 20° it was necessary to modify the input format of the roll drag coefficients. By performing some test runs in SIMLA it was seen that the mean roll angle was reduced to 22° when the roll drag coefficients were set equal to zero for roll angles larger than 25°.

	Φ [deg]				
Ψ [deg]	**0**	**10**	**20**	**25**	**90**
0	d_1	d_2	d_3	0	0
10	d_4	d_5	d_6	0	0
20	d_7	d_8	d_9	0	0
25	d_{10}	d_{11}	d_{12}	0	0
30	d_{13}	d_{14}	d_{15}	0	0
35	d_{16}	d_{17}	d_{18}	0	0
40	d_{19}	d_{20}	d_{21}	0	0
45	d_{22}	d_{23}	d_{24}	0	0
50	d_{25}	d_{26}	d_{27}	0	0
60	d_{28}	d_{29}	d_{30}	0	0
70	d_{31}	d_{32}	d_{33}	0	0
80	d_{34}	d_{35}	d_{36}	0	0
90	d_{37}	d_{38}	d_{39}	0	0

Table A.7: Drag coefficients at 0 m seabed gap for $\mathrm{DOF} = 4$

	Φ [deg]				
Ψ [deg]	**0**	**10**	**20**	**25**	**90**
0	d_{40}	d_{41}	d_{42}	0	0
10	d_{43}	d_{44}	d_{45}	0	0
20	d_{46}	d_{47}	d_{48}	0	0
25	d_{49}	d_{50}	d_{51}	0	0
30	d_{52}	d_{53}	d_{54}	0	0
35	d_{55}	d_{56}	d_{57}	0	0
40	d_{58}	d_{59}	d_{60}	0	0
45	d_{61}	d_{62}	d_{63}	0	0
50	d_{64}	d_{65}	d_{66}	0	0
60	d_{67}	d_{68}	d_{69}	0	0
70	d_{70}	d_{71}	d_{72}	0	0
80	d_{73}	d_{74}	d_{75}	0	0
90	d_{76}	d_{77}	d_{78}	0	0

Table A.8: Drag coefficients at 1.5 m seabed gap for $\mathrm{DOF} = 4$

Appendix B

Verification of the Advanced Hydrodynamic Load Model

The advanced hydrodynamic load model was included as a new feature in SIMLA in February 2010. In order to check if any bugs were present in the new SIMLA code it was decided to perform a verification test. In this connection the surge, sway and heave drag forces were emphasized. The trawl board was positioned in a steady current with an incoming velocity of 3.0 m/s. As seen in Table B.1 the test was executed for several combinations of heading angle Ψ, roll angle Φ and seabed to trawlboard gap Δ.

The drag forces attack at the trawl board centre of gravity where a pipe element of length 200 mm is attached. The pipe element is oriented such that the axial direction coincides with the surge direction. Fixed boundary conditions were imposed at the free end of the pipe element in the degrees of freedom which correspond to surge, sway and pitch. The prescribed values given in Table B.1 were imposed in the degrees freedom which correspond to the heading angle, the roll angle and the seabed gap.

The static load factors approached unit values after 1.0 s analysis time. Thereafter the current was ramped on linearly between 2.0 s and 9.0 s analysis time. At the boundary condition node the pipe element forces were sampled in the surge, sway and heave directions. The reaction forces due to current is denoted R_x, R_y and R_z in Table B.1 and were found as the difference in pipe element forces at 2.0 s and 10.0 s analysis time. D_x, D_y and D_z in Table B.1 refer to the drag forces which are calculated from the input drag coefficient.

Δ [m]	Ψ [deg]	Φ [deg]	D_x [N]	R_x [N]	D_y [N]	R_y [N]	D_z [N]	R_z [N]
0.0	0	0	−15 430	15 430	−3 588	3 588	−4 996	4 996
0.0	30	−10	−5 997	5 504	133 754	−133 120	−5 490	2 809
0.0	30	0	−6 418	6 418	146 821	−146 821	4 021	−4 024
0.0	0	−10	−12 069	12 020	−10 319	10 306	−7 050	7 071
1.5	0	0	−12 688	12 688	−2 820	2 820	−6 214	6 212
1.5	30	−10	−2 247	3 138	130 384	−133 903	-23 579	23 432
1.5	30	0	−4 112	4 040	147 605	−147 605	−23 408	16 702
1.5	0	−10	−9 322	9 326	-13 657	9 551	−6 990	8 269

Table B.1: Verification of drag forces

If the hydrodynamic load model works properly the reaction forces and the drag forces should be of

equal magnitude and have opposite sign. As indicated by the red cells in Table B.1 some errors are present in the magnitude of the drag forces.

When the seabed gap is zero it is seen from Table B.1 that the errors are present only for the surge and heave drag coefficient. During pipeline interference these coefficients are not of major importance. In the 1.0 m span height case the seabed gap is larger than zero only for the last 0.5 s of the simulation. The 0 m span height case has a seabed gap which is slightly larger than zero for 0.6 s. Therefore it is maybe possible to obtain reasonable pull-over simulations even with the errors present.

Appendix C

Contact Problems

C.1 Span Height of 0 m

Initially the boards in Figures 5.3 and 5.4 were modelled by a minimum number of pipe elements. In the 0 m span height case it was observed that the boards were not able to describe the contact geometry properly. This resulted in loss of contact and thereafter violent peaks emerged in the pull-over force time histories when pipeline contact was restored. The problem was solved by introducing shorter elements in the lower part of the trawl board front. The element lengths in Figures C.1 and C.2 were reduced from 550 mm to 200 mm, while the element lengths in Figures C.3 and C.4 were reduced from 300 mm to 100 mm.

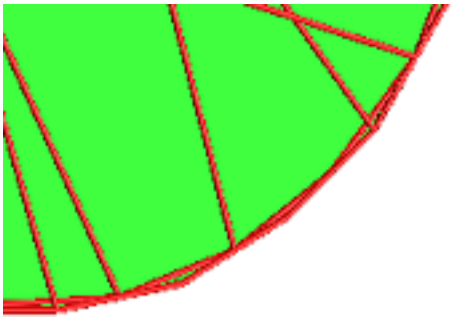

Figure C.1: Original front of polyvalent board

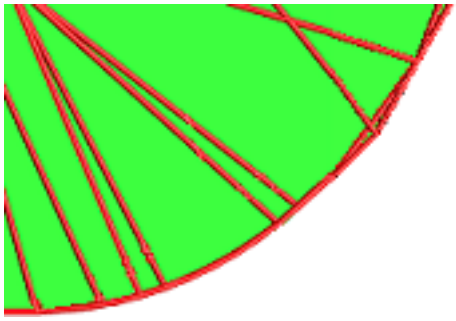

Figure C.2: Modified front of polyvalent board

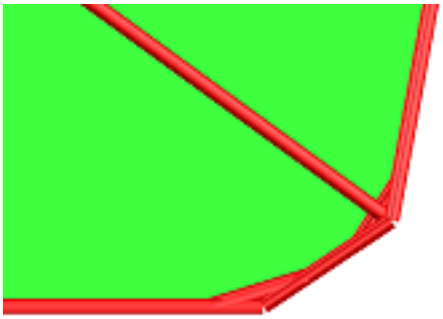

Figure C.3: Original corner of rectangular board

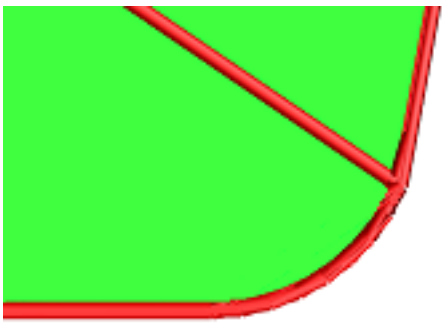

Figure C.4: Modified corner of rectangular board

C.2 Span Height of 1 m

Contact problems related to the lower front corner of the rectangular board occurred when it was lifted upwards at the end of pull-over. To avoid spurious behavior the lower corner was modified as shown in Figure C.5 for hit angles of $-10°$, $10°$ and $30°$. The modification is not believed to influence the pull-over results since the trawl board is lifted quickly upwards and the lower corner interacts with the pipeline for less than 0.1 s. Additional slave elements were attached to the board surface as shown in Figure C.5 to improve the contact ability. Extra slave elements were applied for both boards in the 1 m span height simulations.

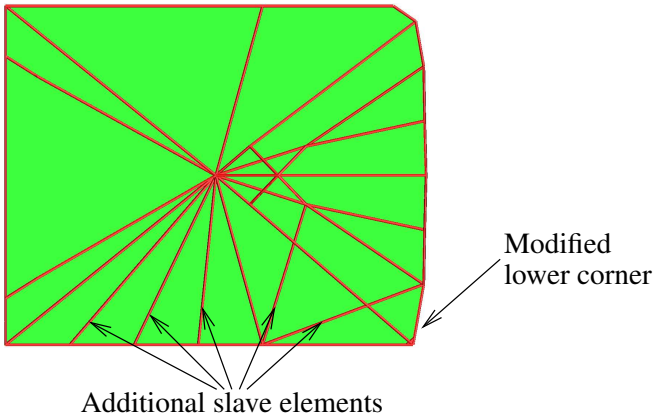

Figure C.5: Modified rectangular board

C.3 General Contact Problem

The master elements attached at the pipeline search for contact towards the corresponding slave elements on the trawl board. As illustrated in Figure C.6 the contact search is only executed in the normal direction of the two slave element surfaces. Loss of contact between trawl board and pipeline can therefore occur at nodal points between inclined slave elements. The problem is eliminated by attaching two more slave elements at the node where the contact failure occurs, see Figure C.7. In all simulations extra slave elements have been attached nearby the nodal points where contact problems occurred.

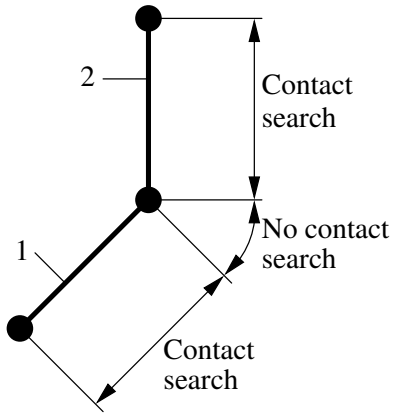

Figure C.6: Possible contact failure

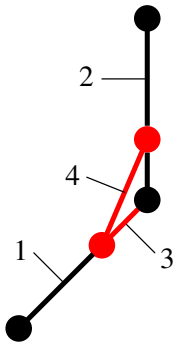

Figure C.7: No contact failure

Appendix D

Pull-over Screenshots

A limited number of the simulations are presented by screenshots in the following pages. The cases with 0 m span height are represented by the polyvalent board, the rectangular board, and the advanced hydrodynamic load model for a hit angle of $0°$.

The 1 m span height cases are represented by the polyvalent board with hit angles of $-20°$, $0°$ and $30°$. Here screenshots of the rectangular board simulations are not included since they resemble on the polyvalent board simulations. The advanced hydrodynamic load model is also presented with screenshots for this span height.

Polyvalent board, infinite fluid added mass, 0 m span height, ψ=0°

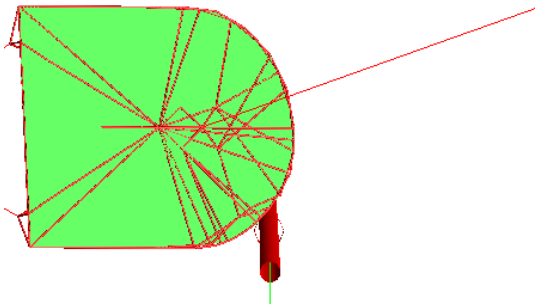

Pull-over time = 0.0 s

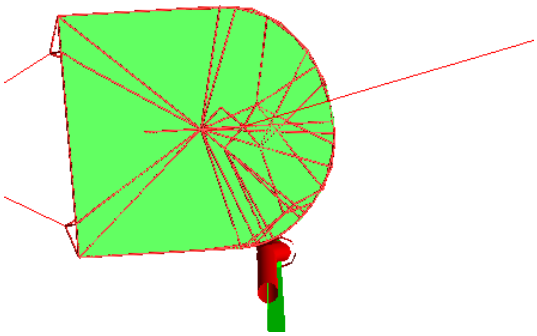

Pull-over time = 0.3 s

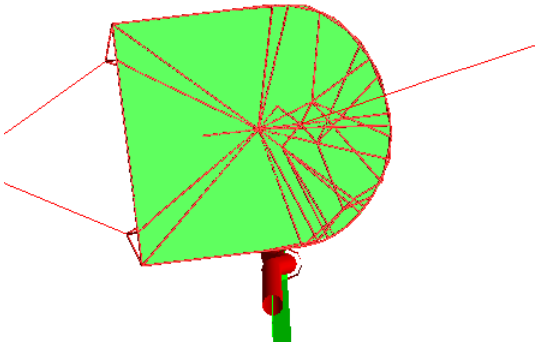

Pull-over time = 0.6 s

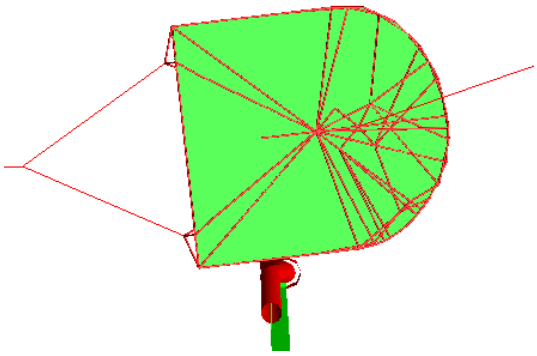

Pull-over time = 0.9 s

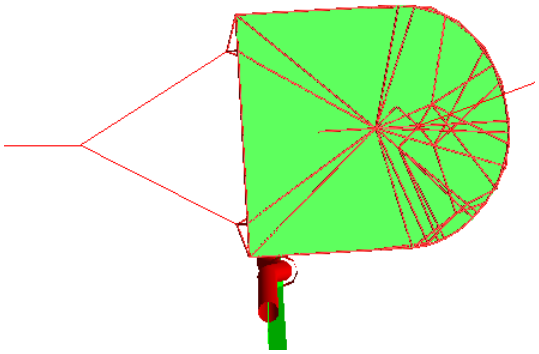

Pull-over time = 1.2 s

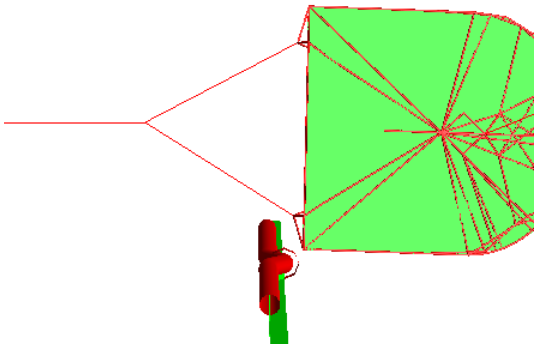

Pull-over time = 1.5 s

Rectangular Trawl Board, 0 m span height, ψ=0°

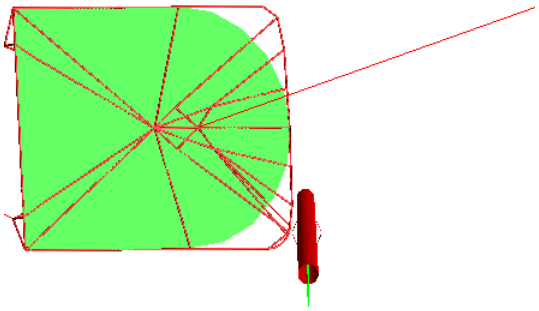

Pull-over time = 0.0 s

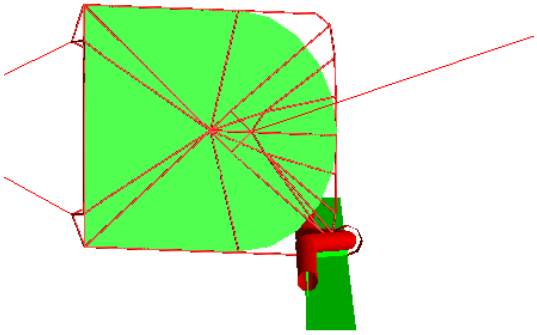

Pull-over time = 0.4 s

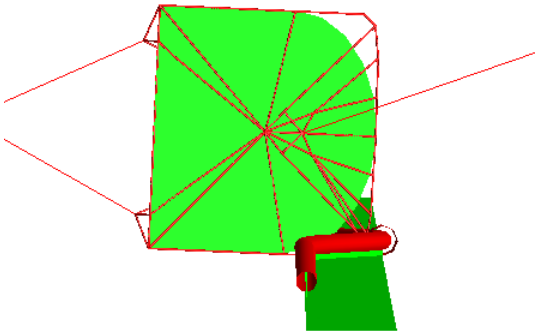

Pull-over time = 0.8 s

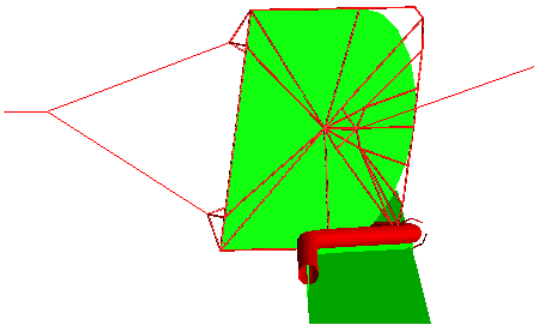

Pull-over time = 1.2 s

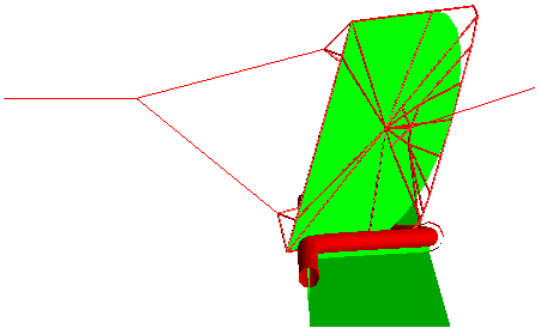

Pull-over time = 1.6 s

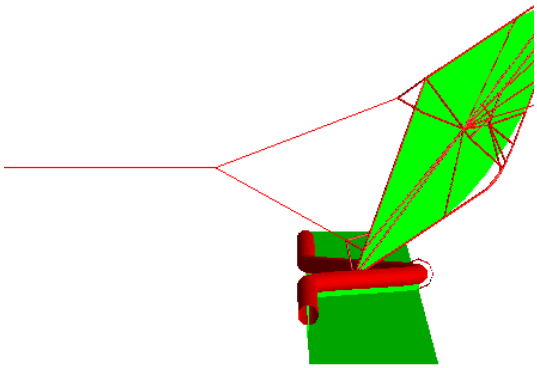

Pull-over time = 2.0 s

Advanced hydrodynamic load model, 0 m span height

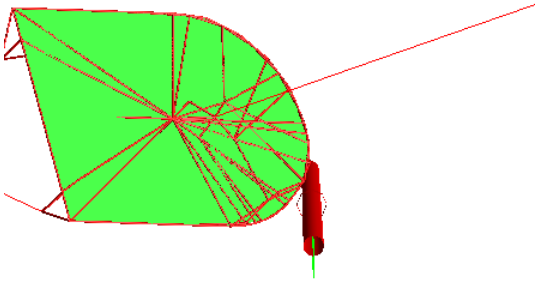

Pull-over time = 0.0 s

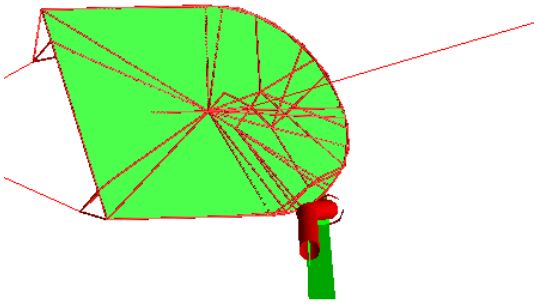

Pull-over time = 0.3 s

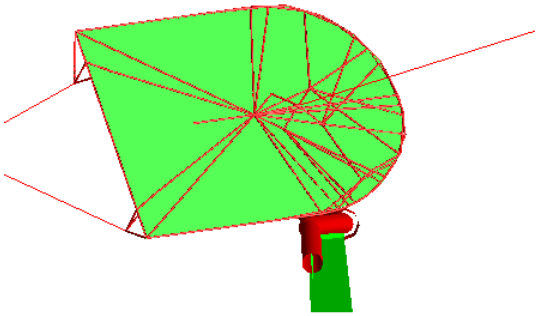

Pull-over time = 0.6 s

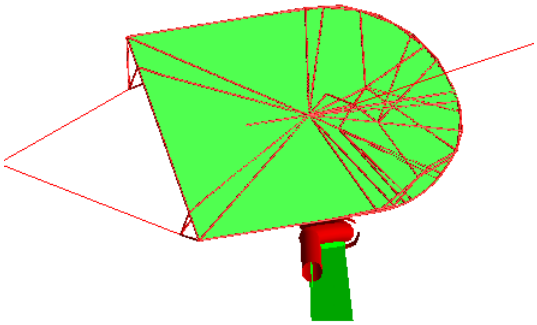

Pull-over time = 0.9 s

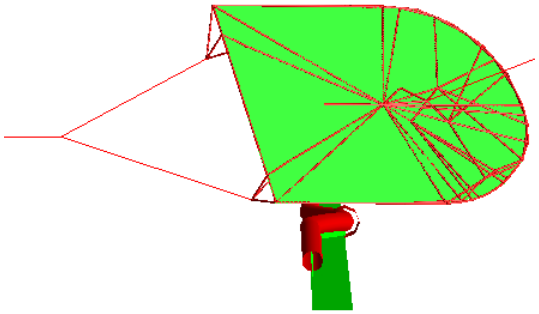

Pull-over time = 1.2 s

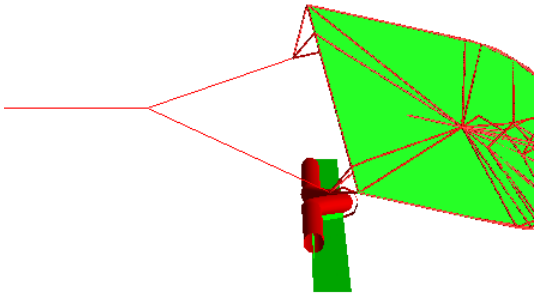

Pull-over time = 1.5 s

Polyvalent board, infinite fluid added mass, 1 m span height, ψ=−20°

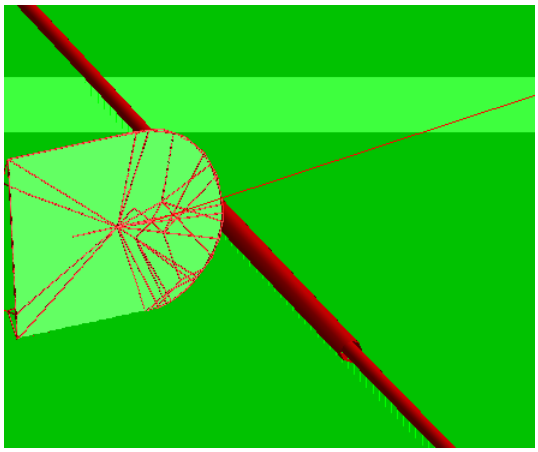

Pull-over time = 0.0 s

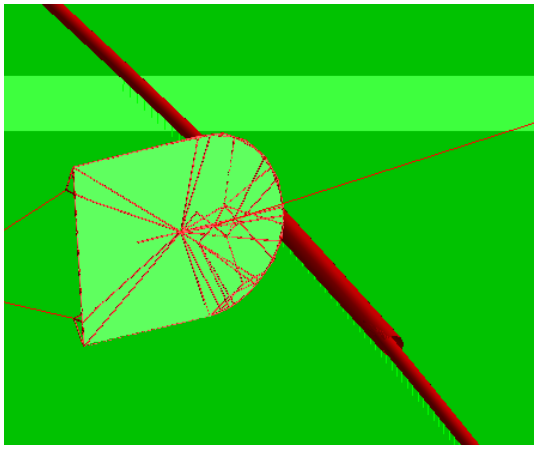

Pull-over time = 0.6 s

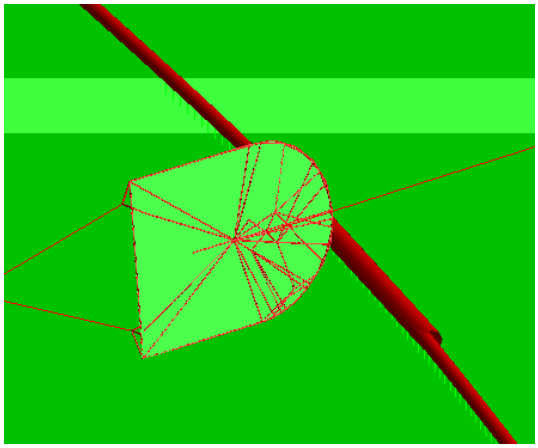

Pull-over time = 1.2 s

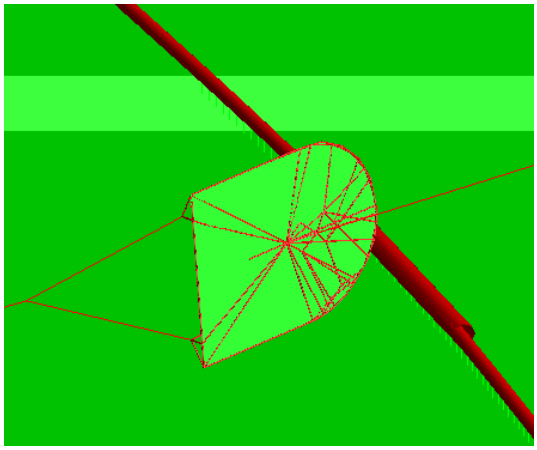

Pull-over time = 1.8 s

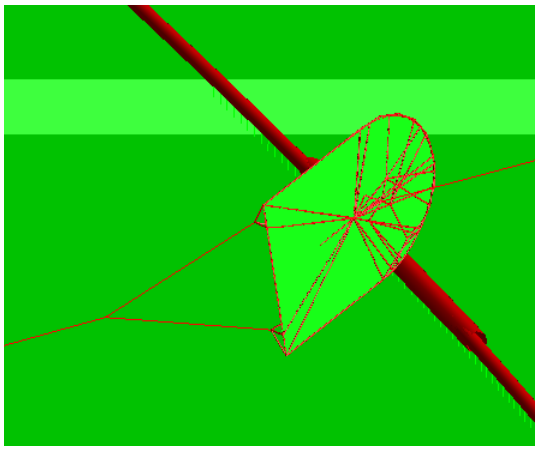

Pull-over time = 2.4 s

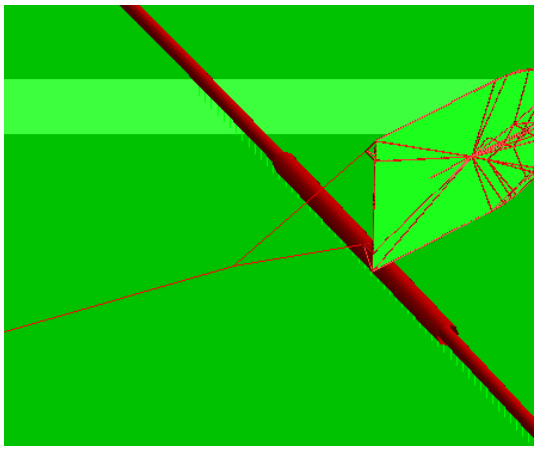

Pull-over time = 3.0 s

Polyvalent board, infinite fluid added mass, 1 m span height, ψ=0°

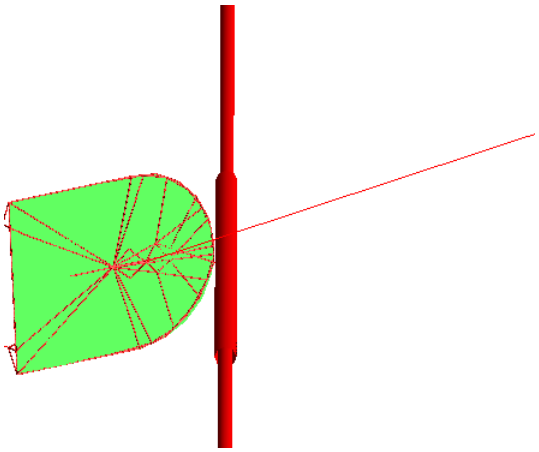

Pull-over time = 0.0 s

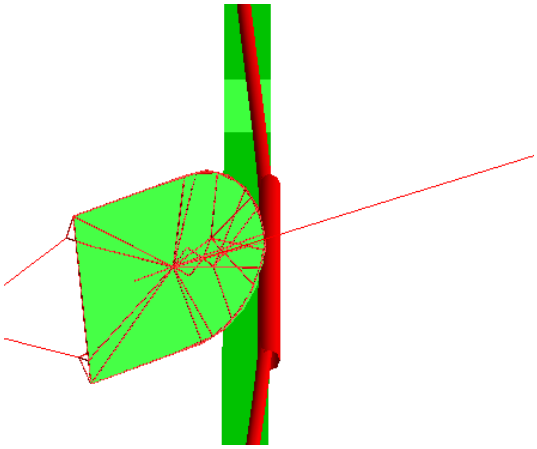

Pull-over time = 0.6 s

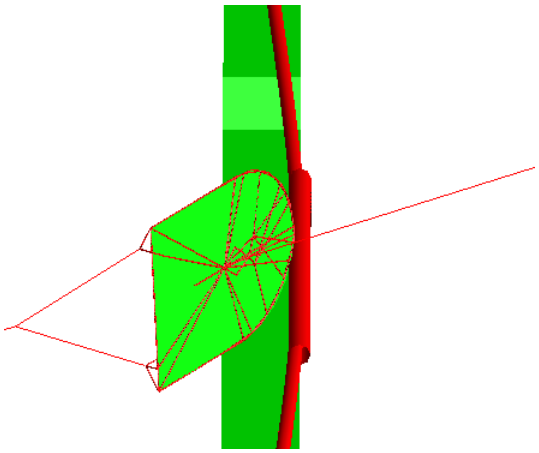

Pull-over time = 1.2 s

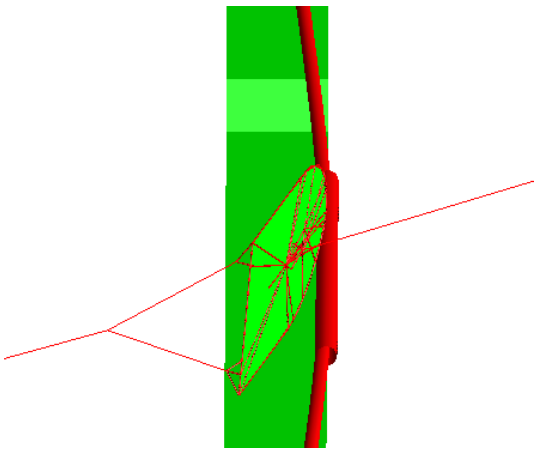

Pull-over time = 1.8 s

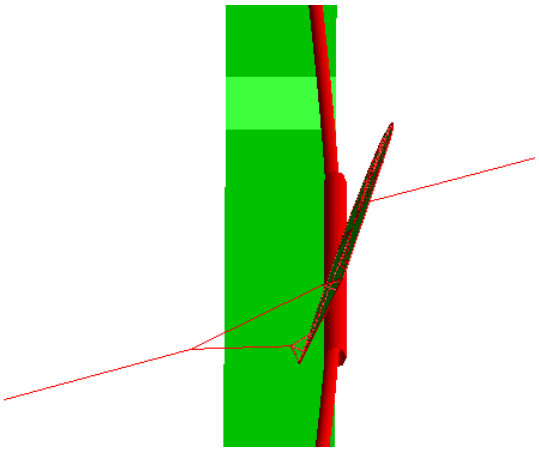

Pull-over time = 2.4 s

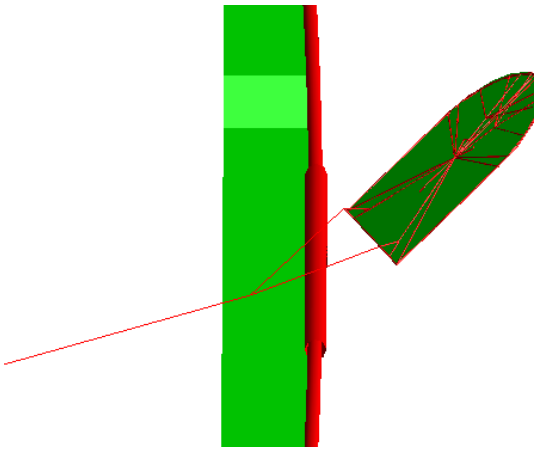

Pull-over time = 3.0 s

Polyvalent board, infinite fluid added mass, 1 m span height, ψ=30°

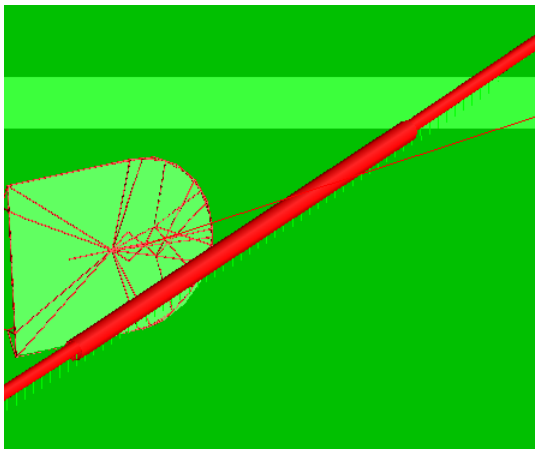

Pull-over time = 0.0 s

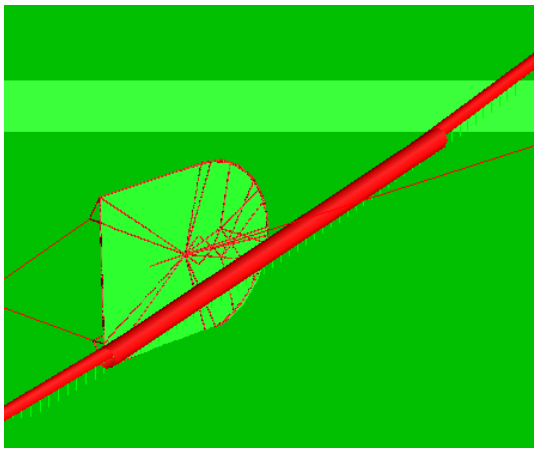

Pull-over time = 0.6 s

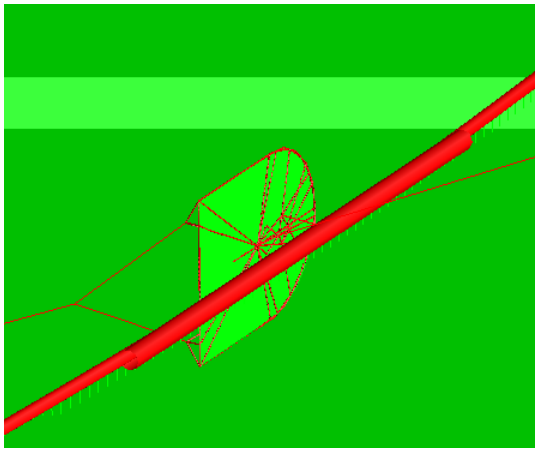

Pull-over time = 1.2 s

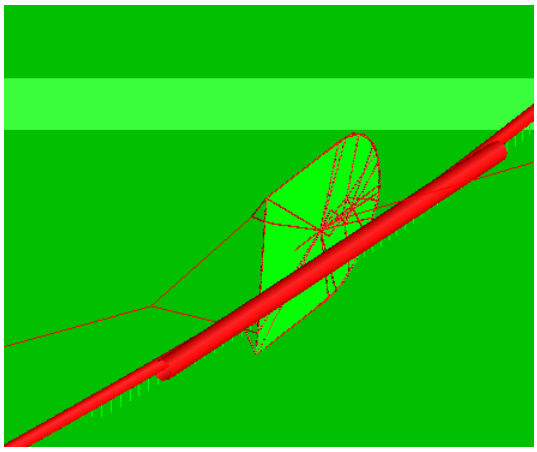

Pull-over time = 1.8 s

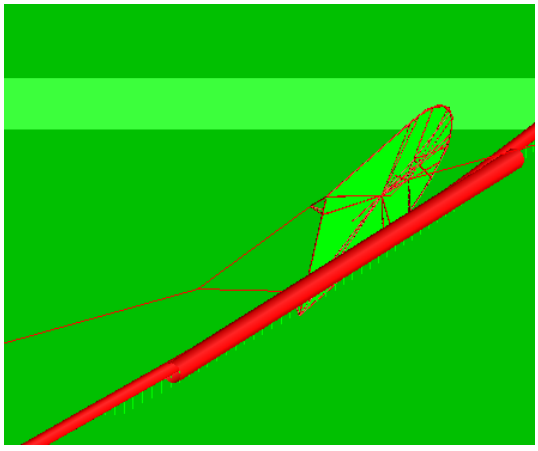

Pull-over time = 2.4 s

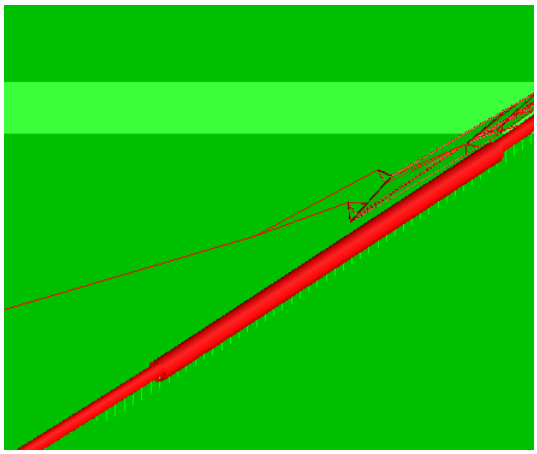

Pull-over time = 3.0 s

Advanced hydrodynamic load model, 1 m span height

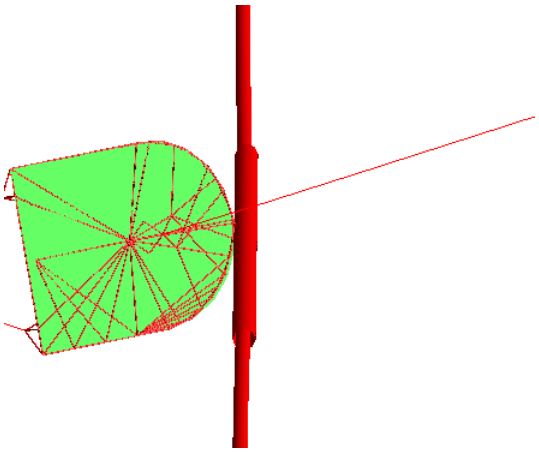

Pull-over time = 0.0 s

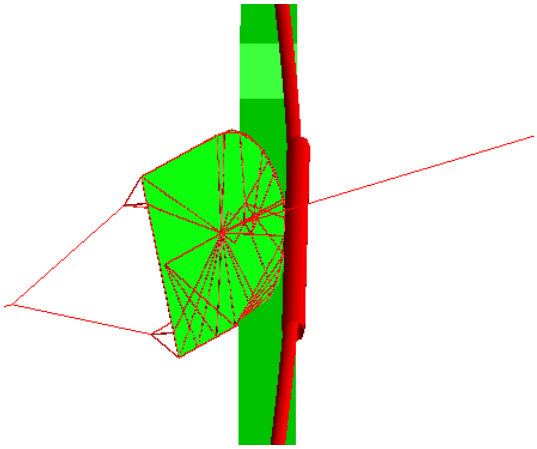

Pull-over time = 0.8 s

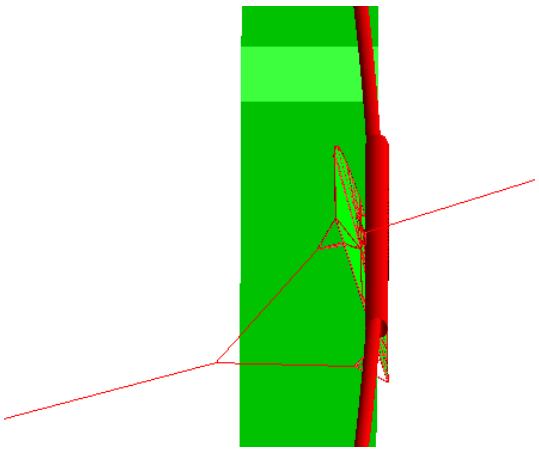

Pull-over time = 1.6 s

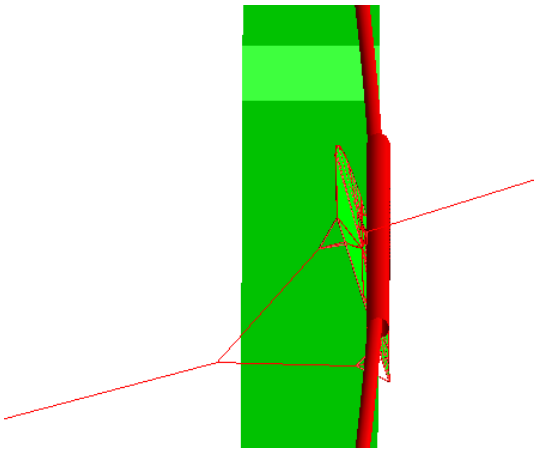

Pull-over time = 2.4 s

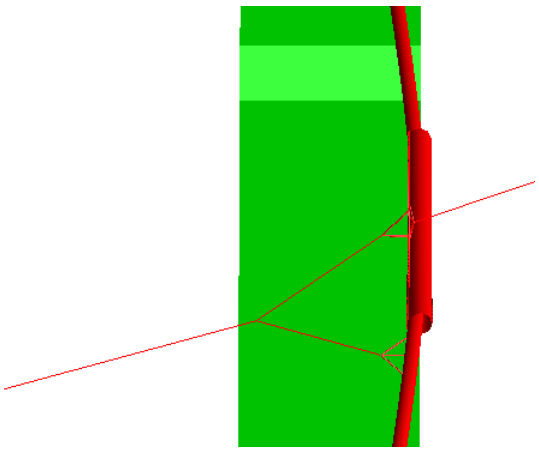

Pull-over time = 3.2 s

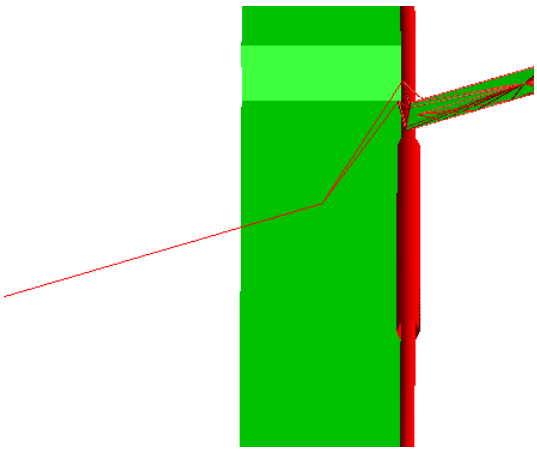

Pull-over time = 4.0 s